Membrane perturbation by the antimicrobial peptide [KIGAKI]$_3$: a simulation study

Störung von Membranen durch das antimikrobische Peptid [KIGAKI]$_3$: Eine Simulationsstudie

Master Thesis

Heinrich-Heine-Universität Düsseldorf

B.Sc. Marianne Schulte

Forschungszentrum Jülich
Institute of Complex Systems 6 - Structural Biochemistry
Multiscale Modelling Group

30th September 2014

Examiner: Jun.-Prof. Dr. Birgit Strodel
Co-Examiner: Prof. Dr. Henrike Heise

Declaration of the author

I, Marianne Schulte, hereby declare that this thesis has been composed by me and is based on my own work, unless stated otherwise. No other person's work has been used without due acknowledgment in this thesis. All references and verbatim extracts have been quoted, and all sources of information, including graphs and data sets, have been specifically acknowledged.

Jülich, 30th of September 2014

Marianne Schulte

Acknowledgments

First of all, I would like to thank my supervisor, Jun.-Prof. Dr. Birgit Strodel, for her encouragement and guidance during my Master Thesis. My sincere thanks to Prof. Dr. Henrike Heise for acting as second supervisor and for her kind aid in the experimental field. I thank my colleagues at the ICS-6 and in the Multiscale Modelling Group for interesting discussions and a very nice working environment, which made working a rewarding and enjoyable time. In particular, I would like to thank Bogdan, Qinqhua, Falk, Philipp and Oliver who helped me solving tricky computer problems and Martin for providing me an awesome poster template.
Many thanks also to Chetan Poojari for the preliminary work and for the great help in my first months at the Forschungszentrum Jülich.
I would like to thank Vineet for his encouragement and the great support during my thesis, especially for checking my written English for all kinds of mistakes.

This acknowledgment would be incomplete without thanking my family for their support and motivation throughout my studies.

Abstract

[KIGAKI]$_3$ is an antimicrobial peptide which is reported to disrupt bacteria cell-membranes without being harmful for mammalian cell-membranes. However, little is know about the adsorption and disruption mechanisms. In this work, we will contribute to the understanding of the adsorption process by analyzing the change in structure of the peptides when adsorbing on the membrane surface, the interaction between [KIGAKI]$_3$ peptides and the bilayer and the perturbation of the membrane. Molecular dynamics (MD) simulations were performed to study the behavior of [KIGAKI]$_3$ on a partly charged POPC/POPG and a pure POPC bilayer on an atomistic level. These bilayer models were used to mimic bacteria (POPC/POPG) and mammalian (POPC) cell-membranes. In total 5.2 μs simulations were analyzed and compared to experimental results.

We observed more [KIGAKI]$_3$ peptides adsorbing on the negatively charged bilayer, leading to membrane perturbation, whereas fewer peptides adsorb to the POPC bilayer, which does not show any changes in membrane properties. These findings agree well with experimentally derived results that show perturbation and leakage only of negatively charged bilayers upon addition of [KIGAKI]$_3$, but not of neutral membranes. On the POPC membrane, [KIGAKI]$_3$ retains its β-hairpin structure, whereas some peptides on the charged bilayer surface unfold, resulting from stronger interactions between the cationic peptide and the negatively charged bilayer.

The attachment of a *L*-CF$_3$-Bpg or a *D*-CF$_3$-Bpg label to the peptide sequence leads to a deviant folding of [KIGAKI]$_3$. The slight difference in the secondary structure results in a different adsorption behavior of the labeled peptides. This might explain the different hemolytic activities among the two labeled and unlabeled peptides, which has been observed experimentally, while the antimicrobial activity is similar.

Contents

1 Introduction **12**

1.1 Mechanism of action of AMPs 13

1.2 The $[KIGAKI]_3$ peptide 14

1.3 Motivation and outline 15

2 Methods **18**

2.1 MD simulations 18

2.2 Integrators 19

2.3 Statistical mechanics 21

2.4 Force field 23

2.5 Analysis methods 25

2.6 Parametrization of CF_3-Bpg 28

3 Simulation Details **30**

3.1 Simulation setup of bilayer systems 30

3.2 Simulation setup of $[KIGAKI]_3$ with CF_3 label in water 31

4 Results and Discussion of $[KIGAKI]_3$ simulations **32**

4.1 Adsorption of $[KIGAKI]_3$ on membrane surfaces 32

4.2 Peptide structures and structural changes on membranes 38

4.2.1 RMSD 38

4.2.2 Secondary structure 39

4.3 Correlation between secondary structure and adsorption 42

4.4 Motion of $[KIGAKI]_3$ on bilayer surfaces 43

4.4.1 Peptide Diffusion 43

4.4.2 Flexibility of peptide residues 44

4.5 Interactions between $[KIGAKI]_3$ and different membranes 45

4.5.1 Hydrogen-bonding 45
4.5.2 Interaction energies 49
4.6 Effects of $[KIGAKI]_3$ adsorption on membrane properties 51
4.6.1 Deuterium order parameter 51
4.6.2 Area per lipid and bilayer thickness 53
4.6.3 Water density 56
4.7 Discussion 57

5 Results and discussion of $[KIGAKI]_3$-CF_3-Bpg simulations 61

5.1 $[KIGAKI]_3$-CF_3-Bpg in water 61
5.1.1 Secondary structure 61
5.1.2 Flexibility 62
5.2 $[KIGAKI]_3$-CF_3 on phospholipid bilayers 63
5.2.1 Adsorption on membrane surfaces 63
5.2.2 Secondary structure 65
5.2.3 Orientation of the CF_3-Bpg label with respect to the bilayer normal . 67
5.2.4 Hydrogen-bonding 70
5.2.5 Interaction energies 71
5.3 Discussion 73

6 Summary and Outlook 76

7 Appendix 78

7.1 Simulation Setup 78
7.2 Lipids 79
7.3 Adsorption of six $[KIGAKI]_3$ peptides in the six-peptide simulations 80
7.4 Secondary structure of six-peptide simulations 82
7.5 Correlation between secondary structure and insertion depth 84
7.6 Na^+ density 86

7.7 Water density 86
7.8 Adsorption of CF_3-labeled peptides 87
7.9 Secondary structure of CF_3 labeled peptides 91

List of Figures

1 Shai-Matsuzaki-Huang model 13

2 Amphipathic presentation of $[KIGAKI]_3$ 15

3 Starting structures 16

4 *L*-CF_3-Bpg label 28

5 Adsorption of $[KIGAKI]_3$ on bilayer surfaces 33

6 Distancemap of $[KIGAKI]_3$ adsorbing on POPC/POPG bilayer 35

7 Distancemap of $[KIGAKI]_3$ adsorbing on POPC bilayer 36

8 Snapshot of cluster3 after 200 ns of simulation 37

9 RMSD of $[KIGAKI]_3$ 38

10 DSSP plots and final snapshot of single-peptide simulations 40

11 Secondary structure content 41

12 RMSF of adsorbed $[KIGAKI]_3$ peptides 45

13 Hydrogen bonds between cluster3 fragments and POPG lipids 46

14 Hydrogen bonds between cluster3 fragments and POPC lipids 48

15 Interaction energies between $[KIGAKI]_3$ and membranes over time 50

16 Deuterium order parameter 52

17 Na^+ coordinated in POPC/POPG headgroup region 53

18 Area per lipid 55

19 Bilayer thickness 56

20 Water density in headgroup region 57

21 Loosely aggregated $[KIGAKI]_3$ peptides 60

22 Secondary structure of $[KIGAKI]_3$-CF_3 in water 62

23 RMSF of $[KIGAKI]_3$ with and without label in water 63

24 Adsorption of $[KIGAKI]_3$-CF_3 on bilayer surfaces 64
25 Average distance between all adsorbed peptides and bilayer surface 65
26 Secondary structure content $[KIGAK]_3$-CF_3 67
27 $[KIGAKI]_3$-CD_3 oligomers 68
28 Orientation of CF_3-Bpg in respect to the membrane normal 69
29 Interaction energies between $[KIGAKI]_3$-CF_3 and membranes over time . . . 73
30 Influence of CF_3 on adsorption 74
31 System setup for single-peptide simulations 78
32 Simulation setup for six-peptide simulations 78
33 Lipid types 79
34 Distancemap of $[KIGAKI]_3$ peptides and POPC/POPG bilayer 80
35 Distancemap of $[KIGAKI]_3$ peptides and POPC bilayer 81
36 DSSP plots of six peptides on POPC/POPG membrane 82
37 DSSP plots of six peptides on POPC membrane 83
38 Na^+ density in respect to the membrane 86
39 Water density comparison of six-peptide simulations 86
40 Distancemap of $[KIGAKI]_3$-8L peptides and POPC/POPG bilayer 87
41 Distancemap of $[KIGAKI]_3$-8L peptides and POPC bilayer 88
42 Distancemap of $[KIGAKI]_3$-8D peptides and POPC/POPG bilayer 89
43 Distancemap of $[KIGAKI]_3$-8D peptides and POPC bilayer 90
44 Secondary structure of $[KIGAKI]_3$-8L on the POPC/POPG bilayer 91
45 Secondary structure of $[KIGAKI]_3$-8L on the POPC bilayer 92
46 Secondary structure of $[KIGAKI]_3$-8D on the POPC/POPG bilayer 93
47 Secondary structure of $[KIGAKI]_3$-8D on the POPC bilayer 94

List of Tables

1 Peptide diffusion coefficients 43

2 Hydrogen bonds between $[KIGAKI]_3$ and membranes 47

3 Interaction energies between $[KIGAKI]_3$ and membranes 49

4 Area per lipid and bilayer thickness 54

5 Hydrogen bonds between $[KIGAKI]_3$-CF_3 and membranes 70

6 Interaction energies between $[KIGAKI]_3$-CF_3 and membranes 72

7 Correlation between secondary structure and insertion depth on POPC/POPG bilayer 84

8 Correlation between secondary structure and insertion depth on POPC bilayer 85

List of abbreviations

AMP Antimicrobial Peptides

MD Molecular Dynamics

PG Phosphatidylglycerol

CL Cardiolipin

PC Phosphatidylcholine

SMH Shai-Matsuzaki-Huang model

POPC 1-palmitoyl-2-oleoyl-*sn*-glycero-3-phosphocholine

POPG 1-palmitoyl-2-oleoyl-*sn*-glycero-3-phospho-(1'-*rac*-glycerol)

CF_3-Bpg 3-(trifluoromethyl)-bicyclopent-[1,1,1,]-1-ylglycine

vdW van der Waals

RMSD Root Mean Square Deviation

RMSF Root Mean Square Fluctuation

MSD Mean Square Displacement

COM Center Of Mass

ATB Automated Topology Builder

QM Quantum Mechanics

AM1 Austin Model 1

B3LYP Becke, three-parameter Lee-Yang-Parr

SPC Simple Point Charge

NMR Nuclear Magnetic Resonance

DSSP Define Secondary Structure of Proteins

LJ	Lennard-Jones
S_{CD}	Deuterium order parameter
APL	Area Per Lipid
P/L	Peptide/Lipid ratio
LUV	Large Unilamellar Vesicle
MIC	Minimum Inhibitory Concentration
TEM	Transmission Electron Microscopy
FRET	Förster Resonance Energy Transfer

1 Introduction

Antibiotic resistant bacteria have become a serious global health problem as pointed out by the World Health Organization in their latest report on antimicrobial resistance [1]. Resistance is an inevitable consequence of the use of antibiotic compounds. This process has been accelerated by negligent antibiotic use [2] and its progressive application in food production [3, 4]. It is therefore of great importance to discover or develop new antibiotics. However, all known classes of antibiotic compounds were discovered between 1908 and 1987; since 1987 there has been a 'Discovery Void' [1]. The preservation of the efficiency of already existing drugs and the development of new treatments are therefore essential for the therapy of infectious diseases.

Antimicrobial peptides (AMPs) are a promising class of molecules under development against bacteria. They were discovered in a wide range of species as part of the innate immune response and show common characteristics of a short sequence (typically between 11-50 amino acids) with an overall positive net charge, typically ranging from +2 to +6, due to lysine and arginine residues present in the peptide sequence [5]. These host defense peptides are composed of hydrophilic, cationic amino acids and nearly 50% of hydrophobic residues. This is why AMPs exhibit hydrophobic and hydrophilic regions upon formation of an amphipathic structure, commonly induced by membrane interaction [6]. Based on their structures, antimicrobial peptides can be divided into four different classes: β-sheet, α-helical, loop and extended peptides [5]. The advantages of using AMPs are an extremely broad antimicrobial activity [7,8] and a rapid killing mechanism (within minutes) in comparison to common antibiotics that need between 4 h and 24 h to kill the target bacteria [9, 10]. They further show synergistic effects in combination with other antibiotic compounds [11]. However, the most important feature is that the emerge of resistance is less probable than for traditional antibiotic compounds. This is because the main target is the bacterial membrane. In order to become resistant, a microbe would have to reorganize its lipids or even change its membrane composition. Both options are energetically costly for most kinds of bacteria. Furthermore, multiple peptides that belong to different structural groups attack the bacteria, hence, resistance against one peptide might not be enough to ward the attack [12].

So why are there only very few antimicrobial peptides in clinical application?

Development of antimicrobial peptides as drugs is a non-trivial process and involves various hurdles. First of all, antimicrobial peptides can be toxic for eukaryotic cells due to the requirement of high dosage [12, 13] and low selectivity [14]. Second, a short half-life of AMPs

in vivo is observed [14] which is due to the sensitivity towards proteolytic degradation in the body [10,15]. The antimicrobial activity is also sensitive towards salt concentration [16] and pH [11]. Apart from pharmacological issues, high manufacturing costs have made the pharmaceutical industry reluctant to invest in the development of AMP drugs [8,11,14].

1.1 Mechanism of action of AMPs

Although the interest in antimicrobial peptides has strongly increased in the last decades, the mechanism of action of these peptides is poorly understood. However, the available information continues to grow and some reasonable models have been developed. We will focus on the Shai-Matsuzaki-Huang (SMH) model of mechanism that is able to explain the activity of most antimicrobial peptides and is explained in Figure 1 [12,17–19].

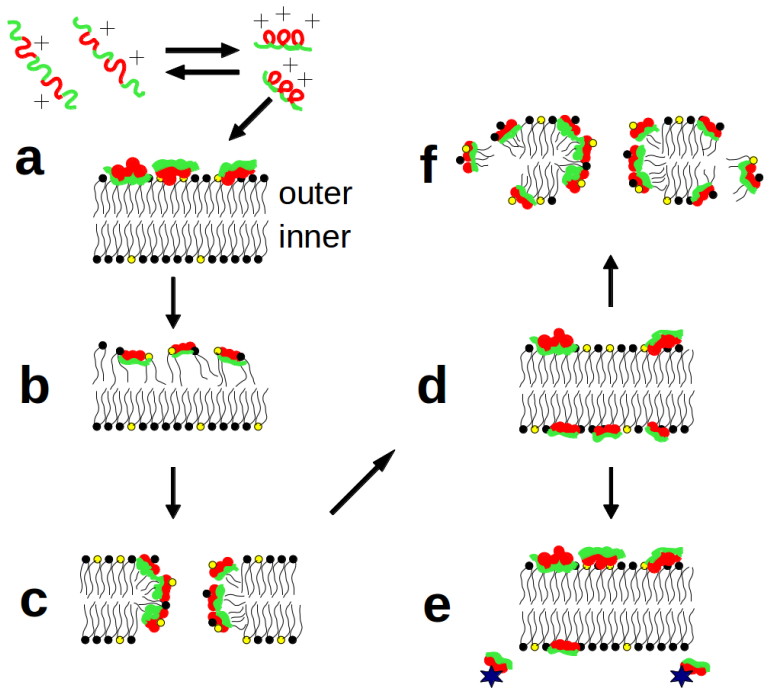

Figure 1: Shai-Matsuzaki-Huang model. Adapted and modified from M. Zasloff [12]. Lipids with yellow headgroups are negatively charged, the ones with black headgroups have no net charge. (a) The AMP in water shows an equilibrium between random coil and amphipathic (here α-helical) structure. The latter one adsorbs onto the membrane surface and carpets the outer leaflet. (b) The peptide integrates into the bilayer and thins out the outer leaflet and hence, leads to expansion of the outer leaflet, relative to the inner leaflet, which further leads to tension within the bilayer. (c) Illustrates the phase transition and pore formation (s. barrel-stave and toroidal pore model [20]). (d) Peptides and associated lipids are transported into the inner leaflet, followed by two possible options: (e) Diffusion of peptides onto targets within the cell (blue stars), or (f) disruption of the bacterial cell-membrane into fragments, implying that the membrane is the target.

The most striking difference between prokaryotic and eukaryotic cell membranes is the composition and arrangement of lipids [21]. The outer leaflet of bacterial membranes that is exposed to the extra-cellular environment contains large amounts of negatively charged phospholipids such as phosphatidylglycerol (PG) and cardiolipin (CL), whereas the outer leaflet of eukaryotic cells consists of zwitterionic, overall neutral phospholipids, mainly phosphatidylcholine (PC) and membrane-stabilizing cholesterol. The majority of lipids containing negatively charged headgroups are segregated into the inner leaflet that faces the cytoplasm of eukaryotic cells [12, 17]. The SMH model proposes the displacement of lipids, change in membrane structure and in some cases the entry of peptides into the interior of the cell upon peptide-lipid interaction. The absence of negative charges in the outer leaflet of mammalian cell membranes and the presence of cholesterol lead to weak interactions between AMPs and the membrane, whereas the negatively charged lipids in the prokaryotic cell-membrane lead to strong, mainly electrostatic interactions between peptides an lipids [12, 17].

1.2 The $[KIGAKI]_3$ peptide

In this work, the novel cationic linear antimicrobial peptide $[KIGAKI]_3$ has been studied, which is designed to adopt a β-sheet conformation [22]. The peptide consists of polar (lysine, glycine) and apolar (isoleucine, alanine) residues, that are present in an alternating sequence. The amphipathic nature of antimicrobial peptides and in particular the one of $[KIGAKI]_3$ is illustrated in Figure 2.

$[KIGAKI]_3$ carries 7 positive charges due to the presence of lysine residues and it is amidated at the C-terminus. Upon interaction with phospholipid membranes it is known to form an amphipathic β-sheet structure [23]. It has been reported that $[KIGAKI]_3$ is effective against the Gram-positive bacteria *S. epidermidis*, *S. aureus* and the Gram-negative strains *P. aeruginosa* and *E. coli*. The minimum inhibitory concentration (MIC) is mostly around 7.5 μM or below [24]. This may result from its ability to disturb and induce leakage in bilayers containing lipids with negatively charged headgroups [22, 25, 26]. Furthermore, Meier et al. [27] and Wadhwani et al. [23] reported that $[KIGAKI]_3$ aggregates and forms amyloid-like fibrils at high peptide/lipid ratios. Amyloids are insoluble fibrous protein aggregates exhibiting β-sheet structure that arise from inappropriately folded proteins.

The aggregation of proteins or peptides into fibrils or plaques are a common characteristic feature of many neurodegenerative diseases such as Alzheimer's and Parkinson's dis-

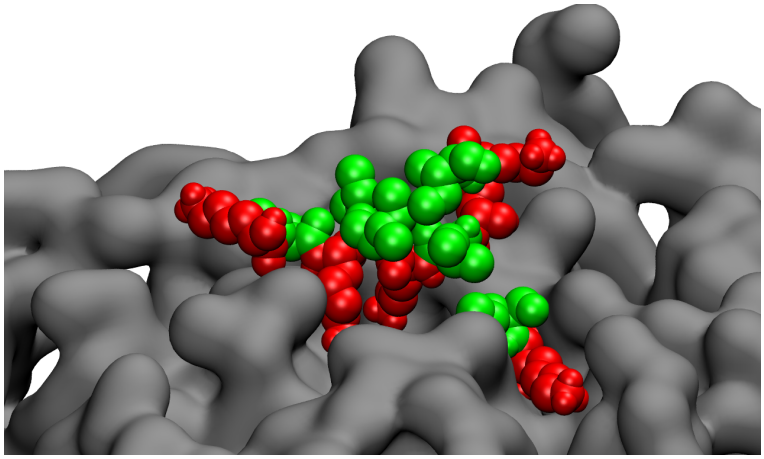

Figure 2: $[KIGAKI]_3$ peptide after 200 ns of simulation on a bilayer surface, presented in 'amphipathic' design. Cationic lysine residues are colored red and hydrophobic isoleucine residues are green. Distinct hydrophobic and cationic/hydrophilic domains can be observed. Other residues are not shown.

ease [28, 29]. The investigation of e.g. Aβ fibril-formation in the laboratory is not a trivial task. Scientists face several problems such as a lack of methods to quantify aggregation, low solubility of the Aβ peptide and high sensitivity of the structure and aggregation process towards the environmental conditions such as pH, temperature and salt concentration [30]. Hence, model peptides for Aβ aggregation are used to gain more insight into the aggregation process.

These model systems should therefore possess the same characteristic properties. These are firstly, strong affinity towards negatively charged lipid membranes, secondly, a transition from random coil to β-sheet conformation upon interaction with membranes and thirdly, self-assembly into oligomers, fibrils and eventually plaques [30]. Since the $[KIGAKI]_3$ peptide shows all of these characteristics, it can be used as a model peptide to study amyloid-formation. However, the main focus of this work will be the investigation of the mechanism of the antimicrobial activity of $[KIGAKI]_3$.

1.3 Motivation and outline

$[KIGAKI]_3$ is an antimicrobial peptide which is known to disrupt bacterial cell-membranes without being harmful to mammalian membranes [25]. However, little is known about the adsorption and disruption mechanisms. The aim of this work is to investigate the adsorption of $[KIGAKI]_3$ to different membranes by analyzing the structural changes of the peptides, when adsorbing on different membrane surfaces, the interactions between $[KIGAKI]_3$ and

the lipid bilayers, and the perturbation of the membranes. To this end, we carried out molecular dynamics (MD) simulations, which will be briefly described in the following.
Three different structures of $[KIGAKI]_3$, presented in Figure 3, were used to initiate the MD simulation, which allows us to conclude whether or not the starting structure affects the results. These three structures correspond to the main conformations obtained from clustering analysis of a 100 ns MD simulation of $[KIGAKI]_3$ in water [31]. In the following they are denoted as cluster1, cluster2 and cluster3.

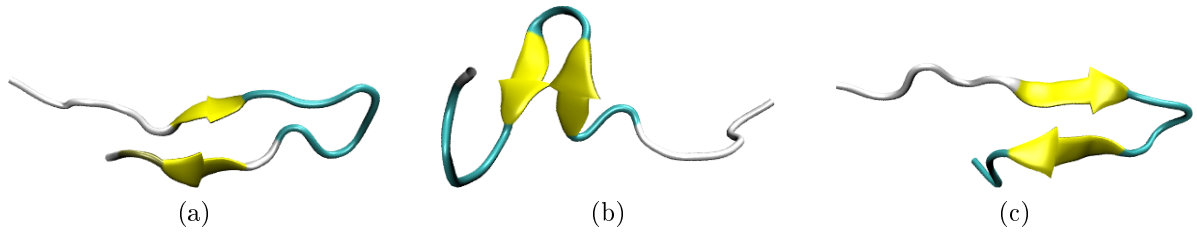

Figure 3: The three starting structures used in the simulations are shown here: (a) cluster1, (b) cluster2 and (c) cluster3. They are the representative structures of the three largest clusters obtained by clustering a 100 ns simulation of $[KIGAKI]_3$ in water, starting from an extend structure [31]. The figure was made with VMD [32] using the new cartoon representation with yellow for β-sheets, cyan for β-hairpin and white for coil.

$[KIGAKI]_3$ on a partly charged POPC/POPG (4:1) bilayer

In the simulation setup, one $[KIGAKI]_3$ peptide was placed approximately 1.5 nm above a POPC/POPG bilayer which resembles bacteria cell-membranes. This 200 ns simulation has been carried out three times with the different starting structures. The aim was to investigate the adsorption process of the peptides and the effects on peptide structure and membrane properties. Furthermore, there are experimental results available which can be used for validation. The initial system is shown in Appendix 7.1

$[KIGAKI]_3$ on a POPC bilayer

The same simulation setup was used as before. The only difference is that here a pure POPC bilayer was used which resembles the mammalian cell-membranes. The results of these simulations allow us to compare the behavior of $[KIGAKI]_3$ peptides on neutral and charged membranes as well as changes in membrane properties.

Six $[KIGAKI]_3$ peptides on a partly charged POPC/POPG (4:1) bilayer

Aggregation of $[KIGAKI]_3$ peptides on membrane surfaces at high peptide/lipid concentration has been previously reported by [23, 24]. However, the role of the aggregates towards the antimicrobial activity of the peptide is not clear. In order to analyze the aggregation mechanism, 3 peptides were placed above the upper-leaflet and 3 peptides were placed

below the lower-leaflet of the bilayer. For this 1 μs simulation only cluster1 was used as starting structure. Apart from the aggregation, another major focus lies on the analysis of membrane properties because the influence on membrane properties of six peptides is likely higher than of only one peptide. The initial system is shown in Appendix 7.1.

Six [KIGAKI]$_3$ peptides on a POPC bilayer

The ability of [KIGAKI]$_3$ to aggregate on membranes has also been reported on neutral bilayers [23, 24], which is the main motivation for this 1 μs simulation. Furthermore, a comparison will be drawn with the previous POPC/POPG simulation to analyze if the peptide aggregation is affected by the membrane charge and if the effects of [KIGAKI]$_3$ on the membrane systems differ.

[KIGAKI]$_3$ peptides with CF$_3$-Bpg label in water

Solid state NMR experiments have been carried out using a 3-(trifluoromethyl)-bicyclopent-[1,1,1,]-1-ylglycine (CF$_3$-Bpg) label, either in the *L*- or *D*- conformation. One label per peptide was attached to the following positions: Ile-6, Ile-8, Ala-10, Ile-12 and Ile-14 of [KIGAKI]$_3$ [23, 24]. The authors already showed that these labels have an influence on the aggregation ability of [KIGAKI]$_3$ and the hemolytic activity. In order to obtain starting structures for the aggregation simulations and to study the effect of the CF$_3$ label, 100 ns simulations in water were performed, starting from an elongated structure of [KIGAKI]$_3$ in either a *L*- or *D*-conformation substituting Ile-8. In addition, the folding process for the labeled and unlabeled [KIGAKI]$_3$ was compared.

Six [KIGAKI]$_3$ peptides with CF$_3$-Bpg label on membranes

In these simulations we will compare the structure, adsorption and aggregation of the labeled and unlabeled peptides. In order to show the behavior of the labeled peptides we performed four 500 ns simulations: six peptides with the *L*-CF$_3$-Bpg and six peptides with the *D*-CF$_3$-Bpg were simulated separately on the individual bilayer systems (POPC/POPG and POPC).

2 Methods

2.1 MD simulations

Experimental methods that are used for the investigation of biological systems provide average or crystal structures which only give limited insight into the dynamics of these systems. In this work, MD simulations were used to explore the dynamics of $[\text{KIGAKI}]_3$. MD simulations are based on classical mechanics, where particles (mainly atoms) interact through Newton's law of motion. The interaction energy is determined by a potential energy function, which is called a force field [33]. Providing initial coordinates, the force that is applied on every particle is calculated at each timestep yielding the acceleration of the particles. Integrating the equation of motion gives a trajectory, containing the positions and velocities of every particle at every time step.
Newton's second law of motion for a particle i is given by:

$$F_i = m_i a_i \tag{1}$$

$$= m_i \frac{dv_i}{dt} \tag{2}$$

$$= m_i \frac{d^2 r_i}{dt^2} \tag{3}$$

with F_i being the force applied on the particle i possessing the mass m_i and the acceleration a_i which is the second derivative of the particle position r_i and the first derivative of the velocity v_i with respect to time. The solution of Newton's equation is required for every particle i in the system of N particles and in each x, y and z direction. The net force F_i, which is exerted on the particle i is given by the negative gradient of the potential-energy function V with respect to the particle position.

$$F_i = -\frac{dV}{dr_i} \tag{4}$$

Combining equations 1 and 4, the acceleration can be related to the potential energy:

$$a_i = \frac{d^2 r_i(t)}{dt^2} = \frac{F_i}{m_i} = -\frac{dV}{dr_i}\frac{1}{m_i} \tag{5}$$

2.2 Integrators

Newton's equation of motion (5) cannot be solved analytically and therefore various algorithms have been developed to integrate it. The most commonly used integrators are presented in the following.

Verlet algorithm

The simple Verlet algorithm [34] calculates the position at $t+\Delta t$ by using the positions and accelerations at times t and $t-\Delta t$, with Δt being the timestep for the integration, which it typically between 1 and 5 fs. It is based on the Taylor series of r at times $t+\Delta t$ and $t-\Delta t$:

$$r(t+\Delta t) = r(t) + \frac{dr(t)}{dt}\Delta t + \frac{d^2r(t)}{dt^2}\frac{\Delta t^2}{2} + \frac{d^3r(t)}{dt^3}\frac{\Delta t^3}{6} + O(\Delta t^4) \tag{6}$$

$$r(t-\Delta t) = r(t) - \frac{dr(t)}{dt}\Delta t + \frac{d^2r(t)}{dt^2}\frac{\Delta t^2}{2} - \frac{d^3r(t)}{dt^3}\frac{\Delta t^3}{6} + O(\Delta t^4) \tag{7}$$

The summation of equations 6 and 7, solving for $r(t+\Delta t)$ yields the new position of particle i which is only dependent on the acceleration at t and particle positions at time t and the previous time step $t-\Delta t$ but not velocities.

$$r(t+\Delta t) = 2r(t) - r(t-\Delta t) + \frac{d^2r(t)}{dt^2}\Delta t^2 + O(\Delta t^4) \tag{8}$$

However, velocities are needed for the computation of the kinetic energy, which allows the determination of temperature.

$$\frac{1}{2}kT = \frac{m}{2}v^2 \tag{9}$$

Therefore, the velocities are calculated by the following formula

$$v(t) = \frac{r(t+\Delta t) - r(t-\Delta t)}{2\Delta t} \tag{10}$$

Leapfrog algorithm

A commonly used integrator is the Leapfrog algorithm which is a slight modification of the

Verlet algorithm and has been used for all simulations in this work. The particle position at time t and velocities at time $t - \frac{\Delta t}{2}$ are used to determine new positions at time $t + \Delta t$ and velocities at $t + \frac{\Delta t}{2}$.

$$r(t + \Delta t) = r(t) + v(t + \frac{\Delta t}{2})\Delta t \tag{11}$$

$$v(t + \frac{\Delta t}{2}) = v(t - \frac{\Delta t}{2}) + a(t)\Delta t \tag{12}$$

Positions and velocities are computed at alternating time steps so that velocities *leap* over the positions and vice versa. This describes the major disadvantage of this algorithm: positions and velocities are determined not at the same time. Since the potential energy is derived from the coordinates and the kinetic energy is calculated via the velocity, they cannot be calculated at the same time which complicates the calculation of the total energy. Hence, an average velocity is assigned to every position which is determined by the following equation.

$$v(t) = \frac{v(t + \Delta t/2) + v(t - \Delta t/2)}{2} \tag{13}$$

At the beginning of a simulation with $t{=}t_0$ this algorithm requires that the velocities at $t_0 - \frac{1}{2}\Delta t$ are available. If this is not the case, initial atomic velocities $v_i, i = 1..3N$ are generated from a Maxwell-Boltzmann distribution [35]:

$$p(v_i) = \sqrt{\frac{m_i}{2\pi kT}} exp\Big(- \frac{m_i v_i^2}{2kT}\Big) \tag{14}$$

where k is the Boltzmann's constant. It yields the probability $p(v_i)$ of particle i obtaining the velocity v_i at a temperature T.

Several other integrators have been developed, like the velocity Verlet algorithm that synchronizes the computation of positions, velocities and accelerations at the same level of precision [33, 36].

2.3 Statistical mechanics

In order to reproduce experimental results in simulations, the experimental conditions such as pressure, temperature and volume should be replicated. However, microscopic mechanical laws do not contain these concepts. Statistical mechanics provide methods to connect these thermodynamic quantities of a macroscopic system to its microscopic constituents. A collection of all possible systems that may have different microscopic states, but belong to the same macroscopic state are defined as an ensemble [33, 37]. Various ensembles exist that obtain different characteristics. In the microcanonical ensemble (NVE) the number of particles (N), system volume (V) and the energy of the system (E) are fixed. This does, however, not correspond to conditions that are present in laboratories, since the system must be in a closed container without any interactions (particle or energy transfer) with the environment. A more commonly used ensemble is therefore the canonical ensemble (NVT) where the temperature (T) is kept fixed instead of the energy. This is in better agreement with real experiments, because it corresponds to a system being enclosed in a box whose walls are heat conducting and impermeable to the passage of particles. The most commonly used ensemble is, however, the isobaric-isothermal (NPT) ensemble, that provides conditions very close to experiments *in vivo* as temperature and also pressure (P) can be controlled due to an adjustable system volume. The grand canonical ensemble (μVT) allows the exchange of particles with the reservoir to maintain a constant chemical potential (μ).
To control temperature and pressure in simulations several algorithms have been developed. The most conventional thermostats and barostats for temperature control and pressure control are briefly described in the following.

Berendsen thermostat
The Berendsen thermostat [38] mimics a weak coupling of the system with an external heat bath given the temperature T_0. Velocities are rescaled in order to match the following equation that slowly corrects the system temperature T.

$$\left(\frac{dT}{dt}\right)_{bath} = 2\gamma(T_0 - T) \tag{15}$$

The coupling time constant is $\tau_T = (2\gamma)^{-1}$ that can be modified by the user to vary the coupling strength. However, since the Berendsen thermostat suppresses fluctuations of the kinetic energy it does not generate a proper canonical ensemble.

Nosé-Hoover thermostat

Instead of using an exponential relaxation as in the Berendsen thermostat, the Nosé-Hoover algorithm [39,40] produces an oscillatory relaxation that takes several times longer to apply the reference temperature T_0 to the system, but it generates a proper canonical ensemble. For this reasons it is preferred to use the Berendsen thermostat for equilibration and the Nosé-Hoover thermostat for the production run. The equations of motion of the particles, given in equation (1) is extended to include a thermal reservoir and a friction term ξ which is a dynamic quantity with its own momentum p_ξ:

$$\frac{d^2 r_i}{dt^2} = \frac{F_i}{m_i} - \frac{p_\xi}{Q}\frac{dr_i}{dt} \tag{16}$$

with the equation of motion for the heat bath parameter ξ being

$$\frac{dp_\xi}{dt} = (T - T_0) \tag{17}$$

Here, the strength of the coupling is described by the so called mass-like parameter Q. This thermostat corresponds to a system that is coupled to a heat bath which can be coupled to a further heat bath and so forth which generates a chain of baths, known as Nosé-Hoover-chain.

Velocity-rescaling thermostat

This thermostat is similar to the Berendsen temperature coupling method with an additional stochastic term that produces a correct kinetic energy distribution. The velocity-rescaling algorithm [41] therefore generates a correct canonical ensemble.

Essentially, the pressure coupling works similar to the temperature coupling, since systems can theoretically be coupled to a pressure bath. The most common pressure coupling methods are the Parrinello-Rahman algorithms [42, 43] and the Berendsen barostat. The latter one works in the same spirit as the temperature coupling analog and will therefore not be described further. Several other pressure coupling approaches exist like the Martyna-Tuckerman-Tobias-Klein (MTTK) implementation [44], which will also not be discussed here.

Parrinello-Rahman barostat

The Parrinello-Rahman approach is similar to the Nosé-Hoover temperature coupling [35]:

$$\frac{db^2}{dt^2} = VW^{-1}b'^{-1}(P - P_{ref}) \tag{18}$$

Box vectors are represented by the matrix b, V corresponds to the box volume and W is a parameter that determines the strength of the pressure coupling. Analogous to the temperature coupling, P is the current, whereas P_{ref} is the reference pressure. Like the Nosé-Hoover thermostat, the Parrinello-Rahman pressure coupling needs a longer time to adjust the system pressure compared to the Berendsen barostat. Furthermore, a larger time constant is used which might result in large box oscillations that can lead to the crashing of a simulation. Therefore, this barostat is not the first choice for an equilibration-simulation.

2.4 Force field

In this work the GROMOS53a6 force field [45], extended to the CKP lipid parameters [46], was used for all simulations. A force field is in general a potential energy function that determines the potential energy of every atom, combined with an appropriate parameter set. The force field parameters of GROMOS53a6 are mainly based on the reproduction of free enthalpies of hydration and apolar solvation, since these properties are crucial for biomolecular processes such as protein folding, membrane formation and biomolecular association. The GROMOS force fields are modeling on an all atom level, however, aliphatic carbons and the associated hydrogen atoms are treated as a single atom in order to reduce the degrees of freedom, hence the computational effort.
The potential energy function can be divided into bonded and non-bonded terms; $V(R) = V_{bond}(R) + V_{nbond}(R)$ with R representing all atomic coordinates. Bonds (19), angles (20), torsion dihedral-angles (21) and improper dihedral-angles (22) are accounted in the bonded interactions, whereas non-bonded interactions incorporate the van der Waals (vdW) (23) and Coulomb interactions (24). The total energy function can hence be written as:

$$V(r) = \sum_{n=1}^{N_b} \frac{1}{4} K_{b_n} [b_n^2 - b_{0_n}^2]^2 \tag{19}$$

$$+ \sum_{n=1}^{N_\theta} \frac{1}{2} K_{\theta_n} [cos\theta_n - cos\theta_{0_n}]^2 \tag{20}$$

$$+ \sum_{n=1}^{N_\varphi} K_{\varphi_n} [1 + cos(\delta_n) cos(m_n \varphi_n)] \tag{21}$$

$$+ \sum_{n=1}^{N_\xi} \frac{1}{2} K_{\xi_n} [\xi_n - \xi_{0_n}]^2 \tag{22}$$

$$+ \sum_{pairs(i,j)} \left(\frac{C12_{ij}}{r_{ij}^{12}} - \frac{C6_{ij}}{r_{ij}^{6}} \right) \tag{23}$$

$$+ \sum_{pairs(i,j)} \frac{q_i q_j}{4\pi\varepsilon_0 \varepsilon_1} \frac{1}{r_{ij}} \tag{24}$$

where $K_{b_n}, K_{\theta_n}, K_{\varphi_n}$ and K_{ξ_n} are the bond length, bond angle, dihedral angle and improper dihedral angle force constants, respectively. Likewise, b_n, θ_n, φ_n and ξ_n are bond length, bond angle, dihedral angle and improper dihedral angle values from the current configuration, while the zero subscript represents the equilibrium values for each of those, defined in the parameters. Bond stretching and covalent bond-angle interactions are described by a harmonic potential by treating the according atoms as balls that are connected by springs, which exhibit the according force constant. The torsional dihedral-angle potential is defined by a trigonometric function. The potential energy is calculated as a sum over N_{φ_n} dihedral angles using the parameters δ_n that describes the phase shift, m_n is the multiplicity of the dihedral potential and φ_n is, as mentioned before, the value of the dihedral angle that is defined by four atoms i, j, k, l. The improper dihedral, that is also called harmonic out-of-plane interaction, is used to keep the structure of chiral centers in a certain configuration, which is especially important for conserving the peptide stereochemistry, and the planarity of aromatic rings. Van der Waals interactions are described by the repulsive and attractive forces between atoms i and j which are not directly bonded to each other, using a Lennard-Jones 12/6 interaction function based on the distance r_{ij} between i and j. Parameters $C12_{ij}$ and $C6_{ij}$ depend on the atom types that are involved in the interaction. For atom pairs that are connected via three covalent bonds, vdW parameters are defined differently. The electrostatic interaction within the cutoff distance is calculated using a Coulomb potential, where q_i and q_j are the point charges of the interacting atom pairs and r_{ij} is the distance between them. ε_0 is the dielectric permittivity of vacuum and ε_1 the relative permittivity of

the medium in which the atoms are embedded. As shown in (24), the electrostatic potential decays slowly with $1/r$. Ignoring these interactions beyond the cutoff distance would lead to artifacts in MD simulations using periodic boundary conditions [47]. A common treatment of the long-range electrostatics is achieved with the particle mesh Ewald method [48, 49] that computes the electrostatic interaction by using a lattice, considering periodic boundary conditions.

2.5 Analysis methods

If not stated otherwise in this section, standard GROMACS tools have been used for the analysis of the MD simulations performed in this work.

RMSD & RMSF

The root mean square deviation (RMSD) is the measure of the difference in structure between two superimposed structures. We have used it to show the structural difference of the sampled conformations relative to the first and last structure of a trajectory. The RMSD can be calculated using the following equation:

$$RMSD = \sqrt{\frac{1}{N}\sum_{i=1}^{N} \|r_i(t) - \tilde{r}_i\|^2} \tag{25}$$

with N pairs of equivalent atoms, with the distance $\|r_i(t) - \tilde{r}_i\|$ between them after superimposing the reference structure $\tilde{r}_i$ with the current structure $r_i(t)$. Mass weighting for superposition has been used by default.

The root mean square fluctuation (RMSF) is quite similar. Here, the deviation between positions of a particle i (e.g. atoms, residues) at time t and a given reference structure $\tilde{r}_i$ is calculated and averaged over the total simulation time T. The RMSF has been used to identify the flexibility of each atom or residue in the investigated peptides and can be calculated using the following equation:

$$RMSF = \sqrt{\frac{1}{T}\sum_{t}^{T} (r_i(t) - \tilde{r}_i)^2} \tag{26}$$

Area per lipid & bilayer thickness

We used the grid based tool g_lomepro [50] that is based on the GridMAT-MD algo-

rithm [51] to calculate both, area per lipid and bilayer thickness. Once all phosphorus atoms are divided into lower and upper leaflet, based on their z-coordinate which is along the membrane normal, they are mapped onto a grid. The membrane thickness is hence determined by considering the pair of opposite cells in the upper and lower leaflets. The area per lipid is given by the average of the areas of all the cells.

Deuterium order parameter

In general, order parameters are a measure of the (dis-)order of a system. The lipid order parameter is defined via and the orientation of the lipid chains and can be calculated in the following way [52, 53]:

$$S_{ij} = \frac{\langle 3cos\theta_i cos\theta_j - \delta_{ij} \rangle}{2} \tag{27}$$

with S_{ij} being elements of the order parameter tensor, θ_i is the angle between the bilayer normal and the molecular coordinate axes (x, y, z) and δ_{ij} denotes Kronecker delta function ($\delta_{ij} = 1$ if $i = j$; $\delta_{ij} = 0$ if $i \neq j$). The brackets indicate that the average is taken over time and molecules. The order parameter can vary between 1 ($\theta_{i,j} = 0°$), corresponding to full order along the bilayer normal and -0.5 ($\theta_{i,j} = 90°$) which implies full order perpendicular to the membrane normal [54]. The deuterium order parameters for saturated lipids can now be calculated as following:

$$S^{CD} = \frac{2}{3}S_{xx} + \frac{1}{3}S_{yy} \tag{28}$$

The molecular axes for the nth CH_2 groups are defined as:

- x: H-H vector of C_n, perpendicular to z and y
- y: bisectrix of HC_nH angle therefore in plane of C_{n-1}, C_n, C_{n+1}
- z: vector from C_{n-1} to C_{n+1}

As mentioned in the beginning, the GROMOS53a6 force field was used, which does not model aliphatic hydrogen atoms (that correspond to deuterium atoms in experiments) explicitly. Therefore the hydrogen atoms have to be reconstructed by assuming an optimal tetrahedral angle of 109.5° between two hydrogens and the corresponding carbon atom. This is considered in equation 28. This calculation has to be modified for double bonds because the carbon atoms which form the double bond (in the case of POPC and POPG these are C_9 and C_{10}) exhibit a sp^2 geometry. The molecular axes x, y, and z are now defined as [55]:

- x: perpendicular to the plane formed by C_9-H bond, C_{10}-H bond respectively and z

- y: is perpendicular to x and z
- z: along the double bond

Douliez et al. showed that the order parameters for the oleoyl chains in POPC can be calculated in the following way [55]

$$S_{9,10}^{CD} = \frac{1}{4}S_{zz} + \frac{3}{4}S_{yy} - \frac{\sqrt{3}}{2}S_{yz} \tag{29}$$

For the calculation we first used the g_order (-unsat) analysis tool. However, there is a known bug (#1166 [56]) in the code of GROMACS version 4.5.4 (and the later ones) which has not been fixed yet. The order parameters for unsaturated chains are not calculated correctly: it seems to be the case, that the axes are defined correctly, but then equation 28 is used, which implies a tetrahedral geometry and not a double bond. The order parameter for C_{10} seemed to fit well with experimental data, but values for C_9 did not match at all. This is why we decided to use a patch, provided by Chris Neale [57]. It calculates the order parameters in a different way: first, the hydrogen atoms are modeled explicitly by assuming the appropriate angle (109.5° for saturated carbons, 120° for unsaturated carbons). Second, the angle θ between the C-H bond and the membrane normal can directly be calculated. Third, a slightly altered version of equation 27 is used to calculate the order parameter:

$$S^{CD} = \frac{\langle 3cos^2\theta - 1 \rangle}{2} \tag{30}$$

The first and terminal carbon atoms are not included in the GROMACS output, because C_1 is in a carbonyl group therefore it is not bound to a hydrogen atom and C_{16} and C_{18} from the two acyl chains are each bound to three hydrogens. This is why the numbering starts with C_2 and ends with C_{15} and C_{17}, respectively.

Hydrogen bonds

The determination of hydrogen bonds was performed by using the standard GROMACS tool g_hbond. By default, OH and NH groups are regarded as donors, whereas O and N are acceptors. If the donor-acceptor distance is within a cutoff radius of 0.35 nm and the donor-H-acceptor angle is less than 35° it counts as a hydrogen bond.

Peptide lateral diffusion coefficient

GROMACS provides a tool (g_msd) for calculating diffusion coefficients D by fitting the mean square displacement: $MSD = \langle (r(t) - r_0)^2 \rangle = 4Dt$, where $r(t)$ is the current positions

and r_0 the initial position of the peptide. Basic requirement is, however, a linear MSD over time which we did not observe in all simulations. Furthermore, we wanted to determine the diffusion of the peptide in relation to the leaflet it is adsorbed to. Therefore, we have chosen a slightly different approach.
After centering the upper leaflet (in the single-peptide simulations all peptides adsorbed to this leaflet and not the lower one), the position of the center of mass (COM) of the peptide was calculated in x- and y-direction. The lateral diffusion coefficient $D_{\Delta t}$ for every step $\Delta t = 20$ ps is calculated using the following relation:

$$D_{\Delta t} = \frac{\Delta x^2 + \Delta y^2}{4\Delta t} \tag{31}$$

where $\Delta x = r_x(t + \Delta t) - r_x(t)$ is the deviation between the positions in x-direction for two consecutive time steps and Δy is calculated accordingly. The diffusion coefficient D is then calculated by averaging $D_{\Delta t}$ over the last 150 ns, hence, after adsorption of all peptides.

2.6 Parametrization of CF_3-Bpg

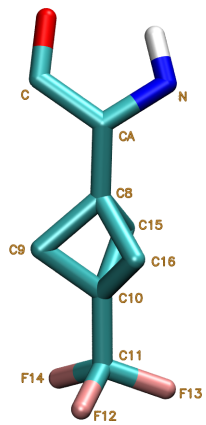

Figure 4: L-CF_3-Bpg

Parameters for L- and D-CF_3-Bpg were derived from the Automated Topology Builder (ATB) [58]. The user is required to provide the overall molecule charge and a PDB file containing three-dimensional coordinates and connectivity data. These input data define the stereochemistry, protonation and tautomeric state of the molecule, which yields a unique description. After the generation of an initial template a geometry optimization using QM calculations at the AM1 level were performed and further optimized at B3LYP/6-31G* level in implicit solvent. From the optimized structure several information can be extracted, such as the bond lengths, bond angles, dihedral angles and the geometry of chiral centers. Furthermore, aromatic rings and planar groups are identified, based on dihedral and improper dihedral angles. These information, along with the connectivity, allow the assignment of atom types. The atomic charges are generated by fitting the electrostatic potential using the Kollman-Singh method [59], considering the symmetry of the molecule. In order to estimate force constants the Hessian matrix is calculated. Since we use the GROMOS53a6 force field, the all-atom topology, which is used for QM calculations, is finally converted into a united-atom topology. The atomic charges

were slightly edited to conserve the backbone charges of isoleucine which has been replaced by the CF_3-Bpg group on position 8 in $[KIGAKI]_3$ while the overall residue-charge of zero is maintained. Finally, the *L*- and *D*-CF_3-Bpg "residues" were added in the "aminoacids.rtp" file.

3 Simulation Details

The GROMACS package [60] was used to build the systems and perform the simulations. Starting conformations correspond to the main conformations of $[KIGAKI]_3$ in water obtained from a 100 ns simulation, which was initiated from an elongated peptide structure [31]. The GROMOS53a6 force field, which is parametrized to reproduce experimental solvation enthalpies for small molecules, was employed to carry out all simulations runs. It was extended to CKP lipid parameters for POPC, POPG-D and POPG-L [46], which are provided in the lipidbook [61].

3.1 Simulation setup of bilayer systems

The Packmol package [62] was used to build the POPC/POPG (4:1) bilayer patch, which was then equilibrated for 200 ns as described in [31].
Initial coordinates of a pure POPC bilayer consisting of 128 lipids, equilibrated with water for 200 ns, were obtained from the work of Piggot et al. on lipid bilayers [46]. For further analysis, this bilayer model was simulated for 10 ns with 3552 SPC water molecules with a box size of $6.2 \times 6.3 \times 6.8$ nm^3. Semi-isotropic Parrinello-Rahman pressure coupling was used along with a Nosé-Hoover thermostat, which provided a constant temperature of 303 K and pressure of 1 atm.

All peptide/membrane systems were solvated using the simple point-charge (SPC) water model to fill the simulation box. Depending on the system, Na^+ or Cl^- ions were used as counter ions to neutralize the systems. The box size for simulations with one peptide on the mixed membrane was set to $6.1 \times 6.1 \times 9.2$ nm^3, while the box size for the according simulations with the neutral membrane was $6.2 \times 6.3 \times 10.0$ nm^3. We increased the size in z-direction slightly to avoid interactions of the peptide with the periodic image of the membrane. This was necessary as the peptides are not as strongly attracted by the neutral membrane as by the charged one. It might be possible for them to unfold and interact with both sides of the membrane when using periodic boundary conditions with a too small box. The box length in z-direction was increased to 16 nm for the simulations with six peptides. Prior to the production MD simulations, 100 ps equilibration in the canonical ensemble (NVT) were performed during which all phosphorus atoms of the lipids in z-direction and all peptide heavy atoms were restrained. The velocity rescaling thermostat with a coupling constant of 0.1 ps was used to regulate the temperature of peptides, lipids and solvent/ions

separately at 303 K to guarantee a fluid membrane. For the subsequent NPT equilibration, we switched to a Nosé-Hoover thermostat with a time constant of 0.5 ps along with a Parrinello-Rahman barostat. Semi-isotropic coupling is employed to allow a separate coupling of the bilayer normal in z-direction and xy-plane with a time constant of 5.0 ps, maintaining a constant pressure of 1 atm. An isothermal compressibility of 4.5×10^5 bar^{-1} was applied in all box dimensions. Force constants restraining the peptides' heavy atoms and lipid phosphorus atoms were reduced from 100,000 kJ mol^{-1} and 10,000 kJ mol^{-1} for simulations containing one and six peptides, respectively to 1000 kJ mol^{-1} during this 6 ns equilibration under isothermal-isobaric conditions. The Particle mesh Ewald method with periodic boundary conditions was used to calculate long-range electrostatics. For short range Coulombic and vdW interactions cutoff was set to 1.2 nm. The LINCS algorithm was used to constrain all bond lengths. For the MD simulations all restrains were removed and the time constant for pressure coupling was set to 2.0 ps. Simulations with unlabeled [KIGAKI]$_3$ peptides were performed for 1 μs whereas the other four simulations with CF_3 labeled peptides were carried out for 500 ns. The integration time step was 2 fs, with coordinates and velocities saved every 20 ps.

3.2 Simulation setup of [KIGAKI]$_3$ with CF_3 label in water

The parameters for the L-CF_3-Bpg and D-CF_3-Bpg label for the GROMOS53a6 force field were obtained by the Automated Force Field Topology Builder (ATB) [58] as described previously. Using VMD, the label was attached to the [KIGAKI]$_3$ peptide. By doing so, the hydrophobic side chain of Ile-8 was removed and the CF_3-Bpg group was attached in the according stereoisomeric geometry. The new residue was declared as LCF3 and DCF3, respectively.

Each labeled peptide was located in the middle of a dodecahedron box and solvated with SPC water molecules. After neutralizing the systems by adding 7 Cl^- counter ions, a 50 ps equilibration in an NVT ensemble was performed. The velocity rescaling thermostat was applied to obtain a temperature of 300 K with a time constant of 0.1 ps. The Parrinello-Rahman barostat was used to regulate the pressure at 1 atm in the following 100 ps NPT equilibration with a time constant of 2.0 ps. To calculate long-range electrostatics, the Particle mesh Ewald method was used with periodic boundary conditions. The Coulombic and vdW cutoffs were set to 1 nm. A production run of 100 ns was carried out using the LINCS algorithm to constrain all bond length and a time step of 2 fs. Coordinates and velocities were saved every 2 ps.

4 Results and Discussion of [KIGAKI]$_3$ simulations

In this section, all simulations without a CF_3 label are analyzed and discussed. The three different starting structures are labeled as cluster1, cluster2 and cluster3. For the 1 μs simulation of six peptides only cluster1 was used as starting structure. In order to distinguish between the different peptides they are denoted as peptides1 to peptide6.

4.1 Adsorption of [KIGAKI]$_3$ on membrane surfaces

It was shown experimentally, that [KIGAKI]$_3$ adsorbs on charged as well as on neutral membrane models [22]. While partly charged POPC/POPG membranes are perturbed, POPC bilayers do not show any effects upon adsorption of [KIGAKI]$_3$, which indicates the selectivity of the peptide due to different peptide-membrane interactions [63].
In this section, the adsorption process of [KIGAKI]$_3$ is described, including the speed of adsorption on different bilayers and the analysis of key interacting residues.

In Figure 5 the distance between each peptide and the corresponding bilayer surface is illustrated.

Starting with one-peptide simulations in Figure 5(a) and (b), we can state that all different starting structures adsorb on the membrane surface within the simulation length. Within 30 ns all peptides are closer than 1 nm to the POPC/POPG bilayer surface. During the simulation they move closer towards the membrane surface. After 200 ns the COM of each peptide is only about 0.5 nm away from the average z-coordinate of the phosphorus atoms, indicating adsorption.
The peptides on the POPC membrane take longer to adsorb. After 30 ns of simulation, the peptides are closer than 1.5 nm to the membrane surface. It takes another 120 ns for the peptides to get closer than 1.0 nm. This different adsorption speed can be explained by the presence of the electrostatic interactions between peptides and membrane. [KIGAKI]$_3$ carries 7 positive charges at the six lysine residues and the N-terminus. The POPC/POPG membrane possesses 13 negative charges on every leaflet. Therefore, [KIGAKI]$_3$ is more attracted by the charged membrane than the neutral bilayer which consists of zwitterionic lipids. For the multi-peptide simulations, Figure 5(c) shows that all six peptides are adsorbed on the POPC/POPG membrane surface within the first 100 ns of the simulation. Over the last 750 ns the COM distance between peptides and leaflet is never larger than

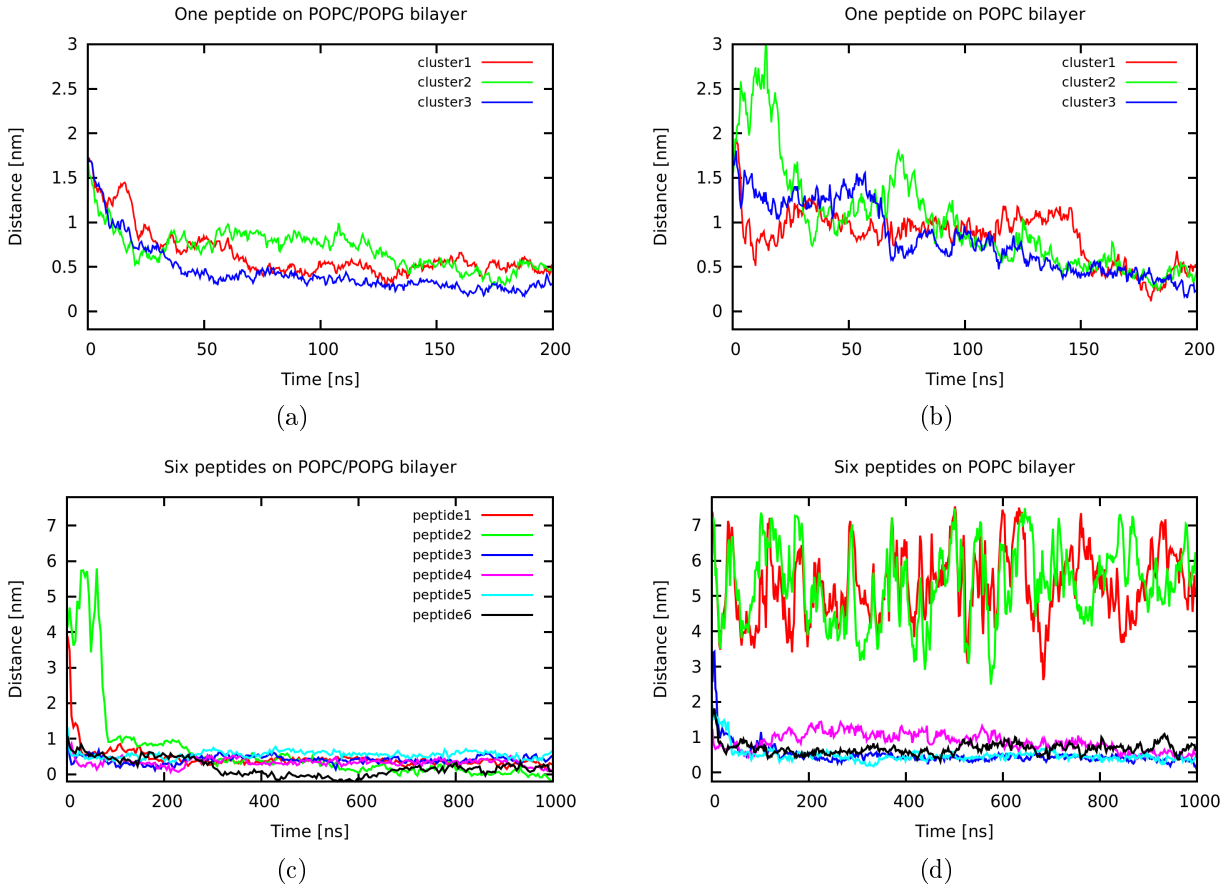

Figure 5: The distance in z-direction between the COM of [KIGAKI]$_3$ and the COM of the phosphorus atoms of the leaflet, which is closest to the peptide in question, is shown. The distances are shown as a function of time, with time averages calculated for every 0.5 ns (single-peptide simulations) and 2 ns (six-peptide simulations) in order to avoid high fluctuations. The results for the single-peptide simulations are plotted in (a) and (b), for the simulations with six peptides in (c) and (d).

1.0 nm. On the zwitterionic POPC membrane the peptides behave differently; only four of the six peptides get adsorbed on the bilayer surface, two on each leaflet. During the simulation the adsorbing peptides move towards the membrane surface, yet it takes them longer to get within 1.0 nm from the membrane compared to POPC/POPG. We can therefore state, that in our simulations 33% less [KIGAKI]$_3$ peptides adsorb on the zwitterionic POPC membrane than on the partly charged membrane. This trend has also been reported by Wadhwani et al. [24], where [KIGAKI]$_3$ peptides were reported to remain in the water phase if not enough negative charges on the membrane are present to compensate the negative charges on the peptides. The presence of 7 positive charges leads to repulsion between the peptides. A partly charged POPC/POPG bilayer is therefore better at compensating

the positive charges than a neutral one. Another clear difference is the adsorption speed. $[KIGAKI]_3$ peptides get faster and more deeply adsorbed on the charged membrane. To illustrate this process the key interacting residues were identified by calculating the distance between each residue and the membrane surface.

Figure 6(a) shows that residues K_1, K_7 and K_{13} of cluster1 are embedded within the charged membrane, whereas the residues from I_{14} to the C-terminus are further away from the membrane surface. Cluster2 exhibits more conformational changes over time. In the first half of the simulation, the C-terminus is circa 2 nm away from the surface, but then adsorbs on the surface after around 120 ns. I_2 points further away from the upper leaflet at the beginning of the simulation but then undergoes a conformational change to point inside the membrane surface after 70 ns. However, this insertion is not stable and only lasts for around 100 ns. At the end of the 200 ns simulation the termini as well as K_{11} are closest to the surface. Cluster3 shows a deep and stable insertion of the C-terminus in the headgroup region of the POPC/POPG bilayer. At the N-terminus, alternate residues (K_1, G_3, K_5 and K_7) point inside the headgroup region. I_{12} and adjacent residues exhibit the largest distance to the surface throughout the simulation.
At first glance, a different adsorption pattern of the three starting structures is observed on a POPC membrane. Cluster1 shows a deep insertion of both termini. After 150 ns a structural change can be observed for residues K_7 to G_{15}. Initially being further away, this region is adsorbed on the membrane surface for the rest of the simulation. The termini of cluster2 initially interact with the membrane surface but then get desorbed, followed by a stable and deep insertion of K_{11}. Towards the end, the termini get readsorbed. At the beginning, cluster3 adsorbs with K_{11}, which gets more deeply inserted during the simulation. Again, the termini as well as G_3, K_7, I_{12} and A_{16} are close to the bilayer surface at the end of the 200 ns of simulation.
The comparison of Figures 6 and 7 show that it takes longer for $[KIGAKI]_3$ to adsorb on POPC bilayer surfaces. For cluster1 and cluster3 on the mixed bilayer one can see that predominantly lysine residues and the N-terminus, which carries two positive charges, point towards the membrane. The same pattern can be observed in the simulations with six peptides (s. Appendix 7.3) showing an average insertion depth of 0.39 nm for lysine and 0.46 nm for the other residues. Also the N-terminus exhibits a clear preference to insert into the headgroup region of the bilayer, having an average insertion depth of 0.08 nm.

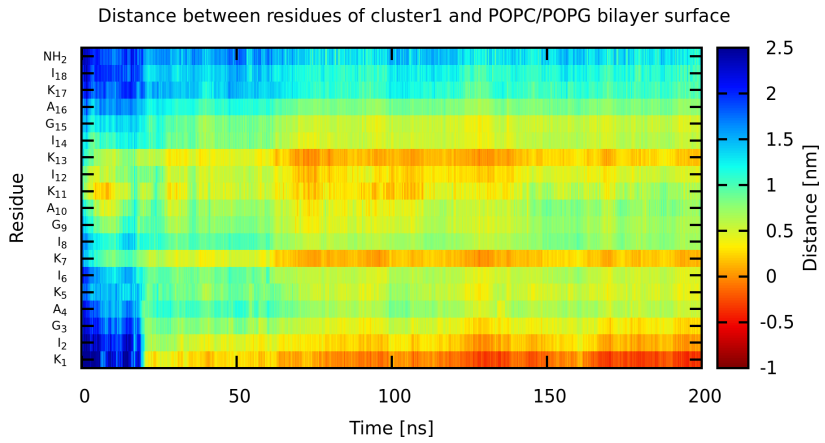

(a)

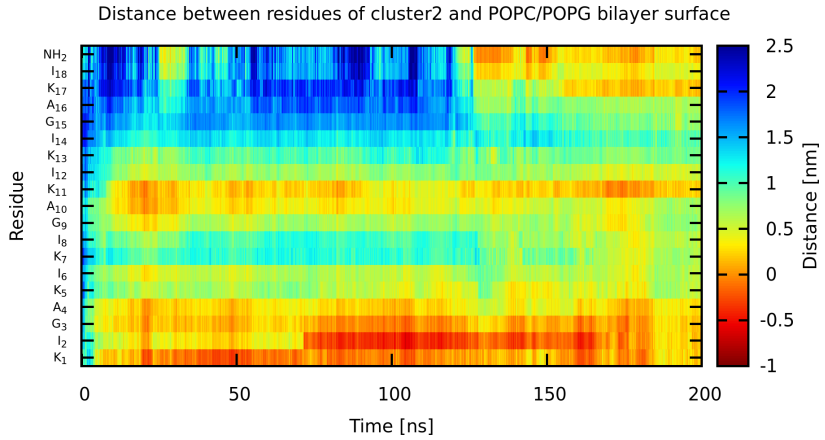

(b)

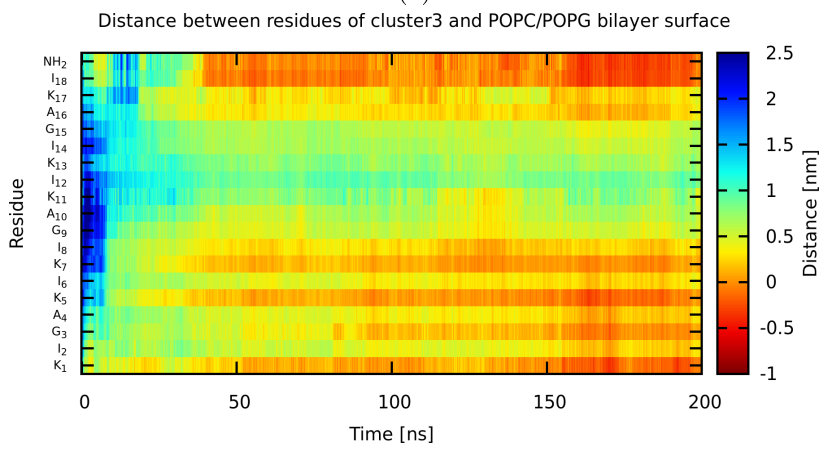

(c)

Figure 6: The distance between each residue of cluster1 (a), cluster2 (b) and cluster3 (c) and the POPC/POPG membrane surface is illustrated here. Amino acids are written in the 1-letter code, the reside index is shown as the subscript. In addition, the amide group at the C-terminus is shown as well. Time is shown on the x-axis, residues on the y-axis and the distance is represented by a color code. The color-bar next to every subfigure shows that blue implies a small distance in z-direction between the COM of the residue and COM of the phosphorus atoms, whereas red color indicates that the residue in question is inserted into the membrane, giving rise to negative distance values.

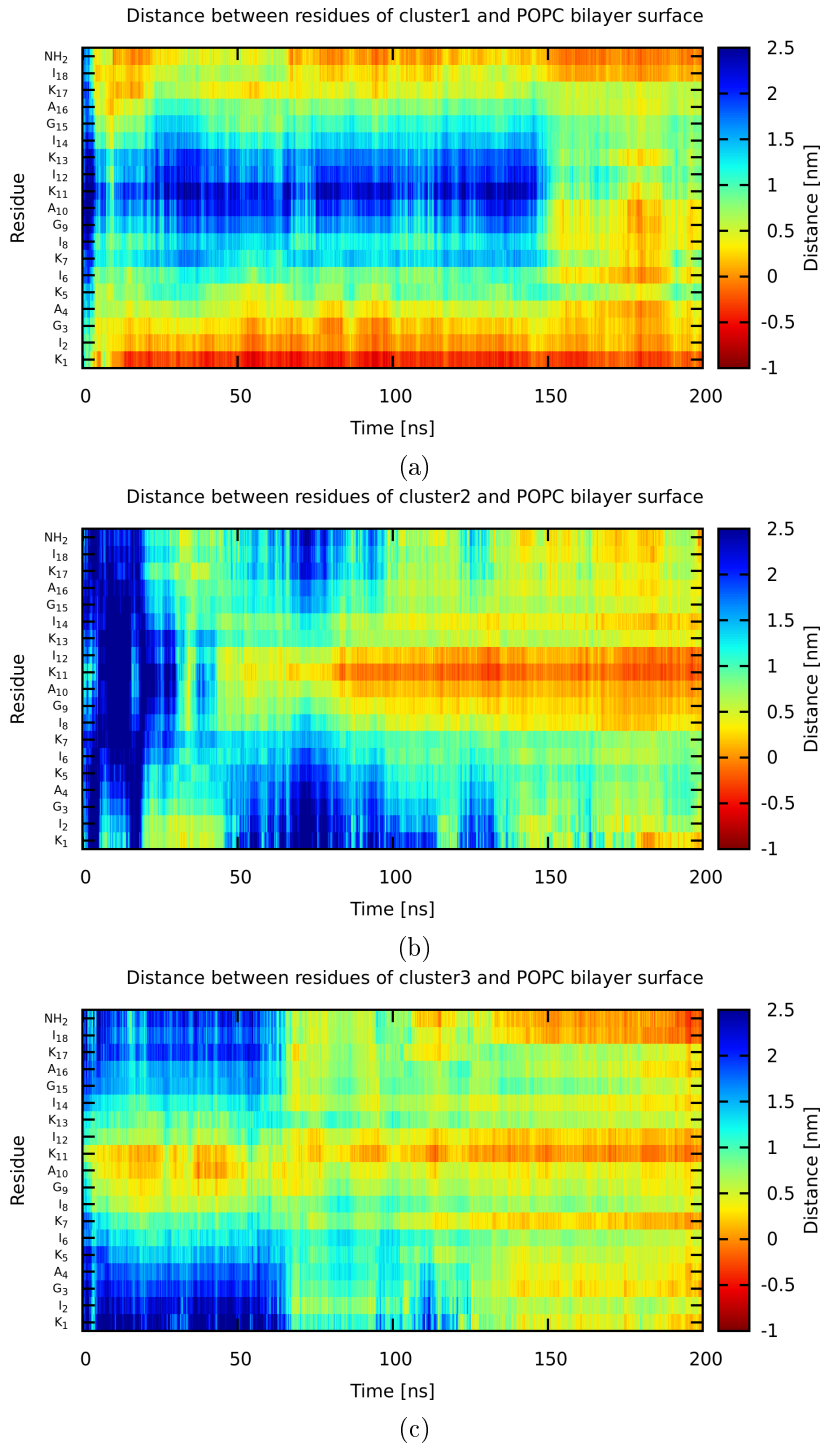

Figure 7: The distance between each residue of cluster1 (a), cluster2 (b) and cluster3 (c) and the POPC membrane surface is illustrated here. A description of the axes and color code is given in the caption of Figure 6.

In the POPC simulations lysine residues occasionally insert deeper into the membrane than other residues, but the average insertion depths for all residue types are between 0.62 nm and 0.64 nm which does not show a clear preference for any residue type to inserting deeply into the membrane. However, the N-terminus exhibits an average distance of only 0.17 nm from the bilayer surface showing the same pattern as in the charged membrane simulation. In contrast to the peptides on the charged membrane, the C-terminus is also relatively close to the bilayer, with a distance of 0.44 nm. The average insertion over all residues is 0.62 nm which is 38% higher than for the charged membrane system.

Initially, we expected isoleucine residues to point inside the membrane since they would prefer to be in a hydrophobic environment and polar lysine residues to snorkel up to the water. However, in the simulations it is mainly the other way around: lysine inserts into the headgroup region, while isoleucine often points away from the membrane into the water phase as shown in Figure 8. This indicates strong interactions between the positively charged lysine and the negatively charged and also the zwitterionic headgroups. In NMR experiments carried out by Wadhwani et al. [23] it was shown that the Cα-Cβ bond of the CF_3-Bpg label, which replaced an isoleucine residue in four of the five cases, is parallel to the membrane normal in [KIGAKI]$_3$ fibrils. This leaves both options open, CF_3-Bpg pointing in- or outwards. So far, the simulation results suggest that it is the lysine that interacts with the headgroup region and therefore points inside the membrane. However, it cannot be excluded that the peptides flip at some point or that the fibril structure shows a totally different behavior than [KIGAKI]$_3$ in the monomeric form.

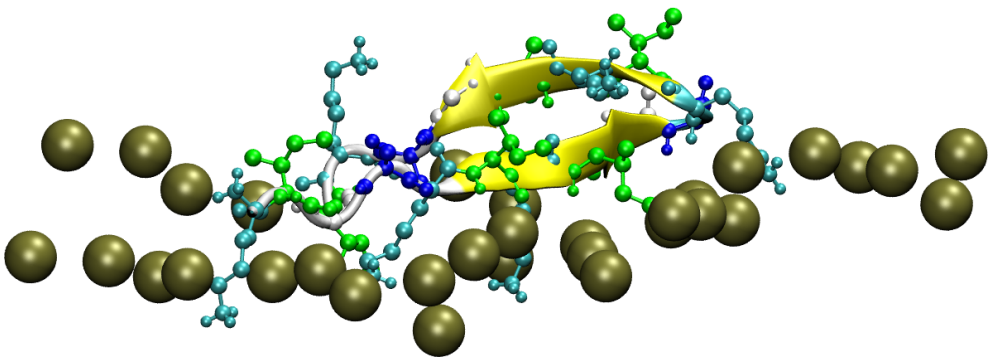

Figure 8: Last frame of cluster3 on the POPC/POPG bilayer is shown. Lysine residues are illustrated in cyan, isoleucine in green, alanine in blue and glycine in white. The tan spheres show the vdW representation of the phosphorus atoms of the lipids within 1.2 nm of the peptide. This figure shows that K_1, K_5 and K_7 enter the headgroup region of the membrane while hydrophobic isoleucine residues point into the water phase.

4.2 Peptide structures and structural changes on membranes

It has been reported by Meier and Seelig [27] that [KIGAKI]$_3$ in buffer (50 μM peptide concentration in 2.5 mM cacodylate at pH 7.4) mainly adopts a random coil structure with around 23% β-structure. However, when bound to a bilayer consisting of 50% negatively charged lipids, the predominantly coil conformation is converted into a stable β-sheet conformation, containing 98% β-structure. This β-sheet $\rightleftharpoons$ coil transition on other bilayers was also observed [22, 24, 25]. In addition, M. Meier et al. and P. Wadhwani et al. [23] report in their work that [KIGAKI]$_3$ peptides aggregate on bilayer surfaces.
In this section, we show the structural changes of the peptide during adsorption by presenting the RMSD values and the secondary structure of the peptides and the aggregation process during the simulations.

4.2.1 RMSD

The RMSD was calculated to compare all structures obtained in the trajectory to the starting and to the final structure of the 200 ns simulations. This analysis was only done for the simulations with one peptide.

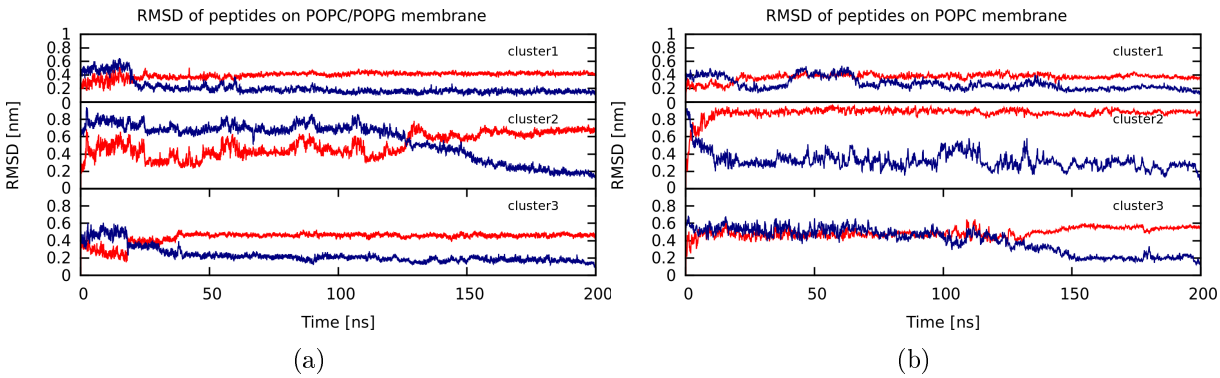

Figure 9: RMSD values of the three starting structures on the POPC/POPG bilayer (a) and the pure POPC bilayer (b). The RMSD is calculated with respect to the starting structure (red) and to the last structure (blue).

In Figure 9(a) the RMSD of all peptides on the POPC/POPG membrane is illustrated. Cluster1 and cluster3 show a structural change after around 20 ns when they adsorb on the bilayer surface (s. Figure 5). The conformation which is adopted after this rearrangement is already very similar to the final structure after 200 ns of simulation, explaining the low RMSD value with respect to the last structure. Cluster2, in contrast, exhibits a high RMSD

during the whole simulation, which suggest a high flexibility of the peptide. After 120 ns when adsorption takes place, the structures become more similar to the last structure than to the starting structure. Figure 9(b) presents the RMSD of the peptides on the zwitterionic membrane. Again, cluster1 exhibits low RMSD values with an average value of 0.27 nm with respect to the last structure. After 20 ns, a structural change can be observed when the peptide adsorbs on the bilayer surface. Between 20 ns and 60 ns the peptide moves slightly further away from the surface (s. Figure 5), which can explain the higher RMSD values during this period. Cluster2 shows a structural change at the very beginning of the simulation when it moves further away from the membrane surface. The peptide gets adsorbed after around 40 ns at the terminal residues. During the simulation, the average value with respect to the last structure is 0.32 nm, whereas the RMSD relating to the first structure is 0.88 nm, which shows a large change in structure. The RMSD values with respect to the first and last structure are similar during the first 110 ns of the simulation of cluster3. After 150 ns a conformational change happens so that the structure becomes more similar to the final structure, as the corresponding RMSD is around 0.2 nm.

4.2.2 Secondary structure

Using DSSP the secondary structure of [KIGAKI]$_3$ on the different bilayer models was determined as illustrated in Figure 10 for the single [KIGAKI]$_3$ simulations. For the six-peptide simulations, the DSSP Figures are given in Appendix 7.4.

After 20 ns on the mixed membrane surface (Figure 10(a)) cluster1 adopts a stable β-sheet between residues 5-8 and 14-17 with bends at residues 4-5 and 10-12. Cluster2 adopts a β-bridge between residues 8 and 13 and bends at residues 7 and 9-13, which mainly dissolve after 115 ns and leave a mostly unstructured peptide behind. For cluster3 a stable β-sheet was sampled between residues 6-8 and 13-15. In the first 40 ns a bend is observed at residues 9-12, which mainly converts into a turn at residues 10 and 11 leading to a β-sheet extension to residues 9 and 12 and thus, retaining a β-hairpin structure like cluster1. The secondary structure of cluster1 on the neutral POPC bilayer differs little from the one which is formed on the charged membrane. An extension of the bend at residues 10-12 to residue 9 is occasionally observed and a missing turn at residues 4-5. In the first 10 ns cluster2 adopts a β-bridge between residues 8 and 13, which was also observed in the POPC/POPG simulation. This β-bridge converts into a stable β-sheet between residues 5-8 and 14-17 leading to the formation of a β-hairpin structure, that is similar to the structure

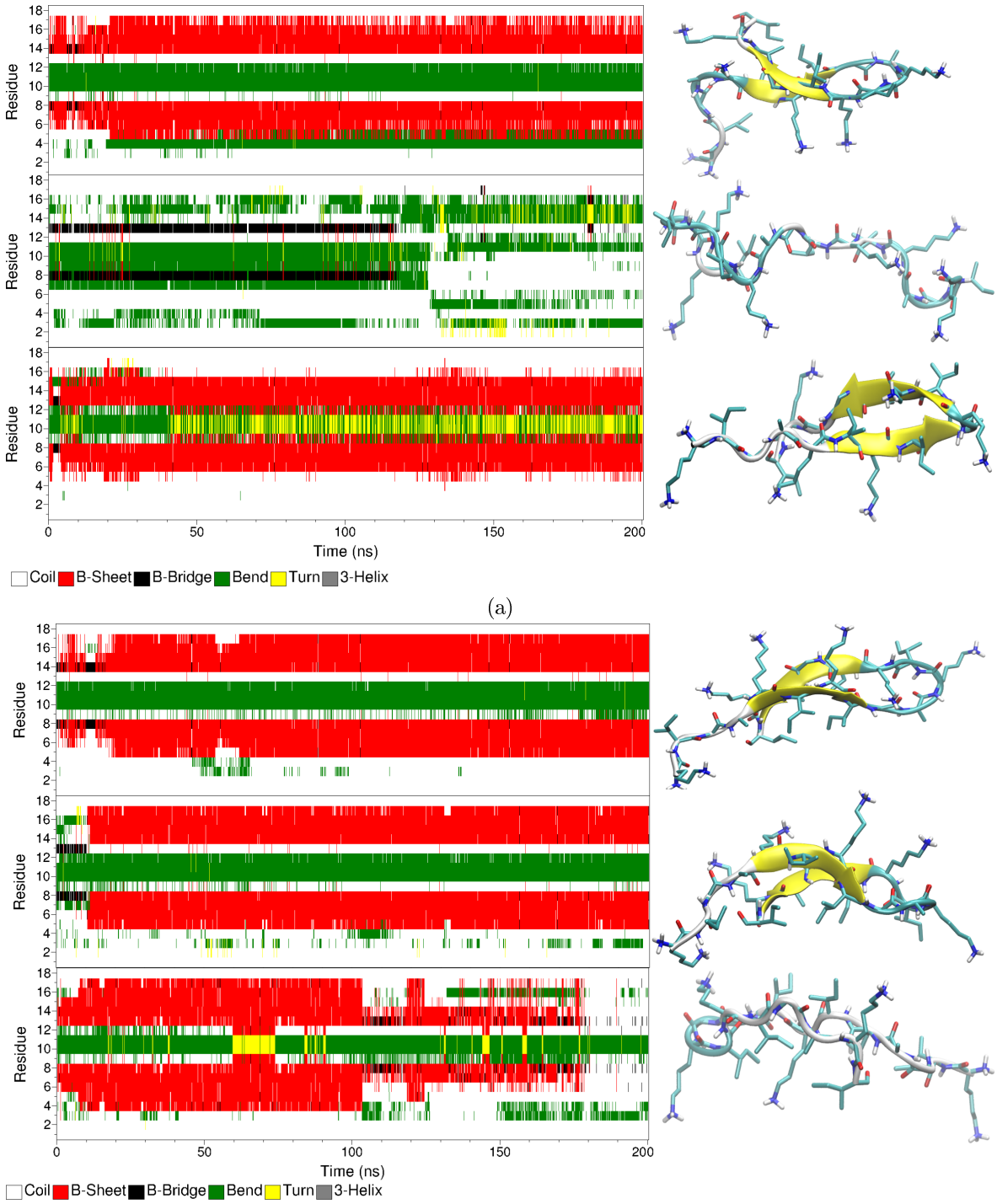

Figure 10: Secondary structure of single [KIGAKI]$_3$ peptides on a POPC/POPG bilayer (a) and on a POPC bilayer (b). On the right, the corresponding final snapshot of the peptides is shown with the membrane normal (z-coordinate) being parallel to the long margin. Lysine residues are illustrated in cyan, isoleucine in green, alanine in blue and glycine in white.

of cluster1. A bend is sampled at residues 10-12 and increasingly at residue 3 at the end of the simulation. Cluster3 adopts a relatively long β-sheet between residues 4-8 and 13-17 in the first half of the simulation. Between 60 ns and 73 ns the β-sheet is extended to residues 9 and 12 under conversion of the bend at residues 10 and 11 into a turn. After 100 ns the β-sheet dissolves which leads to a mostly unstructured peptide. Only the bend at residues 10 and 11 remains stable during the whole simulation. In all simulations the termini exhibit coil structure.

In the simulation of six peptides on the partly charged membrane (s. Appendix 7.4) peptide1 and peptide2 resemble the cluster1 structure on the charged membrane whereas peptide4 resembles the cluster2 structure on a neutral membrane. Peptide3 and peptide4 adopt a relatively weak β-sheet and peptide6 is mostly unstructured.

On the POPC membrane all peptides adopt a stable β-sheet between residues 5-8 and 14-17 with a bend in between, regardless of whether the peptide is adsorbed or not. In all cases, only intramolecular β-sheets are formed which again points out that there is no aggregation during the two 1 μs simulations. At a first glance, it is obvious that the β-sheet content must be higher in the POPC simulation which is further demonstrated in Figure 11.

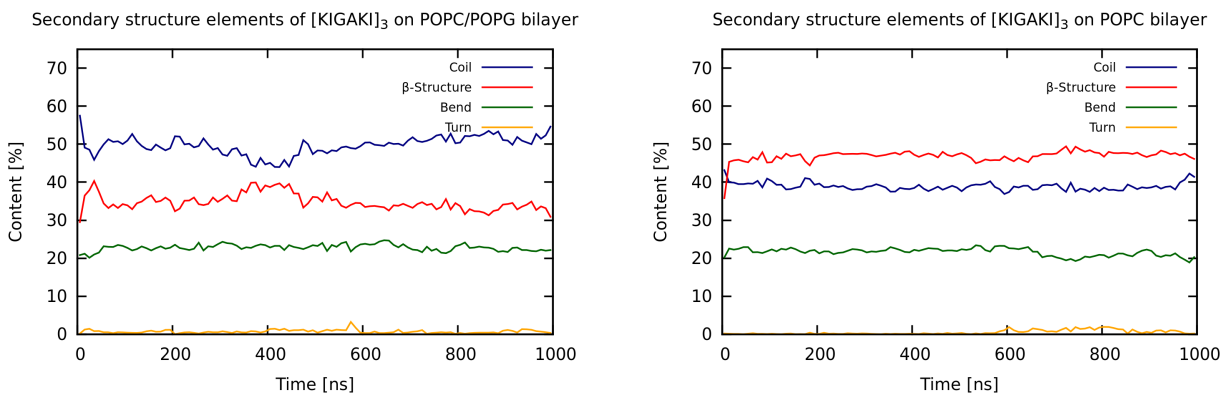

(a) (b)

Figure 11: Secondary structure content of the six-peptide simulations on (a) the POPC/POPG and (b) the pure POPC bilayer. β-Structure contains β-sheet and β-bridge. The plotted values are averages over 10 ns windows.

In both simulations there is a very low turn content and the average bend content has a value of around 22%. However, the β-structure and coil content differ significantly. In the POPC/POPC simulation a fluctuation of the β-structure content can be observed during the first 500 ns, which stays constantly around 34% during the last 500 ns. The coil content proceeds in the opposite way: when the β-content increases, the coil content decreases. During the last 500 ns the coil content stays constantly around 51%. On the POPC bilayer,

the β-sheet content is larger than the coil content with a constant value of around 47% whereas the coil is only sampled for 39% of the residues.

In brief, [KIGAKI]$_3$ peptides tend to adopt a β-hairpin conformation on both the POPC/POPG and POPC bilayer. However, this structure is more stable on POPC, while the peptide structure gets perturbed by the partly charged POPC/POPG membrane. This suggests more interactions between peptides and the charged membrane.
As mentioned, it has been reported that around 23% of peptide residues in solution adopt β-structure [27]. In a previous work [31], a 100 ns simulation of [KIGAKI]$_3$ in water has been performed, which yielded a β-content of 21%, averaged over the last 60 ns of the simulation using the same force field and parameters as in this work. This result shows that the experimental and MD obtained β-content is similar, which indicates that the simulation of [KIGAKI]$_3$ under these conditions gives realistic results. However, this cannot be used as a validation since the significance of such a single short simulation is not high. For [KIGAKI]$_3$ peptides with excess of partly negatively charged lipids (50% POPG), a β-content of 98% has been experimentally reported. This high value suggests that the peptides most likely aggregate in an elongated conformation without a bend or turn. Since a turn or bend in the [KIGAKI]$_3$ peptide consists of at least two residues (s. Figure 10 and Appendix 7.4), the β-content would be much lower than 98% if one of these elements was present. In our simulations, however, we do not obtain a β-content higher than 49%. Thus, we assume that the peptides first must unfold to a certain extent to be able to form intermolecular hydrogen bonds. Furthermore, it is likely that the aggregates consist of elongated structures, as stated before, so that the peptides have to unfold before or while aggregating. In the two simulations with six peptides, the initial structure was cluster1 that contains a β-sheet between residues 6-8 and 13-15. On the POPC/POPG bilayer an unfolding process can be observed for cluster2 in the one-peptide simulation and peptide6 in the six-peptide run. Also peptide3 and peptide4 show a decreased amount of ordered states. On the neutral POPC membrane all peptides adopt a stable β-hairpin structure. This shows that a partly charged POPC/POPG membrane is more likely to induce [KIGAKI]$_3$ unfolding than a neutral POPC membrane.

4.3 Correlation between secondary structure and adsorption

In order to see whether or not the insertion depth correlates to the secondary structure, we calculated the distance between the COM of each residue in the six-peptide simulation and the COM of the phosphorus atoms and determined the the secondary structure propensity

of each residue [64]. The results are shown in Table 7 and Tables 8 in Appendix 7.5. On the POPC/POPG bilayer, β-sheet-forming residues exhibit an average distance of 0.56 nm whereas bend-forming residues (0.28 nm) and coil-forming residues (0.37 nm) are closer to the membrane surface, indicating more interactions with the bilayer headgroup region. On the pure POPC membrane, β-sheet-forming residues have a distance of 0.68 nm, whereas the other residues are on average only 0.54 nm away from the bilayer surface. The pattern on the different membrane systems is the same, but the extent differs. In the POPC/POPG system, β-sheet-forming residues exhibit a 64% larger distance from the bilayer surface than non-β-sheet-forming residues. In the POPC system the distance is only 26% higher for β-sheet-forming residues. This finding shows that on both membranes the β-hairpin of [KIGAKI]$_3$ rather adsorbs than inserts into the membrane. The N-terminus anchors the peptide to the membrane in both cases. And in case of POPC/POPG the bend residues A_{10} and K_{11} also insert more deeply into the membrane compared to the other residues.

4.4 Motion of [KIGAKI]$_3$ on bilayer surfaces

4.4.1 Peptide Diffusion

In order to measure the mobility of [KIGAKI]$_3$ peptides on the POPC/POPG and the neutral POPC bilayer, the diffusion coefficients were calculated.

System		Diffusion coefficient [10^{-7}cm^2/s]
POPC/POPG	cluster1	1.87
	cluster2	2.04
	cluster3	1.40
POPC	cluster1	4.14
	cluster2	4.05
	cluster3	2.95

Table 1: Peptide lateral diffusion coefficients of the [KIGAKI]$_3$ peptides on the different bilayers. The diffusion coefficient has been calculated over the last 150 ns of simulations, hence after adsorption of the peptides.

For low peptide/lipid concentrations it has been reported that [KIGAKI]$_3$ is freely mobile on the bilayer surface [23]. In Table 1 the lateral diffusion is presented for the two bilayer types. Only one-peptide simulations were taken into consideration for this purpose to eliminate any peptide-peptide interactions which could influence the diffusion. Cluster1 and cluster3 show relatively small diffusion coefficients, whereas cluster2 shows the largest motion on this bilayer. The lateral motion of [KIGAKI]$_3$ on the zwitterionic POPC membrane is on average more than twice as large compared to POPC/POPG. Cluster3 moves least in the xy-plane than the two other peptides. It is noticeable, that on the charged membrane β-hairpin structures exhibit the lowest mobility, whereas on the POPC membrane the coil structure shows least motion. These findings correspond also to the number of adsorbed amino acids, which are illustrated in Figures 6 and 7.

4.4.2 Flexibility of peptide residues

In order to make a statement about the flexibility of each residue, the RMSF has been calculated.

On the charged membrane, cluster1 and cluster3 exhibit almost the same pattern: a rigid N-terminus, a minor RMSF increase for residues I_8 and K_{11} and a flexible C-terminus. Cluster2, however, is more flexible. The average RMSF is 0.35 nm, which is about 3 times higher than the RMSF of cluster1 and cluster3. Relatively little flexibility is observed for residues G_3, K_{11} and A_{16}, whereas the termini, K_5, K_7, I_{14} and K_{17} show high RMSF values. On the POPC membrane all peptides exhibit a higher flexibility, but again cluster2 shows the highest RMSF for all residues. An almost alternating pattern for cluster2 is observed: high flexibility at residues K_5, K_7, A_{10} and K_{13}, whereas residues I_6, I_8, G_9, K_{11} and K_{12} are relatively rigid. In contrast to the charged membrane system, cluster1 shows structural flexibility at the N-terminus and less flexibility at the C-terminus. Peaks are observed at residues K_5 and K_{11}. Cluster3 exhibits flexible termini and shows a relatively high RMSF, mainly at lysine residues. Summing up, the main findings are flexible lysine residues and a higher structural flexibility of [KIGAKI]$_3$ on the zwitterionic POPC membrane than on the charged POPC/POPG bilayer. Only cluster2, which is in an unstructured state, exhibits high RMSF values on the charged membrane as well.

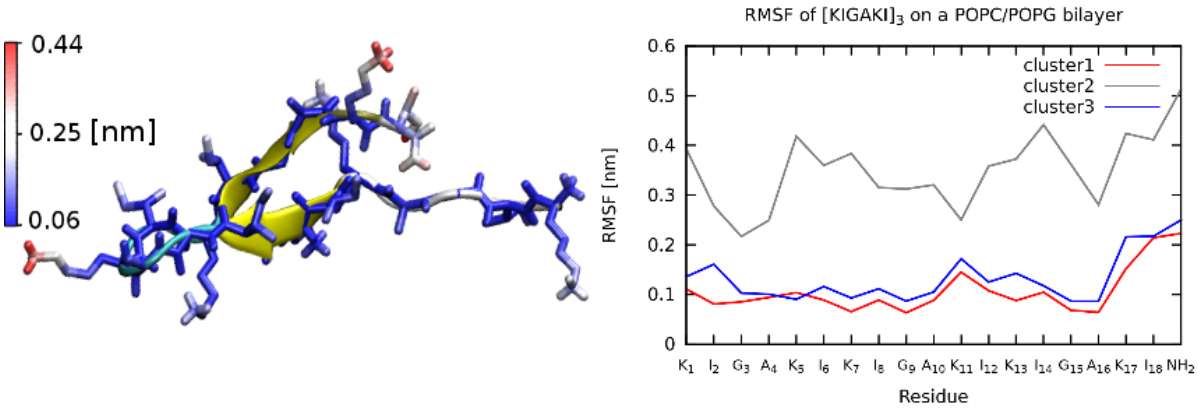

(a)

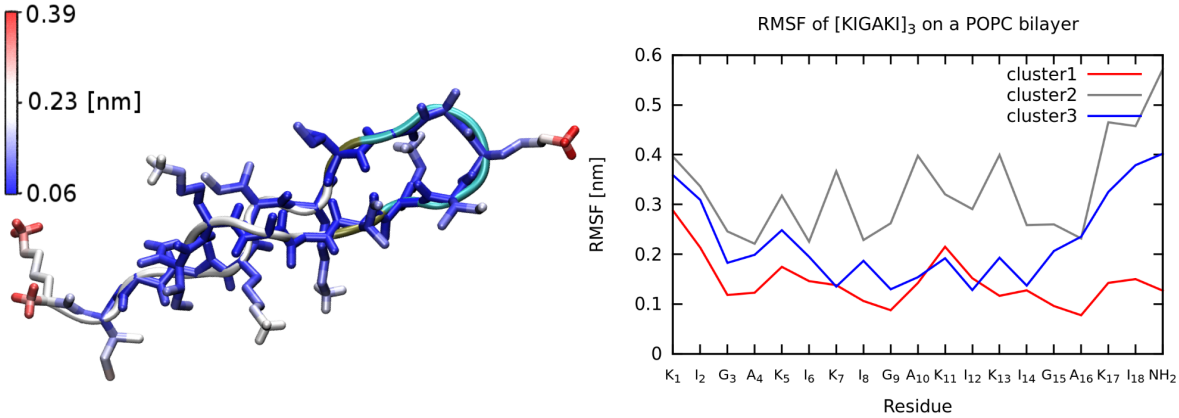

(b)

Figure 12: RMSF values of monomeric [KIGAKI]$_3$ peptides on (a) POPC/POPG and (b) POPC bilayers. On the left, the starting structures (after equilibration) of cluster1 on the corresponding bilayers are shown using the New Cartoon presentation for the backbone and Licorice for the side chains, where the color code corresponds to the RMSF: blue for low RMSF and red for high RMSF. On the right, the RMSF is plotted for the three peptide per bilayer.

4.5 Interactions between [KIGAKI]$_3$ and different membranes

4.5.1 Hydrogen-bonding

In order to understand which residues and lipids are crucial for peptide-membrane interactions, the hydrogen-bonds will be discussed in this section.

Table 2 lists hydrogen-bonds between both lipid types and [KIGAKI]$_3$ and only lysine residues, respectively. In general, 93% more hydrogen-bonds are formed between [KIGAKI]$_3$ and the mixed bilayer than between [KIGAKI]$_3$ and the zwitterionic POPC membrane, considering the total number of hydrogen-bonds.

However, for all structures more hydrogen-bonds between [KIGAKI]$_3$ and the neutral POPC lipids are formed. As mentioned in the simulation setup, the lipid ratio is POPC:POPG (4:1). Therefore it is more likely for [KIGAKI]$_3$ to interact with POPC lipids, simply because 80% of the bilayer consists of these lipids. Nevertheless, a preference towards POPG lipids was observed for cluster1, cluster2 and the six-peptide simulation since the hydrogen-bond ratio is larger than 0.2, which corresponds to the lipid ratio. When considering only hydrogen-bonds formed by lysine residues, this preference becomes even more distinct with an average POPG:POPC ratio for H-bond formation of 0.36.

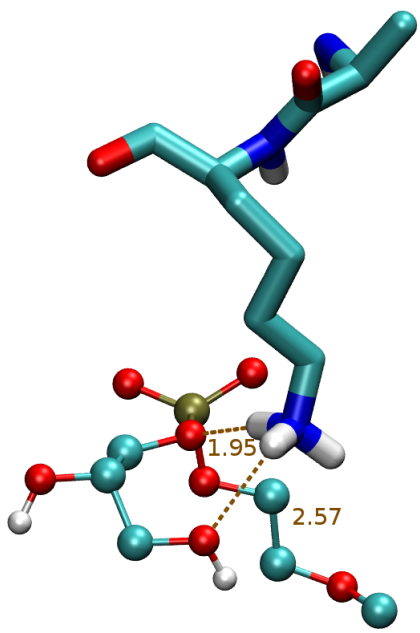

Figure 13: Lysine residue K_{11} of cluster3 interacting with a negatively charged POPG lipid. All distances are in Å.

When determining hydrogen-bonds between each residue and the bilayer, it was observed that the majority of hydrogen-bonds are formed by the positively charged lysine residues. Overall, 67% - 68% of all hydrogen-bonds between the phospholipid bilayers and [KIGAKI]$_3$ are formed by lysine in both membrane systems.

Lysine has a higher affinity to form hydrogen-bonds with negatively charged lipids, as expected, because it carries a NH_3^+, which is electrostatically attracted by negatively charged headgroups. As shown in Table 2, all hydrogen-bonds formed between cluster1 or cluster3 and POPG lipids are formed by lysine residues. Figure 13 shows one of these LYS-POPG interactions. One of the ammonium hydrogens is attracted by the PO_4^- group and another one by the oxygen of the terminal OH of the lipid headgroup.

Figure 14 illustrates the strong interactions between the lysine and zwitterionic POPC headgroups. The K_7 residue is buried relatively deep inside the membrane headgroup region and therefore the NH_3^+ does not interact with the PO_4^- but with the O16 and O33 atoms (lipid structures are given in Appendix 7.2). In this case, it is possible for the backbone atoms to form hydrogen-bonds with the PO_4^- and also with the $N(CH_3)_3^+$ group.

System		POPC		POPG		POPG:POPC	
		Pep	LYS	Pep	LYS	Pep	LYS
POPC/POPG	cluster1	7.03	5.44	2.53	2.53	0.36	0.47
	cluster2	6.89	4.01	2.63	1.45	0.38	0.36
	cluster3	10.32	5.46	1.62	1.62	0.16	0.29
	6 peptides ∅	9.06	6.16	3.05	2.17	0.34	0.35
	all ∅	**8.73**	**5.76**	**2.79**	**2.07**	**0.32**	**0.36**
POPC	cluster1	7.65	4.23				
	cluster2	4.75	3.29				
	cluster3	9.57	6.83				
	6 peptides ∅	5.28	3.64				
	all ∅	**6.16**	**4.13**				

Table 2: Average number of hydrogen bonds between [KIGAKI]$_3$ peptides (Pep) and lipids and between lysine residues (LYS) and lipids, where H-bonds with POPC and POPG have been distinguished. For the POPC/POPG systems, the ratio of the H-bonds between POPG and POPC is given in the last column. For the one-peptide system, the H-bonds were averaged over all fully adsorbed peptides over the last 100 ns, while the last 900 ns were considered for the six-peptide simulations.

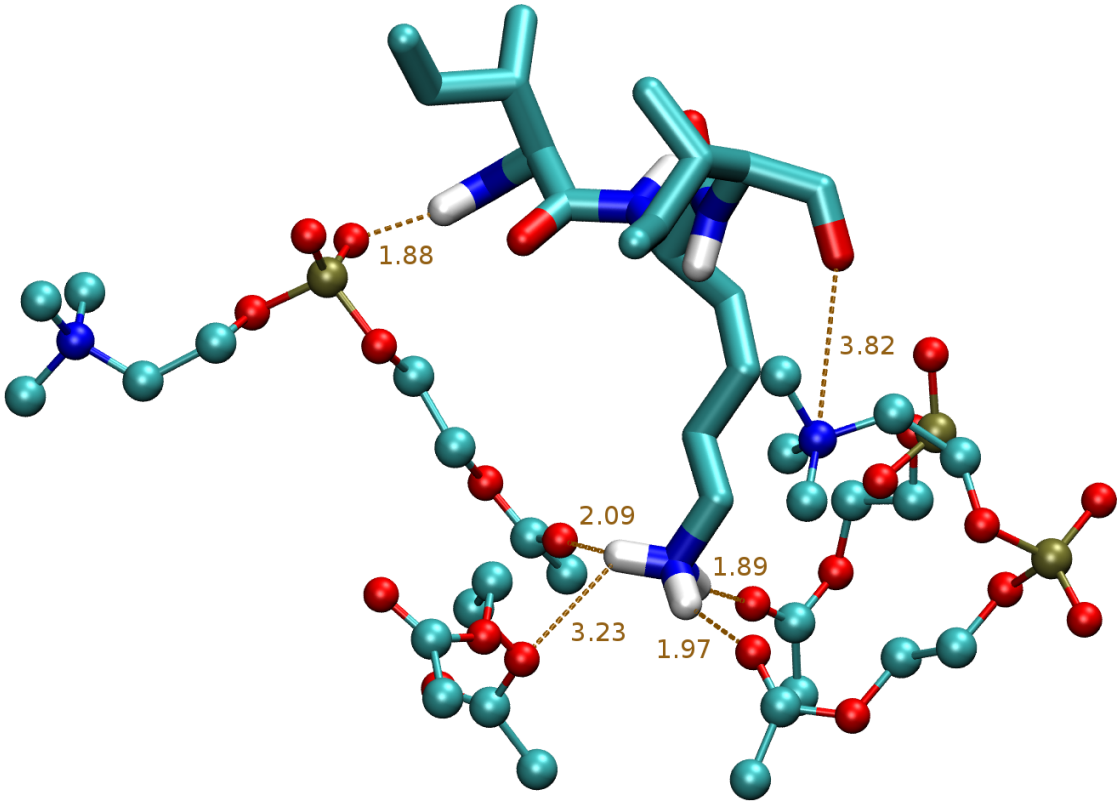

Figure 14: Hydrogen bonds between residues I_6, K_7, I_8 of cluster3 and surrounding POPC lipid fragments are illustrated. Distances are shown in Å. The structure corresponds to the last snapshot of the simulation with POPC. The ammonium hydrogens of the NH_3^+ of K_7 are attracted to the oxygen atoms in the lipid molecules and form strong hydrogen bonds, which explains the little lateral movement of [KIGAKI]$_3$ after adsorption. The insertion of the peptide is deep enough, to enable backbone atoms of the neighboring residues to form hydrogen bonds to the lipid PO_4^- and $N(CH_3)_3^+$ groups, which forces the hydrophobic side chains of I_6 and I_8 to remain in the polar water environment.

4.5.2 Interaction energies

The Coulomb and Lennard-Jones (LJ) interaction energies for the interaction between [KIGAKI]$_3$ and the lipids along with the contribution of the lysine and isoleucine residues are listed in Table 3.

System		LJ energy [kJ/mol]			Coulomb energy [kJ/mol]		
		Pep	LYS	ILE	Pep	LYS	ILE
	cluster1	-208.6	-83.4	-90.3	-1004.9	-916.7	-38.0
	cluster2	-327.5	-113.6	-153.4	-952.7	-772.0	-90.2
POPC/POPG	cluster3	-339.2	-127.0	-157.4	-1102.7	-862.5	-109.4
	6 peptides ∅	-320.8	-91.8	-156.4	-1129.8	-938.5	-75.5
	all ∅	**-311.1**	**-97.2**	**-148.9**	**-1093.3**	**-909.1**	**-76.7**
	cluster1	-14.0	-4.5	-7.6	-277.0	-275.3	-0.9
	cluster2	-57.2	-10.6	-33.0	-213.0	-174.5	-10.9
POPC/POPG	cluster3	-28.2	-10.6	-15.6	-220.8	-221.3	-0.6
	6 peptides ∅	-66.1	-10.1	-39.1	-304.0	-265.9	-17.1
	all ∅	**-55.1**	**-9.6**	**-32.3**	**-281.6**	**-251.8**	**-12.7**
	cluster1	-255.3	-50.4	-148.7	-694.1	-540.9	-44.0
	cluster2	-209.5	-58.0	-104.0	-446.1	-361.7	-36.6
POPC	cluster3	-270.9	-65.9	-131.6	-852.2	-699.0	-48.6
	6 peptides ∅	-232.3	-69.4	-121.7	-711.9	-691.7	-54.6
	all ∅	**-237.8**	**-64.6**	**-124.4**	**-691.4**	**-624.1**	**-49.7**

Table 3: Energies for the interaction of the lipids with [KIGAKI]$_3$, lysine and isoleucine residues, respectively. For the POPC/POPG bilayer system, the interacting lipid type(s) has been underlined. Interaction energies were calculated for snapshots taken every 200 ps for the last 50 ns of each simulation. So overall 250 structures were averaged.

In the charged membrane system the interactions between [KIGAKI]$_3$ and the bilayer is dominated by electrostatic interactions. The LJ energy accounts only for 22% of the total interaction energy and mainly involves isoleucine residues, which have an aliphatic side chain. The electrostatic interaction is mainly (83%) between the bilayer and lysine residues. We expected the majority of interactions to be between lysine, carrying a NH_3^+, and the negatively charged POPG lipids. However, only 23% of the Coulomb energy arises from lysine residues interacting with POPG lipids, which is only slightly more than the POPG lipid

content 20%. The interaction between [KIGAKI]$_3$ peptides and the pure POPC membrane is weaker by a factor of around 2, considering the total interaction energy, in comparison to the the charged membrane model. This pattern has been reported earlier in [63]. Although the interaction with [KIGAKI]$_3$ is twice as strong in the charged bilayer model, there are not twice as many interactions between the peptide and the negatively charged lipids. This fits well to the insertion results, which revealed that [KIGAKI]$_3$ inserts deeper into the headgroup region of the charged bilayer, which allows more interactions between [KIGAKI]$_3$ and POPC lipids. For the pure POPC systems, the percentage of the LJ energy is 28%, which is slightly higher than in the charged membrane system. Lysine residues form 90% of the Coulomb interactions, which leaves only 10% electrostatic interactions between the lipids and the other 12 residues.
Figure 15 illustrates the time evolution of the interaction energies between the [KIGAKI]$_3$ peptides and the bilayer in the six-peptide simulations.

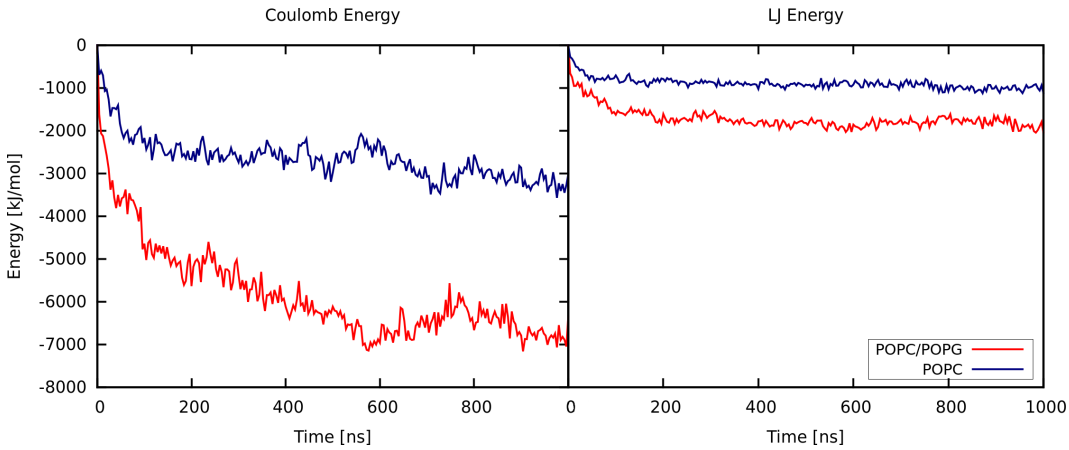

Figure 15: Interaction energy over time for the two six-peptide simulations. The energy was calculated for structures taken every 4 ns from the trajectory.

The Coulomb energy of the POPC/POPG bilayer system decreases rapidly at the beginning when the adsorption process takes place, which suggests that the adsorption is mainly triggered by electrostatic attraction. After 500 ns the Coulomb energy reaches its minimum and increases slightly before it starts decreasing again. The Coulomb energy in the neutral system also decreases rapidly at the beginning, but not as much as in the charged system. Afterwards, this energy decreases slightly during the whole simulation without any significant fluctuations.
The LJ energy contribution is much smaller in both bilayer systems. At the beginning the energy decreases before reaching a plateau for the rest of the simulation. The LJ energy in the charged bilayer system needs longer to converge and exhibits more fluctuations.

4.6 Effects of [KIGAKI]$_3$ adsorption on membrane properties

4.6.1 Deuterium order parameter

Deuterium order parameters (S_{CD}) are a measure of the order of lipid acyl chains. Figure 16 presents the deuterium order parameters of the two bilayer systems, showing the values for POPC and POPG in the charged membrane system separately. Palmitoyl chains (sn1) are presented in the left part of each figure, oleoyl chains (sn2) in the right part. The major difference between the two chains, apart from the chain-length, is the double bond between C_9-C_{10} in the sn2 chain. The S_{CD} has its minimum value at C_{10}, which is in good agreement with experimental results [65], since the atoms involved in the double bond possess a different orientation, which leads to this outstanding value. The results for POPC show that lipids in the charged bilayer are more ordered than lipids in the neutral POPC membrane. That pure POPG bilayers are more ordered than pure POPC bilayers has been reported in other simulation studies [66, 67], which is due to electrostatic interactions between Na^+ and POPG lipid headgroups [66]. We observed 23 Na^+ ions out of 26 Na^+ ions being coordinated with the headgroup region of the POPC/POPG bilayer in the simulation without [KIGAKI]$_3$. The average density of sodium ions relative to the phosphorus-atom density is presented in Appendix 7.6. We added ions only to neutralize lipid and peptide charges, therefore the single-peptide systems contain 19 Na^+ ions, whereas all six-peptide simulations and all simulations with pure POPC bilayers contain Cl^- ions to neutralize the positive charges of the [KIGAKI]$_3$ peptides. The decrease in Na^+ concentration might therefore also add to a decreased lipid order, i.e. to lower S_{CD} values. On the other hand, the NH_3^+ group of [KIGAKI]$_3$ can replace these electrostatic interactions between Na^+ and PG headgroups, and thus induce lipid order to a certain extent, however NH_3^+ is sterically more demanding and less flexible than sodium ions.
Unlike for the POPC bilayer, the order parameters of POPC and POPG lipid acyl chains in the charged membrane increase up to C_5, and then significantly decrease for the terminal carbons which are located in the membrane core. Nevertheless, even the ends of lipid acyl chains in the charged membrane are more ordered than those in the neutral bilayer.
The influence of a single peptide on the order parameters in the charged membrane system is little apart from the POPG-sn1. For this acyl chain the order decreases in the cluster3 simulations generally, similarly as in the six-peptide simulations. This might be due to the larger insertion depth of cluster3 into the POPC/POPG membrane (s. Figure 5). Six [KIGAKI]$_3$ peptides decrease the lipid acyl chain order significantly, whereupon S_{CD} of POPC and POPG lipids are about equally reduced in POPC/POPG.

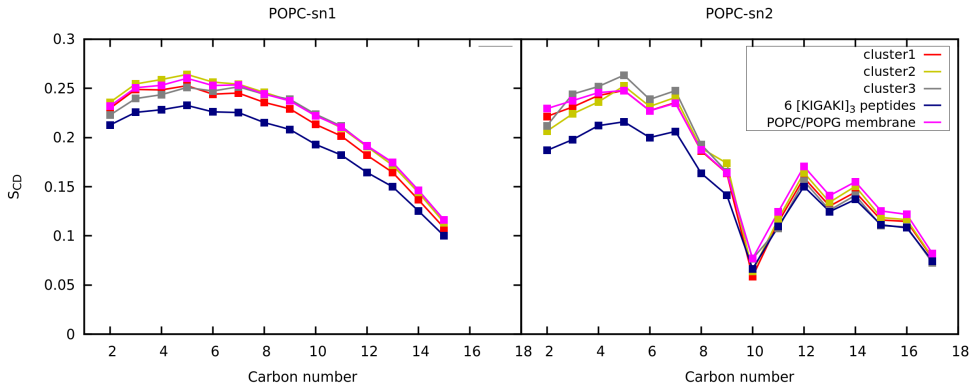

(a)

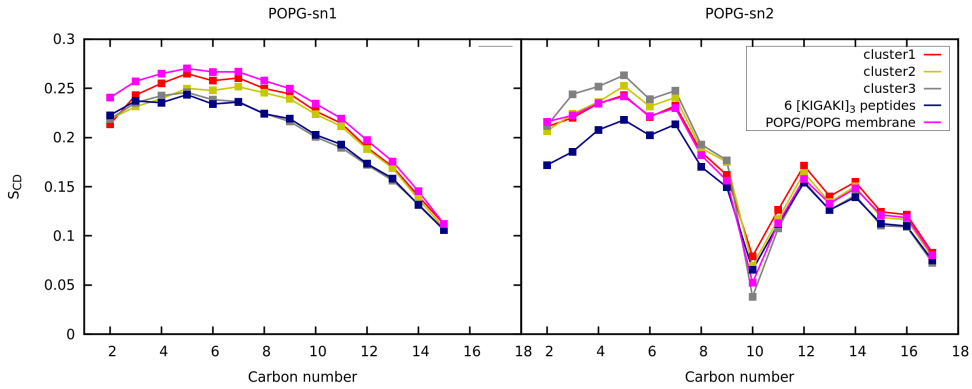

(b)

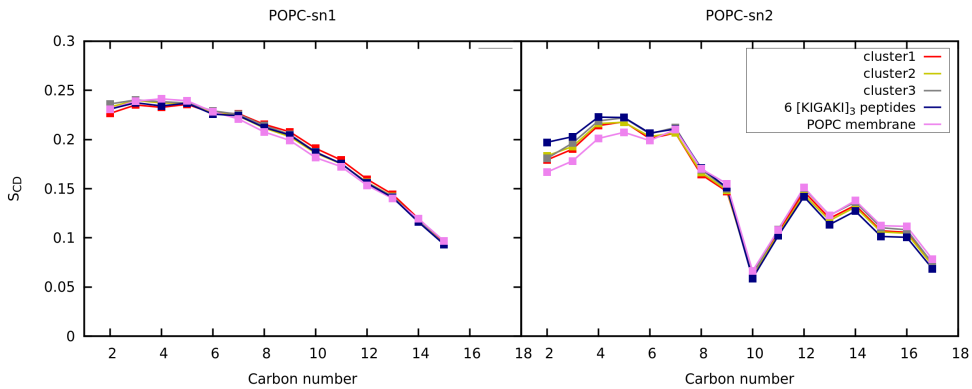

(c)

Figure 16: Deuterium order parameters are illustrated for (a) and (b) for POPC/POPG and (c) the POPC simulations. Values are calculated over the last 100 ns of simulation for single-peptide simulations and over the last 900 ns of the simulation time of the six-peptide simulations. In the left part of the figure the order parameters for the palmitoyl (sn1) chains and in the right part the order parameters of the oleoyl (sn2) chains are shown.

Unlike the palmitoyl chain, only the headgroup region of the oleoyl chain is strongly affected

by [KIGAKI]$_3$ peptides. Remarkably, adsorption of cluster3 leads to an increased order of the sn2 chain, while the order of the sn1 chain is reduced. In the POPC simulations no significant change in lipid order is visible for the sn1 chain. The order parameters for the carbon atoms close to the surface in the oleoyl chain exhibit slightly higher S_{CD} values for the single-peptide systems and even more order for the six-peptide system. This suggests a stabilization of the headgroup region of the POPC bilayer by [KIGAKI]$_3$ peptides. Interestingly, C_7-C_{17} in the sn2 chains do not show any change in comparison with the pure membrane model. The difference in perturbation of different membrane types has also been reported in experimental work [26]. ^{31}P NMR experiments revealed a minimal influence of [KIGAKI]$_3$ peptides on a POPC bilayer, but a moderate perturbation of a POPC/POPG (4:1) bilayer. This is in agreement with the findings of this work.
Overall, S_{CD} values for POPC lipids are slightly higher than determined experimentally [65,68], but in very good agreement with the work of Piggot et al. on POPC bilayers using the same force field and lipid parameters [46].

4.6.2 Area per lipid and bilayer thickness

The area per lipid (APL) and bilayer thickness are commonly used quantities to characterize bilayer systems. In this work, they are calculated using the g_lomepro tool [50]. Table 4 presents the average values for all simulations and experimental values if available.

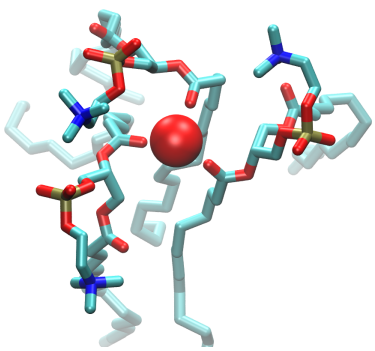

Figure 17: Coordination of Na^+ (red ball) to three O16 atoms of lipids in POPC/POPG membrane.

Elmore [67] and Zhao et al. [66] showed in their work that pure POPG bilayers exhibit a remarkably small APL in comparison with a pure POPC membrane. This is explained by POPG lipids possessing a tight binding through relatively strong salt-bridges between PG headgroups and sodium ions in the headgroup region. Sodium ions coordinating to oxygen atoms in lipids could also be observed in the simulation of the pure POPC/POPG membrane. Na^+ and phosphorus atom densities are presented in Appendix 7.6. A snapshot of one Na^+ ion interacting with three O16 atoms (lipid structure is given in Appendix 7.2) in the charged bilayer is illustrated in Figure 17. Our APL values are, of course, larger since only 20% of the bilayer consists of POPG lipids. But the trend of a smaller APL in the charged membrane system, compared to the neutral system, can be observed. By adding one peptide to the system and reducing the number of sodium ions from 26 to 19,

System		APL [nm^2]	Thickness [nm]
POPC/POPG	cluster1	0.66	4.03
	cluster2	0.65	4.07
	cluster3	0.65	4.05
	6 peptides	0.69	3.89
	membrane	0.65	4.03
	POPG (exp)	(0.56^d), (0.53^e)	(4.27^d), (4.39^e)
POPC	cluster1	0.68	3.87
	cluster2	0.68	3.87
	cluster3	0.67	3.89
	6 peptides	0.67	3.89
	membrane	0.68	3.85
	POPC (exp)	0.68^a, 0.63^b, 0.64^c, (0.68^d), (0.66^e)	3.7^a, 3.91^c, (3.67^d)

Table 4: Average APL and bilayer thickness are presented. Values are obtained from the second half of the simulations and averaged over lipids and time. Experimental values are taken from *a* Kučerka et al. (2005) at 303 K [69]; *b* Smaby et al. (1997) at 297 K [70]; *c* Kučerka et al. (2011) at 303 K [71]. No experimental results for a POPC/POPG membrane or pure POPG bilayer could be found, therefore simulation results are presented: *d* Elmore (2006) pure POPG and POPC bilayer at 310 K [67], *e* Zhao et al., pure POPG and POPC bilayer also at 310 K [66].

no change in APL is observed. However, in the six-peptide simulation the APL increases by 6.2% to 0.69 nm^2. It is possible that the absence of stabilizing sodium ions triggers the increase of APL. However, the [KIGAKI]$_3$ peptides possibly restore the attractive electrostatic interactions. This is indicated in Figure 18 which shows a local decrease of APL close to [KIGAKI]$_3$ peptides for four out of six peptides on the POPC/POPG bilayer. Since the peptides hardly move on the membrane surface, which is illustrated by the low diffusion coefficients, the snapshot can be considered as representative with respect to peptide locations. The APL for the pure POPC membrane is higher, than for the POPC/POPG membrane, which agrees well with the experimental and simulation results shown in Table 4. The average APL of the pure POPC membrane matches exactly the results obtained by Kučerka et al. [69] and Elmore [67]. Adsorption of [KIGAKI]$_3$ peptides has, in our simulations, no effect on this quantity. As shown before, the peptides interact less with the POPC bilayer and are therefore more mobile on the membrane surface. Hence, there is no significant local decrease in APL observed for lipids close to [KIGAKI]$_3$ peptides. In comparison with the partly charged bilayer, the fluctuation of the APL among the lipids is

remarkably low; the APL in the POPC system spreads form 0.55 nm^2 to 0.90 nm^2, whereas in the POPC/POPG system it reaches values between 0.42 nm^2 and 1.06 nm^2.
The bilayer thickness of the two membrane systems differs as well. As shown in Table 1 the thickness for a pure POPG bilayer is found to be larger than for the pure POPC membrane, which can be explained by the long-range electrostatic repulsion of the negatively charged headgroups. By adding six [KIGAKI]$_3$ peptides, which decrease the charge density on the bilayer surface due to their lysine NH_3^+ groups, a decrease in bilayer thickness of 3.5% is observed. The decrease in surface charge density has been reported experimentally by Lu et al. [63] where an up-field shift of POPC and POPG ^{31}P isotropic peaks in a mixed bilayer (3:1) was observed due to addition [KIGAKI]$_3$, which suggests a decrease in surface charge density. Figure 19(a) shows a clear localized decrease in bilayer thickness around [KIGAKI]$_3$ peptides. For lipids close to the peptide it further decreases down to 3.18 nm, which is by far less than observed for the POPC bilayer. However, lipids that are further away from the peptides possess a significantly higher thickness, up to 4.28 nm. The pure POPC bilayer shows the opposite behavior. Starting with a neutral membrane, the surface charge increases after adsorption of four peptides, each carrying 7 positive charges. The increase of bilayer thickness can be explained by the electrostatic long-range repulsion of the positive charges of [KIGAKI]$_3$ peptides.

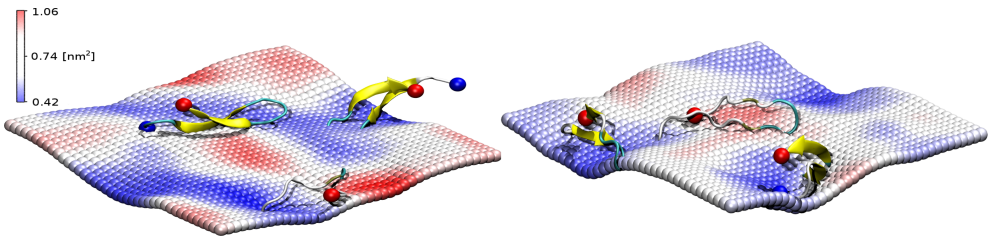

(a)

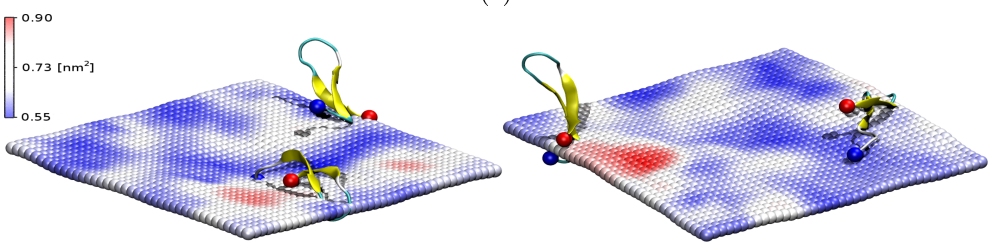

(b)

Figure 18: Average area per lipid of the POPC/POPG (a) and POPC (b) membrane in the six-peptide simulation. The peptide structures are taken from a snapshot after 254 ns (a) and 40 ns (b). The upper leaflet of the POPC/POPG bilayer is shown on the left side with three peptides being adsorbed, the lower leaflet with the remaining peptides is illustrated on the right side. In the POPC system peptide1 and peptide2 stay in the water phase and are therefore not shown in this figure. The N-terminus is highlighted by blue spheres, C-terminus by red spheres.

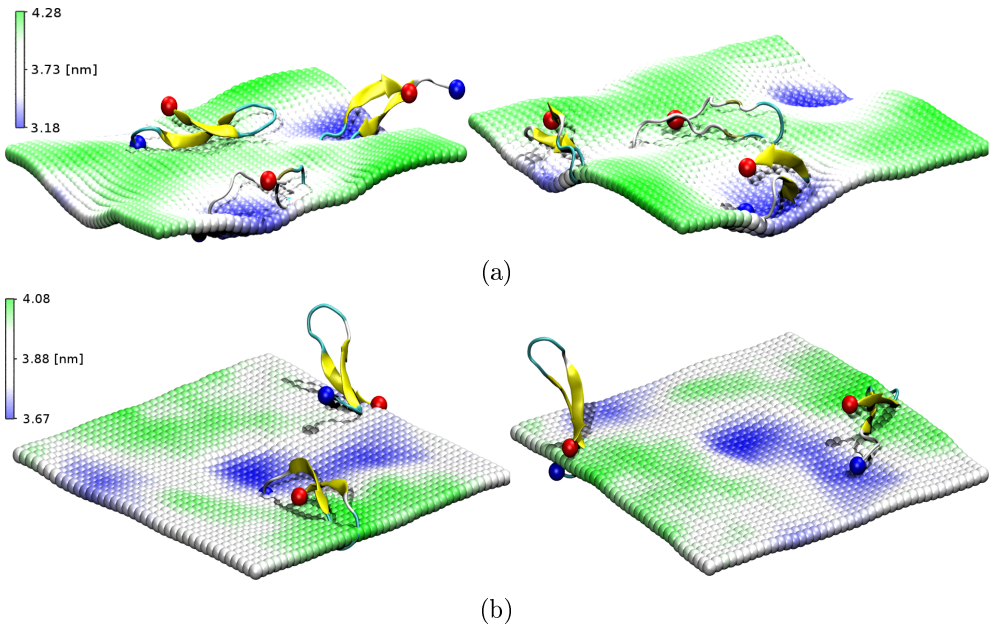

Figure 19: The bilayer thickness of the POPC/POPG (a) and POPC (b) bilayer is illustrated. For further details see Figure 18.

4.6.3 Water density

Leakage of anionic large unilamellar vesicles (LUVs) promoted by [KIGAKI]$_3$ peptides has been reported in experimental work [22, 25]. At high peptide/lipid (P/L) ratio, leakage in the form of calcein release was observed for LUVs containing negatively charged POPG lipids. Among other bilayers, the leakage of POPC/POPG (4:1) and POPC bilayers was investigated. In both experiments [KIGAKI]$_3$ was able to induce leakage in POPC/POPG LUVs at P/L ratios $>$ 1:8. Jin et al. [25] further observed no calcein release for POPC vesicles at a very high P/L ratio of 1:2.

In order to investigate membrane leakage in our simulations, the water density along the z-coordinate and water flux using the Gridcount package [72] was calculated. Since the simulation length is on a completely different time scale than leakage observed experimentally, the effects will not be as evident as in the experiments.

Figure 20 presents the water density along the z-coordinate for the POPC/POPG (a) and POPC (b) systems. Adding one [KIGAKI]$_3$ peptide to the partly charged bilayer reduces the water density slightly in the headgroup region. This can be explained by the presence of the peptide, which pushes water molecules aside. Six peptides, however, have a remarkable influence on the water density. Water molecules are able to insert deeper into the membrane headgroup region. It has been shown before that the bilayer thickness is reduced, which

certainly contributes to the increased water density, however, the decrease in thickness is nearly negligible compared to the change in water density. This effect is more than compensated as shown in Figure 20(a). The reduced lipid order for this system enables H_2O to enter the membrane more easily. The water density in the POPC headgroup region shows no significant changes among the simulations. Only the cluster1 system shows slightly more water in the bilayer headgroup region. A comparison between the water density of the two six-peptide systems can be found in Appendix 7.7.

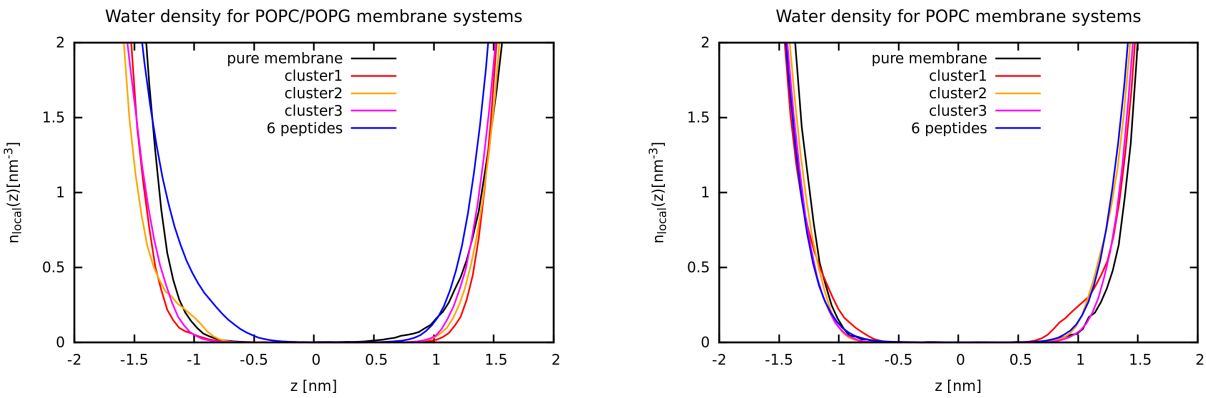

(a) (b)

Figure 20: Water density of the six-peptide simulation with the POPC/POPG membrane (a) and with the zwitterionic POPC bilayer (b). Water density is calculated by counts per nm^3 over the second half of the simulation. The COM of all membranes is set to $z = 0$.

In addition to the water density, also the water molecules crossing the bilayer during the whole six-peptide simulations were determined. In the neutral membrane system 12 H_2O molecules passing through the membrane were observed, whereas 16 water molecules were counted in the POPC/POPG simulation. Without [KIGAKI]$_3$ there are 3 H_2O molecules crossing during the 200 ns simulation of the POPC/POPG membrane, thus, there is no significant change upon addition of 6 peptides. For the POPC bilayer, we only performed a 10 ns simulation, hence, no representative results were obtained for this system.

4.7 Discussion

Membrane selectivity

Our MD simulations demonstrated that 50% more [KIGAKI]$_3$ peptides adsorb on the negatively charged POPC/POPG (4:1) membrane surface than on a zwitterionic POPC bilayer resulting from strong electrostatic interactions between the charged bilayer and the peptides, which trigger the adsorption and are able to reduce electrostatic repulsion between

the positively charged peptides. The POPG lipids allow $[KIGAKI]_3$ to insert more deeply into the headgroup region of the charged bilayer compared to the pure POPC bilayer. This allows the formation of more hydrogen-bonds between peptides and lipids not only with POPG, but also with POPC.

The adsorption on the neutral POPC bilayer is also dominated by electrostatic interactions between peptides and membrane, however, the overall interaction energy is 51% less than in the charged bilayer system, which leads to a higher lateral mobility of $[KIGAKI]_3$ on the POPC bilayer surface. The average distance between peptides and POPC surface is around 40% higher, which is in line with only around half as many peptide-lipid hydrogen-bonds in comparison to the charged membrane systems.

A difference in the effect of the $[KIGAKI]_3$ peptides on the membrane systems was also observed. Whereas only minor effects on the POPC membrane occurred, even for high peptide-to-lipid ratios, the properties of the charged bilayer changed significantly. A decrease in lipid order for both lipid types in the charged membrane was observed for a P/L ratio of 6:128. However, it is not completely clear whether this decrease arises from the peptides or the different Na^+ concentrations. Since ions were only used for neutralization in our simulations, the number of Na^+ ions differs, depending on the number of $[KIGAKI]_3$ peptides present in the system. In the pure POPC/POPG membrane system, 26 sodium ions were used to compensate for 26 negative charges at the POPG lipids. The sodium ions are found to be coordinated in the headgroup region (s. Appendix 7.6), which probably leads to a higher order of the lipid acyl chains. By adding more peptides (and thus reducing the number of sodium ions at the same time) the lipid order decreases. It is unclear to which extent this reduction results from the lower Na^+ concentration and/or higher $[KIGAKI]_3$ concentration. Further simulations with 100 mM NaCl added to each system will help answering this question.

The same applies for the increase in the area per lipid that might also be influenced by the sodium ion concentration. Since sodium ions cause a tighter packing of lipids [66], the absence would lead to an increase of the area per lipid. Nevertheless, we could show a localized decrease in APL for lipids close the the peptides, which suggests that the Na^+ ions get replaced by NH_3^+ groups in lysine. These saltbridges with the lipids then lead to a tight packing of the lipids.

A decrease of the bilayer thickness for POPC/POPG was also observed, which suggests a reduction of the electrostatic repulsion of the two partly negatively charged leaflets due to the reduced surface charge density. Moreover, an increase in water density in the headgroup region was observed for high P/L (6:128) ratio.

Key interacting residues

The lysine residues of [KIGAKI]$_3$ were identified as key interacting residues. Apart from forming the majority of hydrogen bonds and electrostatic interactions between [KIGAKI]$_3$ and both bilayers, it also inserts more deeply into the headgroup region of the POPC/POPG bilayer compared to the other residues. Wadhwani et al. [23] reported, that the CF_3 label, which replaced an isoleucine side chain for ^{19}F NMR measurements, is parallel to the membrane normal in [KIGAKI]$_3$ fibrils. This leaves two options open: either lysine residues point into the bilayer and isoleucine point outwards or vice versa. Since the amphiphilic [KIGAKI]$_3$ peptides consists of alternating polar and apolar residues, all lysines are expected to be on one side in the extended structure [22]. Polar lysine residues prefers to be in the headgroup region [73], whereas hydrophobic isoleucines would certainly prefer to insert into the lipophilic bilayer interior, but this is not observed in our simulations. In the neutral membrane system we do not see a preference for any residue-type to insert deeper than the others, while in the POPC/POPG bilayer system the lysine residues penetrate most deeply into the membrane. This behavior arises from the very strong electrostatic interactions between lysine an the lipids, which are able to compensate for the unfavorable position of the isoleucine side chains in the water environment. Furthermore, the hydrophobic isoleucine side chain consists of four carbons, which is short compared to the polar headgroups of both POPC and POPG. Hence, the peptide would need to insert relatively deep into the headgroup region of the membrane in order for the isoleucine side chains to reach the hydrophobic core.

In summary, in our simulations, [KIGAKI]$_3$ peptides are in the monomeric form and show a different behavior than the fibrils observed in experiment [23]. An intramolecular β-sheet is formed and not all lysine and isoleucine residues flank on either side. This makes it difficult to infer the behavior of [KIGAKI]$_3$ fibrils from our results.

Aggregation of [KIGAKI]$_3$ peptides

As stated in the beginning, one of our goals was to investigate the aggregation of [KIGAKI]$_3$, which has been reported in the work of Wadhwani [23, 24] and M. Meier [27]. In our two 1 μs simulations, containing six [KIGAKI]$_3$ peptides each, no permanent aggregation was observed. The starting structure for these simulations possesses a stable β-sheet conformation, which first must unfold for the peptide to be able to form intermolecular hydrogen bonds and thus assemble into fibrils. On the POPC membrane, no perturbation of the intramolecular β-sheets was observed, during the whole simulation. This suggests that the neutral membrane is less able to destabilize the β-hairpin structure. However, a temporary

assembly of peptide3 and peptide4 was observed at the bilayer surface during the first 200 ns of the simulation, which is shown in Figure 21. The strongest hydrogen bonds between peptide3 and peptide4 are formed by G^3_9-G^4_{15}, G^3_9-K^4_{13} and occasionally also by K^3_{13}-K^4_{17} (peptide index in superscript). These residues from peptide3 are not involved in the β-sheet, whereas in peptide4 these residues are part of the β-sheet. The hydrophobic isoleucine side chains in the β-sheet region from both peptides point towards each other.

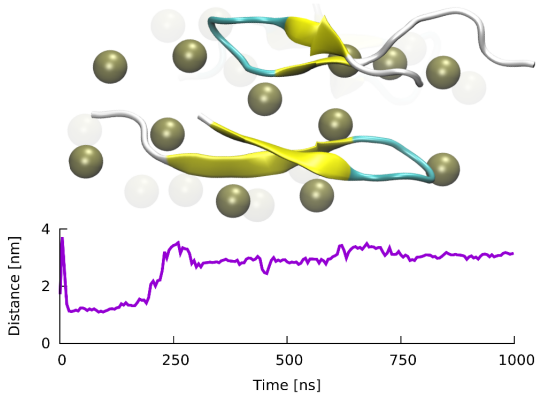

Figure 21: Temporary aggregation of peptide3 and peptide4 on the POPC bilayer. Distance between the COM is shown.

However, the hydrogen bonds dissolve completely after 190 ns which leads to dissociation of the peptides, which repel each other without any balancing charges due to +7 charge per [KIGAKI]$_3$. Furthermore, it has been reported [27], that [KIGAKI]$_3$ peptides exhibit 98% β-content (on a negatively charged membrane), which leads to the conclusion, that they aggregate in an elongated conformation, which has not been observed in this work. This implies the unfolding of the β-hairpin structure. On the charged bilayer, a decrease in β-content was observed due to the strong interactions between peptides and the bilayer, leading to the destabilization of the β-sheets and conversion into an unstructured conformation. This might be the pre-stage of the aggregation process. The lack of aggregation on the bilayer surface in our simulations might be due to the low diffusion of lipids or the relatively short simulation length.

Overall, we showed that fewer peptides adsorb on the neutral membrane, which is probably due to electrostatic repulsion between the positively charged peptides that are not balanced by the zwitterionic lipid headgroups. Moreover, the interaction between peptides and POPC membrane is relatively weak, which makes neutral membranes less effective in dissolving the intramolecular β-sheets. We assume, that this is needed for the [KIGAKI]$_3$ peptides to aggregate in an elongated conformation. These results, and the lower peptide concentration at the POPC surface, suggest, that aggregation of [KIGAKI]$_3$ is more likely on charged membranes than on neutral ones. It still remains unclear how the aggregation contributes to the antimicrobial activity of [KIGAKI]$_3$ peptides.

5 Results and discussion of [KIGAKI]$_3$-CF$_3$-Bpg simulations

For ^{19}F-NMR experiments on the [KIGAKI]$_3$ peptide, P. Wadhwani et al. [23, 24] used *L*-CF$_3$-Bpg and *D*-CF$_3$-Bpg labels. In each measurement the label replaced a single isoleucine residue at positions I$_6$, I$_8$, I$_{12}$ and I$_{14}$. The authors showed that the label and its stereochemistry have an influence on the aggregation propensity and fusogenic activity but not on the antimicrobial activity. While [KIGAKI]$_3$-*L*-CF$_3$-Bpg ([KIGAKI]$_3$-L) shows comparable antimicrobial, fusogenic and hemolytic activities to the unlabeled peptide, the *D*-enantiomer is 4-5 times less hemolytic and also shows a decrease in induced fusion. This has been explained by the decreased tendency of [KIGAKI]$_3$-*D*-CF$_3$-Bpg ([KIGAKI]$_3$-D) to aggregate. It was found that a higher P/L ratio is needed for [KIGAKI]$_3$-D to aggregate. The biologically active concentration in order to see an antimicrobial effect is low, however, with a minimum inhibitory concentration (MIC) of 7.5 μM that corresponds to a P/L ratio of around 100:1. Therefore it is likely that the peptides are aggregated on charged membranes [24]. However, since less [KIGAKI]$_3$ adsorbs on neutral membranes [23], as we have also shown in this work (section 4.1), the concentration of peptides on these membrane surfaces is reduced. This might be the reason for the prevention of fibril formation of the [KIGAKI]$_3$-D peptides. The experiments were carried out with the label placed at positions Ile-6, Ile-8, Ile-12 and Ile-14 [24], however, our simulations focus on [KIGAKI]$_3$ labeled at position Ile-8, due to the availability of more published experimental data. Our goal was to investigate the folding process in water and the behavior of [KIGAKI]$_3$-8L and [KIGAKI]$_3$-8D on POPC/POPG (4:1) and POPC bilayer surfaces in order to analyze structural differences and contribute to the understanding of the remarkably different hemolytic activity.

5.1 [KIGAKI]$_3$-CF$_3$-Bpg in water

5.1.1 Secondary structure

An elongated structure, built with VMD [32], was used as starting conformation for the 100 ns MD simulations of both peptides in water. The DSSP plots in Figure 22 show that [KIGAKI]$_3$-8L forms a β-bridge between residues 14 and 17 from 25 ns to 45 ns and from 64 ns to 73 ns. Also in the unlabeled [KIGAKI]$_3$ this β-bridge was observed within the first 40 ns of simulation [31]. Apart from the β-bridge, the peptide is mostly unstructured.

[KIGAKI]$_3$-8D adopts a β-sheet between residues 12-13 and 16-17 from 15 ns to 40 ns. Another β-sheet in the terminal region was sampled between residues 2-3 and 7-8. This pattern was not found in the [KIGAKI]$_3$ simulation in water [31].

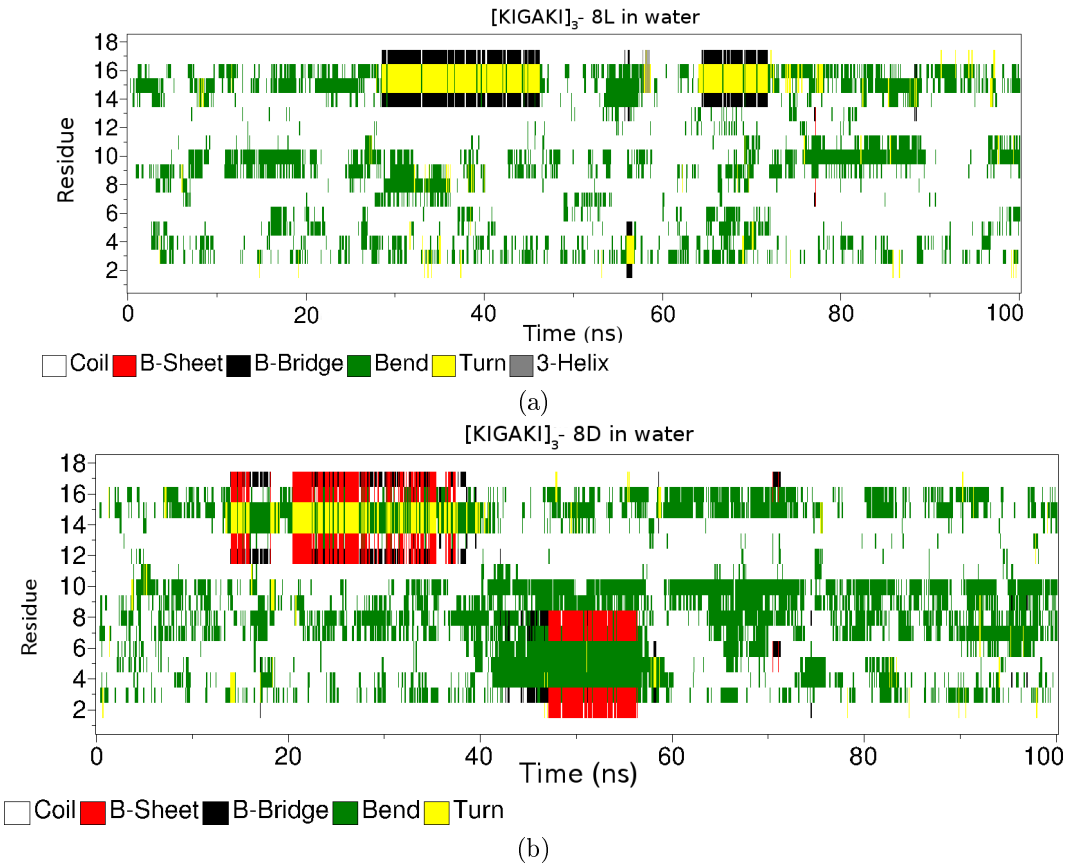

Figure 22: DSSP plots of [KIGAKI]$_3$-8L (a) and [KIGAKI]$_3$-8D (b) during a 100 ns simulation in water.

Again, the other residues are in random coils or bends. No stable β-sheet has been formed within 100 ns of simulation. This is different to the unlabeled peptide, where a stable β-sheet formed when applying exactly the same simulation conditions. These results show that the labeled peptides have less intramolecular order than the unlabeled [KIGAKI]$_3$ peptide, which may has an influence on the formation of aggregates. However, only a single 100 ns simulation was performed for each peptide. So more or longer simulations would be necessary to base this conclusion on better statistics.

5.1.2 Flexibility

In order to determine the flexible regions in the peptides, the RMSF was calculated, which is presented in Figure 23. Both enantiomers have highly flexible termini, whereby the N-

terminus possesses higher RMSF values than the C-terminus. Residues I_6 and I_{12} show reduced fluctuations, whereas K_5, K_7 and K_{11} show local RMSF maxima. The CF_3 label does not induce a change in local flexibility with regards to the other residues and the unlabeled peptide. In general, [KIGAKI]$_3$ in water exhibits the same RMSF pattern. The only remarkable differences are the smaller flexibility at the N-terminus combined with a higher flexibility at the C-terminus and K_{11}.

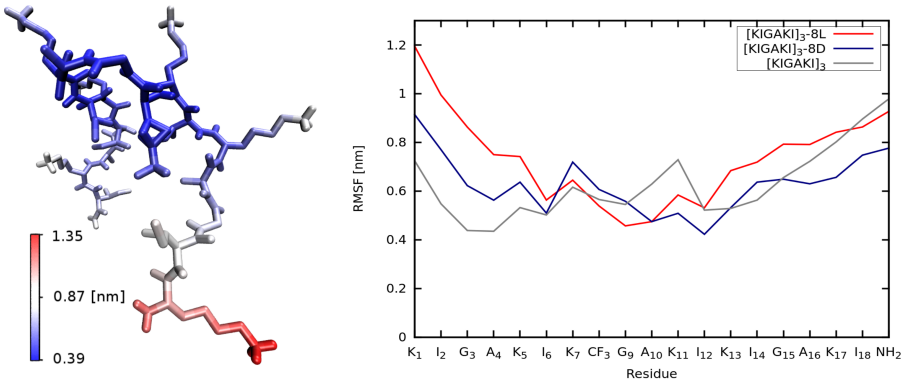

Figure 23: RMSF per residue of [KIGAKI]$_3$-8L (red), [KIGAKI]$_3$-8D (blue) and the unlabeled [KIGAKI]$_3$ peptide (gray) are presented on the right. The structure on the left side corresponds to the [KIGAKI]$_3$-8L last snapshot of the 100 ns simulation. The RMSF of the individual atoms is illustrated with a color scheme. All values are averaged over the whole simulation time.

5.2 [KIGAKI]$_3$-CF$_3$ on phospholipid bilayers

The last snapshot of the simulation of the labeled peptides in water was used as starting structure for the 500 ns six-peptide simulations on a POPC/POPG and a pure POPC bilayer. In this section, the adsorption and interaction between the labeled peptides and the bilayer is presented and compared to the results obtained for unlabeled [KIGAKI]$_3$.

5.2.1 Adsorption on membrane surfaces

In order to investigate the adsorption of the peptides in each 500 ns simulation, the COM distance between the peptides and bilayer surface was calculated. The results are presented in Figure 24. As in the unlabeled [KIGAKI]$_3$ simulations, all six peptides adsorb to the charged bilayer surface. The average distance between the labeled peptides and the surface (0.46 nm for [KIGAKI]-8L, 0.48 nm for [KIGAKI]-8D) is slightly higher than for the unlabeled peptides. All *L*-labeled peptides were adsorbed within the first 50 ns of simulation, whereas the *D*-enantiomer fully adsorbed after 100 ns.
On the POPC bilayer, peptide1 and peptide4 of [KIGAKI]$_3$-8L, which were furthest away

from the surface in the setup system, stay in the water phase. The other four peptides adsorb, though peptide3 exhibits a relatively large distance to the membrane surface. [KIGAKI]$_3$-8D shows a similar behavior, the only noticeable difference is the motion of peptide3. After 80 ns peptide3 adsorbs on the membrane surface, mainly with residue G_9 (s. Appendix 7.8), but gets desorbed after 100 ns. Thus, compared to the unlabeled and *L*-labeled peptide, fewer [KIGAKI]$_3$-8D peptides adsorb on neutral membranes, which resemble mammalian cell-membranes, whereas the same amount of peptides is bound to the charged bilayer.

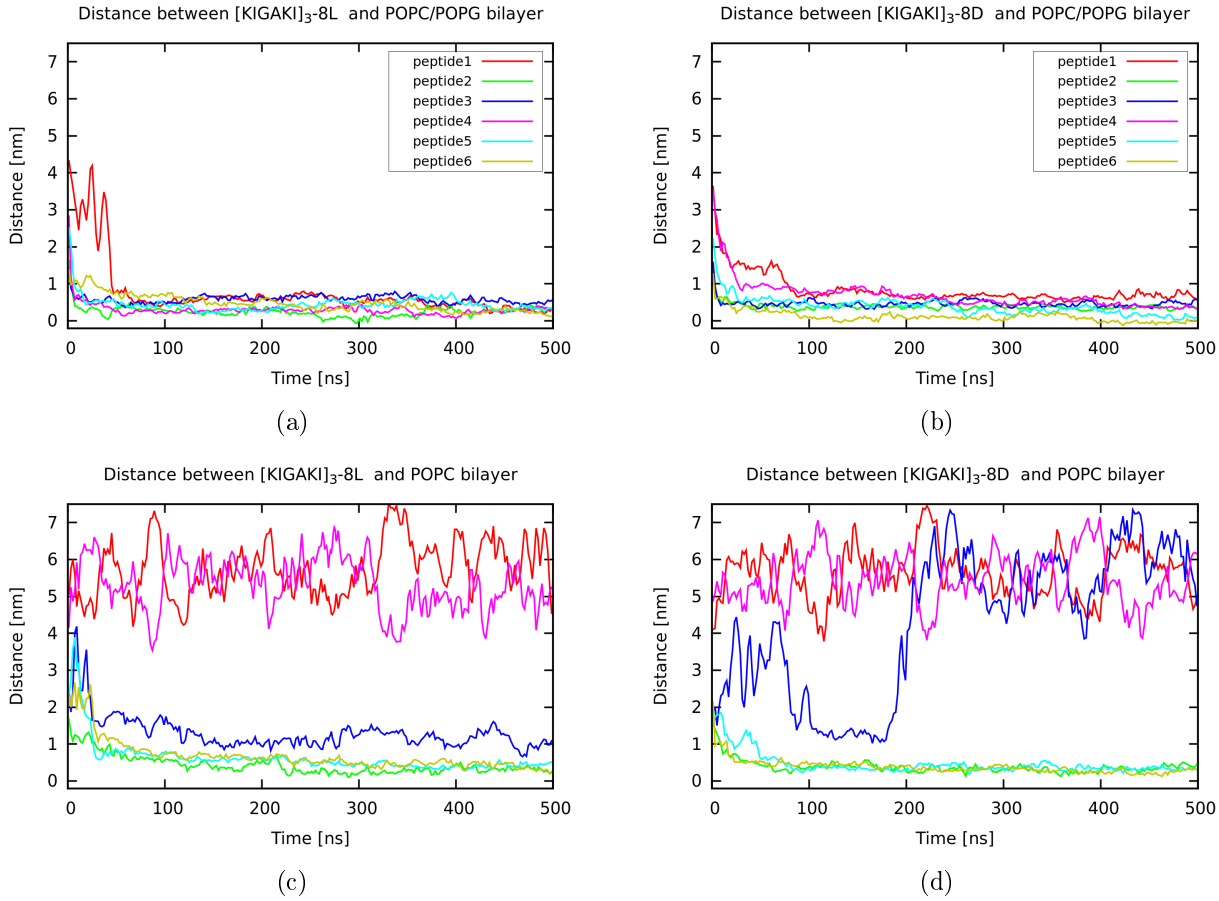

Figure 24: The distance along the membrane normal between the center of mass (COM) of each peptide and the COM of the phosphorus atoms of the leaflet, which is closest to the according peptide, is shown. The peptides are presented with the same color in every subfigure. (a) shows [KIGAKI]$_3$-8L on the charged bilayer, (b) presents the adsorption process of the [KIGAKI]$_3$-8D on POPC/POPG. In both simulations, peptides 1-3 adsorb on the upper leaflet, while peptides 4-6 adsorb on the lower leaflet. (c) and (d) illustrate the adsorption of the peptides on the neutral POPC membrane. In these systems, peptide 2 (and 3) adsorb on the upper leaflet, while peptides 5 and 6 adsorb on the lower leaflet.

To investigate the distance between each residue and the surface in the specific bilayer system, we calculated the average distance between each residue and the membrane surface, averaged over time and adsorbed peptides, shown in Figure 25. The figures that show the distance of each residue per peptide over time can be found in the Appendix 7.8. In general, lysine residues insert more deeply into the headgroup region of the bilayer, apart from [KIGAKI]$_3$ and [KIGAKI]$_3$-8L on POPC. The latter has its smallest distance to the bilayer at residues I_{12} and I_{14}, which are, however, still more than 0.4 nm away from the surface. The CF$_3$-Bpg label is, averaged over all peptides and simulations, more than 0.6 nm away from the surface. The unlabeled peptide on the POPC bilayer shows the same distance for position 8, whereas Ile-8 in [KIGAKI]$_3$ on the charged bilayer is closer to the membrane surface (around 0.4 nm). The *L*-labeled peptides insert deeper into the POPC/POPG membrane, which is expected from the previous results for [KIGAKI]$_3$, but for [KIGAKI]$_3$-8D it is the other way around. The average distance between the D-labeled peptide and membrane surface is 17% lower in the POPC bilayer system.

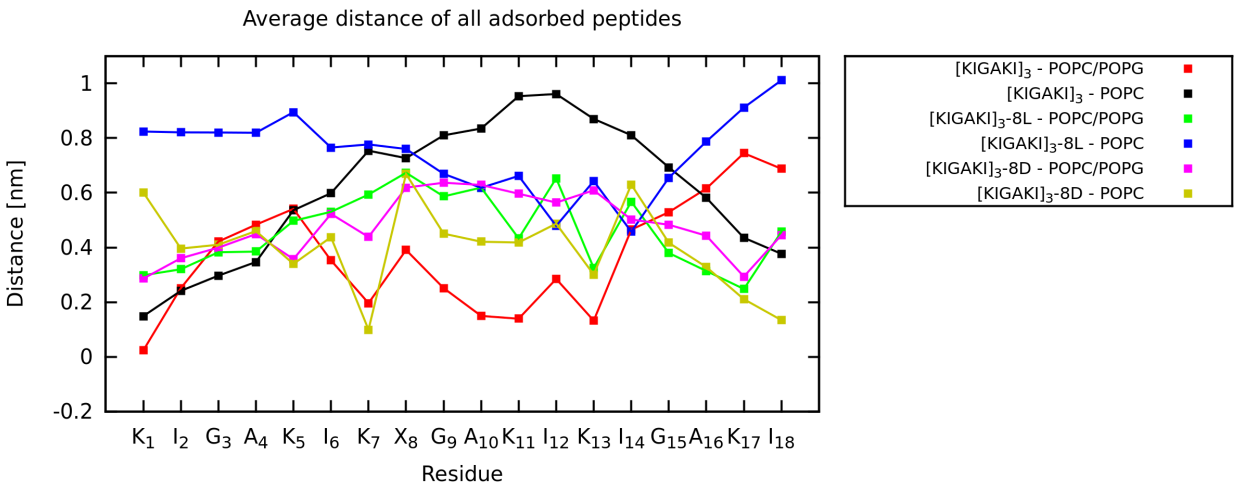

Figure 25: Distance between each peptide residue and the bilayer surface, averaged over time and all fully adsorbed peptides in the respective simulation. In the unlabeled [KIGAKI]$_3$ simulations X_8 corresponds to I_8, while in the labeled [KIGAKI]$_3$ simulations X_8 corresponds to *L*-CF$_3$ and *D*-CF$_3$ respectively.

5.2.2 Secondary structure

The simulation of [KIGAKI]$_3$-CF$_3$ in water already showed that the labeled peptides adopt different conformations than the unlabeled peptide. In this section, the secondary structure of [KIGAKI]$_3$-8L and [KIGAKI]$_3$-8D is in the presence of membranes is presented. The time evolution of the secondary structure elements is illustrated in Figure 26. The DSSP

plots showing the secondary structure for each residue over time are in Appendix 7.9.
In comparison with [KIGAKI]$_3$, the β-content of the *L*-form is remarkably lower, in favor of the drastically higher coil proportion. The *D*-enantiomers show an even lower β-content with an average of 6.1%. As it has been observed for the unlabeled peptide, the β-structure content is slightly higher in the POPC membrane system. On the POPC bilayer, the *L*-labeled peptides 3 and 6 form stable intramolecular β-sheets, which are slightly different from the ones for unlabeled [KIGAKI]$_3$. The majority of β-sheet forming [KIGAKI]$_3$ structures adopt a β-hairpin with the β-sheet between residues 5-8 and 14-17 and the a bend at residues 10-12, while residues 9 and 13 remain unstructured. [KIGAKI]$_3$-8L exhibits slight variations of this β-hairpin structure. Peptides 2 and 3 on the charged membrane show an extended bend at residues 9-11 and no coil-forming residues between the β-sheets and the bend. Peptide1 on the charged, and peptides 3 and 6 on the neutral membrane have a turn consisting of two residues at positions 8,9 and 10-11, respectively between the β-sheets, that are slightly similar to the cluster3 structure on the charged POPC/POPG bilayer. Also the only β-hairpin structure on the neutral membrane of *D*-labeled [KIGAKI]$_3$ (peptide3) possesses this structure with the turn at residues 8 and 9.
Another remarkable difference is the amount of intermolecular interactions between the peptides leading to dimer and trimer formation as illustrated in Figure 27. Peptides 1 and 4 of the *L*-labeled peptides with the POPC membrane form a stable dimer in water (Figure 27(a)). *D*-labeled peptides 1, 3 and 4 form a loose trimer in the water phase in the POPC bilayer system (Figure 27(d)). On the charged membrane, [KIGAKI]$_3$-8D peptides even aggregate to a relatively stable trimer on the lower leaflet, consisting of peptides 4-6 and a dimer on the upper leaflet, which is stable from 410 ns to 480 ns, formed by peptides 1 and 2 (Figure 27(b)+(c)). This oligomer formation is connected to an increase in β-sheet formation, which is best illustrated for the [KIGAKI]$_3$-8L dimer in the POPC system shown in Figure 27(a). Apart from the named peptides, the other monomeric ones are mostly unstructured, only a β-bridge between residues 13 and 17 is occasionally formed in all systems. The increased formation of intermolecular β-sheets in these simulations compared to the previous ones can have various reasons. The most important difference is believed to be the starting structure. Since labeled [KIGAKI]$_3$ did not form an intramolecular β-structure within a 100 ns simulation in water, a random coil conformation was used as a starting structure in the membrane simulations. Having no intramolecular hydrogen bonds, which would compete with intermolecular hydrogen bonds, the formation of intermolecular β-sheets is more favorable. Interestingly, we observed the formation of a dimer by [KIGAKI]-8L and a trimer by [KIGAKI]$_3$-8D in water. This was not expected since every peptide

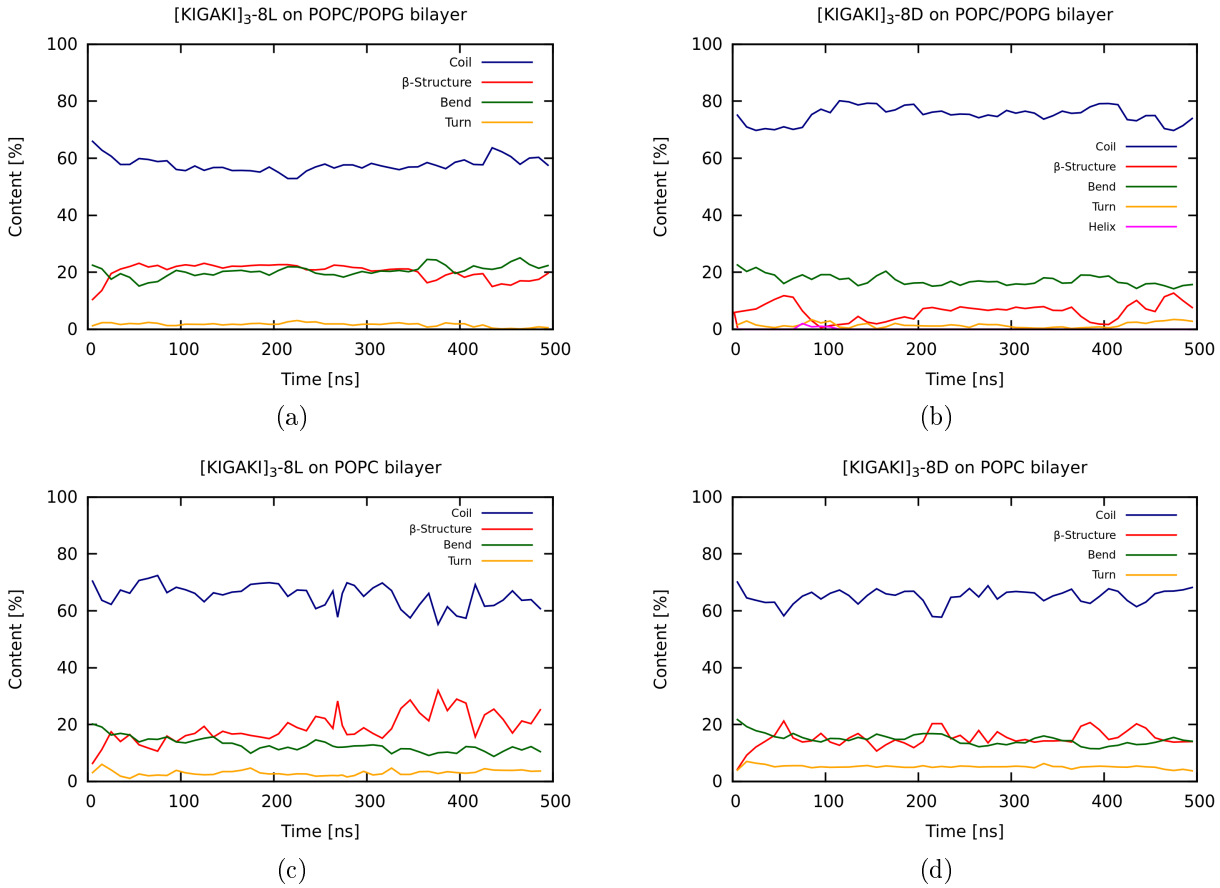

Figure 26: The secondary structure content of [KIGAKI]$_3$-CF$_3$ on the POPC/POPG and POPC bilayer is presented. β-structure includes β-sheet and β-bridge.

carries 7 positive charges, which repel each other. In these aggregates, the NH_3^+ groups in the lysine side chains point away from the β-sheets to gain the largest possible distance from each other as possible. Transmission electron microscopy (TEM) images of [KIGAKI]$_3$ fibrils in water already proved the existence of this species [23]. The authors stated, that this result suggests a pre-oligomerization or aggregation of the peptides before adsorption to membranes. However, this has not been observed in our simulations. The oligomers in the POPC systems did not adsorb on the bilayer surface within the simulation time and the oligomers on the POPC/POPG surface were formed on the bilayer leaflets, not in water. But this might be different on a larger timescale.

5.2.3 Orientation of the CF$_3$-Bpg label with respect to the bilayer normal

It has been suggested, that the label would prefer to insert in the hydrophobic environment of the membrane core, similar to the isoleucine it replaces [23].

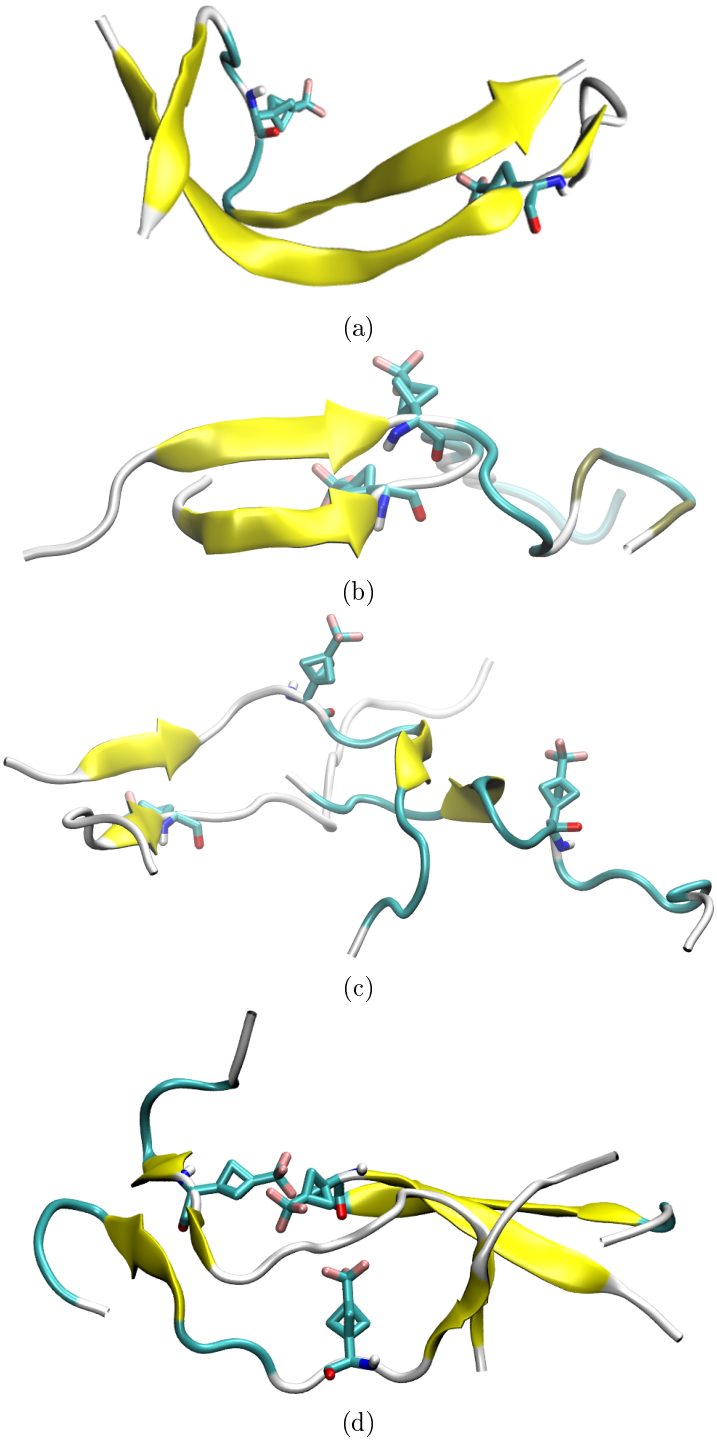

Figure 27: Assembly of labeled [KIGAKI]$_3$-CF$_3$ peptides. (a) shows *L*-labeled peptides 1 and 4 forming a stable dimer in water in the POPC system (snapshot taken after 310 ns). (b) and (c) illustrate the dimer (peptides 1 and 2) and trimer (peptides 4-6) formed by *D*-labeled peptides on the POPC/POPG bilayer surface (snapshot taken after 450 ns). (d) presents the trimer, which consists of *D*-labeled peptides 1, 3 and 4 that loosely aggregate in water in the neutral membrane system (snapshot taken after 430 ns). The CF$_3$ label is shown explicitly using the Licorice drawing in VMD [32].

In order to see if the CF$_3$-Bpg label has a preferred orientation with respect to the membrane, we calculated the angle between the CA-C8 bond vector (C8 corresponds to CB in the label) and the membrane normal for all adsorbed peptides. The angle distribution is presented in Figure 28.

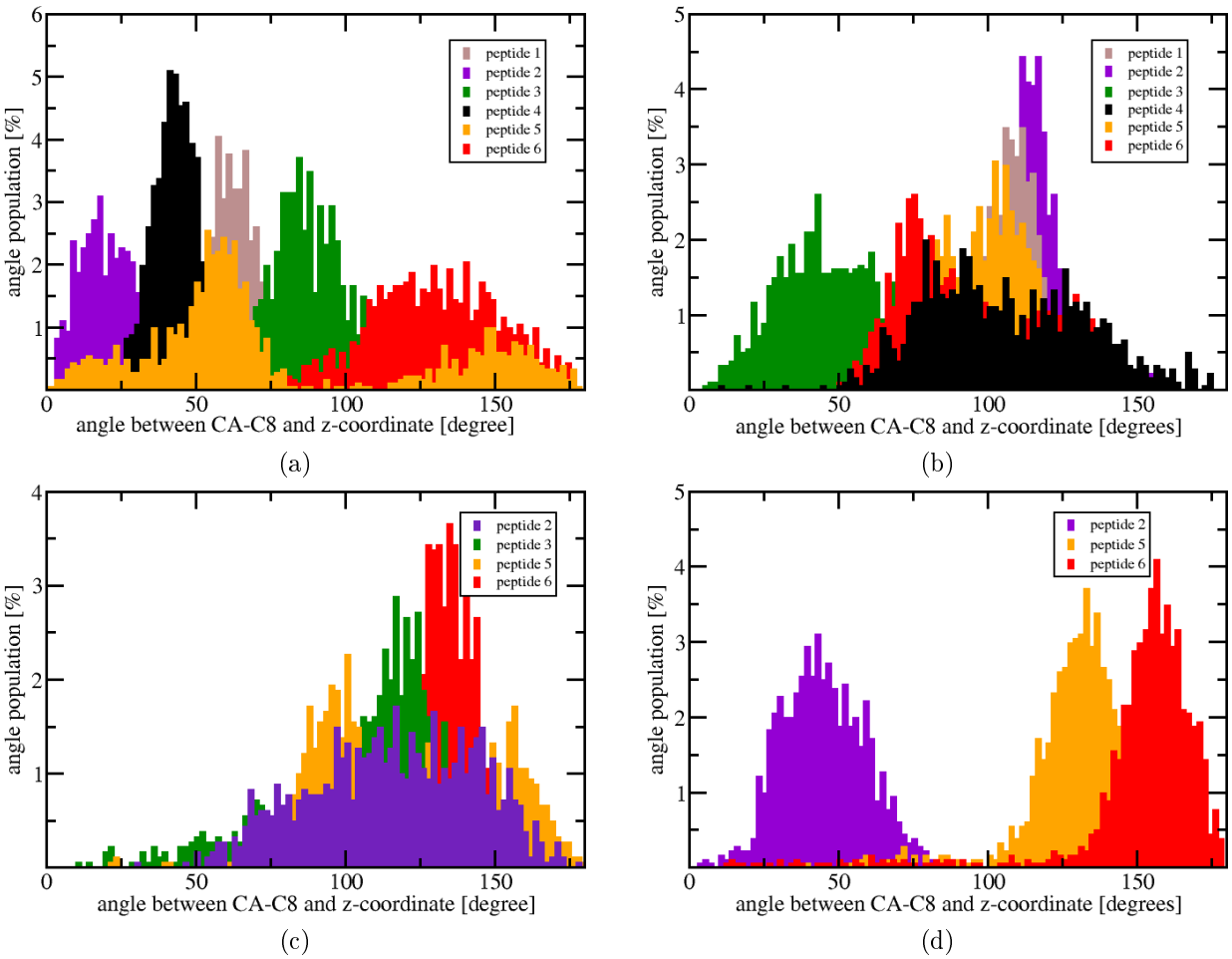

Figure 28: Distribution of the angle between the CA-C8 bond, connecting the CF$_3$ label to the backbone, and the membrane normal for: (a) [KIGAKI]$_3$-8L peptides on the POPC/POPG membrane (upper leaflet: 1,2,3; lower leaflet: 4,5,6), (b) [KIGAKI]$_3$-8D on POPC/POPG (upper leaflet: 1,2,3; lower leaflet: 4,5,6), (c) [KIGAKI]$_3$-8L on POPC (upper leaflet: 2,3; lower leaflet: 5,6) and (d) [KIGAKI]$_3$-8D on the POPC bilayer (upper leaflet: 2; lower leaflet: 5,6).

In all simulations, a wide distribution of the angle between the CF$_3$-Bpg label and the membrane normal is observed. In the *L*-labeled peptides 1, 2, 5 and 6 on the charged bilayer surface the label points mostly away from the surface, whereas in peptides 4 and 5 it point towards the membrane (Figure 28(a)). The *D*-labeled peptides, however, show the highest population around 100° for this angle. Only the *D*-CF$_3$ label of peptide3, which is the only monomer in this simulation, exhibits a preference to point away from the charged

membrane surface (Figure 28(b)). On the POPC bilayer, the *L*-label of peptides 2 and 3 has the tendency to point towards the bilayer surface, whereas the CF$_3$-Bpg group of peptides 5 and 6 show the opposite behavior (Figure 28(c)). All [KIGAKI]$_3$-8D peptides, that are adsorbed on the POPC bilayer, have a tendency to insert deeply into the headgroup region with K$_7$ (s. Appendix 7.8) so that the adjacent label sticks out and points away from the surface (Figure 28(d)).
In general, the angle distribution suggests that CF$_3$-Bpg points away from the membrane surface and therefore hardly interacts with the bilayer. This conclusion is supported by the rather large distance of > 0.6 nm, on average, between the label and the membrane (s. Figure 25). To describe the interaction between the CF$_3$ label and the bilayer, the following sections will present the hydrogen-bonds of specific residues, including residue 8, which carries the CF$_3$ label, and the interaction energies with the membrane.

5.2.4 Hydrogen-bonding

The interaction between the labeled peptides and the membrane models are analyzed in terms of hydrogen-bonds. Table 5 presents the hydrogen-bonds between the peptides, with specific residues given explicitly, and the lipids. Again, the hydrogen-bond ratio of the POPG and POPC lipids is shown to illustrate if the peptides prefer to interact with either of them.

System		POPC			POPG			POPG:POPC		
		Pep	LYS	CF$_3$	Pep	LYS	CF$_3$	Pep	LYS	CF$_3$
POPC/ POPG	[KIGAKI]$_3$-8L	6.91	5.10	0.10	5.18	3.34	0.13	0.75	0.66	1.30
	[KIGAKI]$_3$-8D	6.37	4.50	0.32	4.68	2.86	0.04	0.73	0.64	0.13
POPC	KIGAKI]$_3$-8L	7.21	4.89	0.04						
	KIGAKI]$_3$-8D	14.20	10.67	0.07						

Table 5: Number of hydrogen-bonds between the peptide (Pep), lysine residues (LYS) or CF$_3$-Bpg and POPC and POPG lipids. The hydrogen-bond ratio between the POPG and POPC lipids in the charged bilayer is shown as well. Averages are taken over the last 400 ns of simulation and all adsorbed peptides.

L- and *D*-enantiomers form nearly the same total number of hydrogen-bonds to the POPC/POPG bilayer. More than 66% of these hydrogen-bonds involve lysine residues, which play a crucial role in the interaction between [KIGAKI]$_3$-CF$_3$ and the bilayer. The CF$_3$-Bpg-residue

hardly forms hydrogen-bonds to the bilayer, which is expected since there is no donor or acceptor in the side chain, only in the backbone. Furthermore, the CF$_3$-Bpg-residue is generally not close to the bilayer surface (s. Appendix 7.8), and its backbone atoms are too far away to form stable hydrogen-bonds. The ratio between the hydrogen-bonds to the POPG and POPC lipids is striking. Keeping in mind, that the lipid ratio is POPG/POPC=0.2, the preference towards the POPG lipids is remarkable. Unlabeled [KIGAKI]$_3$ peptides show a similar preference, albeit to a lower extend. The average POPG/POPC ratio for the H-bond formation in the unlabeled [KIGAKI]$_3$ simulations is 0.36, which is 52% less than in the [KIGAKI]$_3$-8L and 51% less than in the [KIGAKI]$_3$-8D simulations. The total number of hydrogen-bonds has decreased around 23%, whereas the number of hydrogen-bonds to charged lipid increased. The formation of oligomers on the bilayer surface probably plays a role in the decreased number of hydrogen-bonds to the membrane surface. However, the shorter simulation length of 500 ns might also also play a role. The hydrogen-bonds between peptides and lipids steadily increased during the simulation and did not reach a steady value as it has been the case for the two 1 μs simulations with unlabeled [KIGAKI]$_3$. Thus, in the future the simulations with labeled [KIGAKI]$_3$ should be extended to 1 μs.
The number of hydrogen-bonds between [KIGAKI]$_3$-8D and the charged bilayer is comparable to [KIGAKI]$_3$-8L, whereas the total number of hydrogen-bonds between [KIGAKI]$_3$-8D and the POPC bilayer is clearly higher. This was not expected, because only three *D*-labeled peptides adsorbed on the bilayer surface, whereas four *L*-labeled peptides adsorbed on the neutral membrane. The stronger interaction between [KIGAKI]$_3$-8D and the POPC membrane (s. also Table 6) explains, however, the small distance between these peptides and the membrane surface, which was observed in Figure 25. Lysine residues of [KIGAKI]$_3$ form 75% of the hydrogen- bonds and are therefore responsible for the deep insertion of the peptides.

5.2.5 Interaction energies

In order to further investigate what influence the CF$_3$-Bpg label has on the interaction between peptides and each bilayer type, their interaction energy was calculated. The results are shown in Table 6.

The overall energy is similar to the unlabeled [KIGAKI]$_3$ interaction energies: the interaction between peptides and bilayer is in all cases dominated by electrostatic interactions. The key interacting residues are again lysine residues, which contribute more than 80% to the Coulomb energy. Furthermore, the interactions with the charged bilayer are stronger than

System		LJ energy [kJ/mol]			Coulomb energy [kJ/mol]		
		Pep	LYS	CF$_3$	Pep	LYS	CF$_3$
POPC/POPG	[KIGAKI]$_3$-8L	-315.1	-107.7	-13.7	-1244.7	-1058.5	-3.6
	[KIGAKI]$_3$-8D	-308.0	-111.1	-14.8	-933.4	-757.8	-16.1
POPC/POPG	[KIGAKI]$_3$-8L	-92.8	-33.0	-4.8	-438.8	-383.2	-1.8
	[KIGAKI]$_3$-8D	-82.9	-29.5	-4.1	-330.1	-273.9	+1.1
POPC	[KIGAKI]$_3$-8L	-257.7	-69.7	-13.1	-689.9	-556.6	-11.3
	[KIGAKI]$_3$-8D	-364.0	-116.0	-16.9	-1358.7	-1165.4	-16.4

Table 6: Energies for the interaction of the lipids with CF$_3$-labeled [KIGAKI]$_3$ (Pep), lysine (LYS) and CF$_3$-Bpg-residues respectively. For the POPC/POPG bilayer system, the interacting lipid type(s) has been underlined. Interaction energies were calculated for snapshots taken every 200 ps for the last 50 ns of each simulation. Thus, 250 structures were considered. The energies are averaged over these structures and the adsorbed peptides.

with the zwitterionic one. As indicated by the hydrogen-bonds, the interactions between the labeled peptides and the charged POPG lipids is higher compared to the unlabeled [KIGAKI]$_3$ peptides and the according lipid type. 35% of the electrostatic interactions between the CF$_3$-labeled peptides and the bilayer involve POPG lipids, whereas only 26% were contributed by POPG lipids in the unlabeled [KIGAKI]$_3$ systems. A marked difference is, however, the electrostatic interaction between the CF$_3$-residue and the negatively charged POPG lipids. The *L*-enantiomer shows a weak attraction like the [KIGAKI]$_3$, whereas the *D*-labeled analog shows a repulsion of +1.1 kJ/mol per adsorbed peptide. This can be explained with the negative partial charges of the fluorine atoms that are repeled by the negatively charged headgroup of the POPG lipids. This increases the energy barrier for CF$_3$-Bpg groups to insert into the bilayer, which has been hardly observed in our simulations (s. Figure 28 and Appendix 7.8). The attraction of [KIGAKI]$_3$-8D towards the neutral POPC bilayer is in total 81% higher than [KIGAKI]$_3$-8L, which mainly arises from stronger electrostatic interactions of lysine residues in [KIGAKI]$_3$-8D with the membrane. The interaction over time is illustrated in Figure 29.

As it has been observed for the unlabeled peptides, the LJ energy decreases at the beginning and reaches a constant value after around 100 ns, whereby the interaction between the

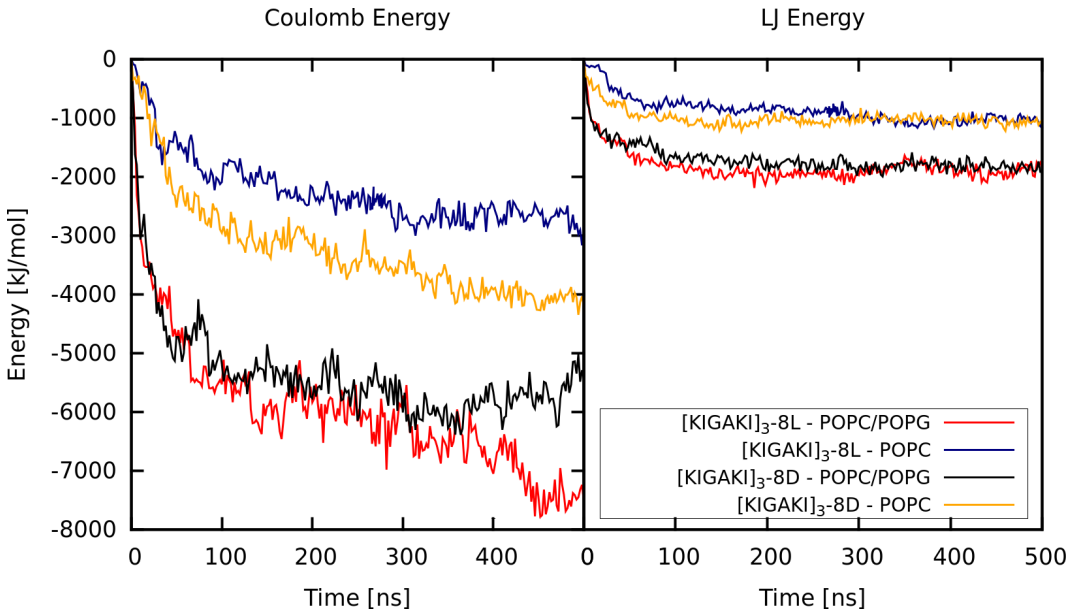

Figure 29: Interaction energies between CF$_3$-labeled peptides and the different bilayers over time and averaged over peptides.

peptides with the charged membrane is by a factor of 2 stronger compared to the zwitterionic one. The adsorption is triggered by electrostatic interactions, especially in the charged membrane system where a rapid decrease in Coulomb energy is observed at the very beginning of the simulation. The electrostatic interaction energy between [KIGAKI]$_3$-8D and the POPC membrane is lower than for the *L*-labeled peptide. On the charged membrane, however, [KIGAKI]$_3$-8L forms stronger interactions to the membrane, especially in the last 100 ns this Coulomb energy decreases drastically. This can be explained by a deeper insertion of the peptides (s. Figure 24) into the headgroup region of the bilayer. At the same time, the electrostatic interaction energy between [KIGAKI]$_3$-8D and the charged bilayer increases, which is possibly due to enhanced oligomer formation and therefore less interactions between peptides and membrane.

5.3 Discussion

The simulations of [KIGAKI]$_3$-CF$_3$-Bpg in water showed that the folding of the labeled peptides differ from that of the unlabeled [KIGAKI]$_3$ peptides. Only unstable β-sheets and β-bridges were formed in the termini region of the peptide. This leads to a mostly unstructured conformation, which hardly forms any intramolecular interactions or hydrogen bonds.

The simulations involving the bilayer models showed formation of oligomers in water and on

partly charged membrane surfaces. As the monomeric structure in water has a low tendency to form intramolecular hydrogen-bonds as opposed to the unlabeled peptide, the formation of intermolecular β-sheets is certainly easier. The aggregation of [KIGAKI]$_3$ in water has been shown experimentally [23] as well as the formation of aggregates on membrane surfaces [23, 27]. The membrane selectivity, which has been observed for unlabeled [KIGAKI]$_3$ peptides, is found in the simulations on the CF$_3$-labeled [KIGAKI]$_3$ as well. All *D*- and *L*-labeled peptides adsorbed on the partly charged bilayer, whereas four of the six [KIGAKI]$_3$-8L peptides and only three of the six [KIGAKI]$_3$-8D peptides adsorbed on the zwitterionic POPC bilayer.

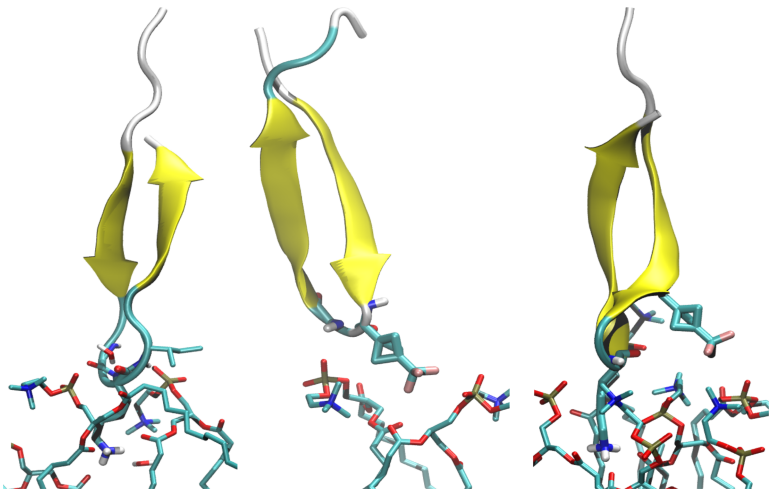

Figure 30: Cluster2 after 70 ns (left), peptide3 of [KIGAKI]$_3$-8D after 180 ns (middle) and peptide3 of [KIGAKI]$_3$-8L after 50 ns (right) on the POPC bilayer.

This leads to a lower concentration of [KIGAKI]$_3$-8D on the POPC bilayer surface. It has been reported that, in comparison with unlabeled [KIGAKI]$_3$ and [KIGAKI]$_3$-8L [24], a higher concentration of [KIGAKI]$_3$-8D peptides is needed for the peptides to aggregate. This might be a result of the reduced adsorption of [KIGAKI]$_3$-8D on POPC. The active concentration, which is needed in order to observe an antimicrobial effect, is a minimum inhibitory concentration of 7.5 μM [24]. This was estimated to correspond to a P/L ratio of 100:1 that strongly suggests [KIGAKI]$_3$ to be aggregated. Hence, the aggregates are believed to be the toxic species [24]. Therefore, the reduced tendency of [KIGAKI]$_3$-8D to adsorb on neutral membranes might contribute to the reduced hemolytic activity, while the adsorption on charged bilayers shows only small differences in respect to the unlabeled and *L*-labeled peptides. The average insertion depth of labeled and unlabeled peptides on the POPC/POPG bilayer (s. Figure 25) is quite similar, however, the N-terminus and residues I$_6$-K$_{13}$ of [KIGAKI]$_3$ are around 0.3 nm closer to the surface, whereas the C-terminus is around 0.2 nm further away from the bilayer surface than in the labeled [KIGAKI]$_3$ analogs. The relatively large distance between the central

residues of labeled [KIGAKI]$_3$ may result from the repulsion between the CF$_3$ label and POPG headgroups, which has been observed earlier (s. Table 6). The difference in the secondary structure may contribute to the different adsorption behavior on the neutral POPC membrane. The presence of CF$_3$-Bpg in the peptide sequence leads to an extended β-sheet in the β-hairpin structures and a conversion of the bend, consisting of 5 residues (G$_9$-K$_{13}$) in [KIGAKI]$_3$, into a turn, consisting of only 2 residues (s. Figures 45 and 47 in Appendix 7.9). The turn in [KIGAKI]$_3$-8L on the POPC membrane is at residues A$_{10}$ and K$_{11}$, whereas the turn in [KIGAKI]$_3$-8D is formed at residues DCF3 and G$_9$. As shown in Figure 30, K$_{11}$ of [KIGAKI]$_3$ (left) and [KIGAKI]$_3$-8L (right) inserts into the headgroup region of the POPC bilayer and anchors the peptide in the membrane. The turn of [KIGAKI]$_3$-8D is, as mentioned, at residues DCF3 and G$_9$, which do not have a side chain that can insert deeply into the headgroup region of the bilayer and form stable hydrogen-bonds. Moreover, Figure 30 also illustrates that the bulky CF$_3$-Bpg group of [KIGAKI]$_3$-8D, when close to the headgroup region, holds the peptide backbone further away from the bilayer surface. This might prevent [KIGAKI]$_3$-8D from forming stable hydrogen-bonds with the lipid bilayer and thus lead to the desorption or reduced adsorption of [KIGAKI]$_3$-8D, which has been observed in this work and is in good agreement with experimental findings, as discussed previously in this section. However, this result is based on one [KIGAKI]$_3$-8D and two [KIGAKI]$_3$-8L peptides that form a β-hairpin structure on the POPC bilayer. Therefore, these results should be treated with caution and more simulations that focus on the adsorption process should be performed in order to validate these findings.

6 Summary and Outlook

In this work we have analyzed the adsorption process and the behavior of $[KIGAKI]_3$ on two different membrane systems using molecular dynamics (MD) simulations. We observed more peptides adsorbing to the negatively charged POPC/POPG bilayer than to the neutral POPC membrane, which results from strong electrostatic attraction between the negatively charged membrane and the cationic $[KIGAKI]_3$ that also leads to a faster and deeper insertion of $[KIGAKI]_3$ into the POPC/POPG headgroup region. Differences were also observed in the secondary structure of $[KIGAKI]_3$. On POPC/POPG, some peptides unfold, which leads to a lower β-content than in the POPC simulation where $[KIGAKI]_3$ retains its β-hairpin structure. Upon addition of six peptides, the membrane properties of the neutral POPC membrane did not change, whereas the charged bilayer got perturbed. However, the increased area per lipid (APL) and the decrease in deuterium order parameters S_{CD} that were observed for the POPC/POPG bilayer may be due to either the addition of $[KIGAKI]_3$ peptides or the reduction of Na^+ ions as discussed previously. In order to clarify the involvement of the peptides in membrane perturbation, the simulations should be carried out again, retaining a constant salt concentration.
The attachment of the CF_3-Bpg label to the peptide leads to differences in the secondary structure. During a 100 ns simulation in water no β-hairpin structure was observed for the labeled peptides, which was present for $[KIGAKI]_3$. Also, fewer *D*-labeled $[KIGAKI]_3$ peptides adsorb on the POPC bilayer compared to *L*-labeled and unlabeled peptides. This may result from the formation of an extended β-sheet in $[KIGAKI]_3$-8D on POPC that leads to a smaller turn region, which does not involve a lysine residue that is able to anchor into the bilayer surface. In addition, oligomers in water and on the membrane surface were observed with both bilayer systems for *D*- and *L*-labeled peptides, but not for $[KIGAKI]_3$. It is not clear, however, if the different starting structure for the six-peptide simulations leads to the aggregation of $[KIGAKI]_3$ or the attachment of the CF_3-Bpg label. Therefore, the influence of the starting structure on oligomer formation in the labeled $[KIGAKI]_3$ simulations will be further analyzed by performing two additional six-peptide simulations in which the starting structures of $[KIGAKI]_3$ and labeled $[KIGAKI]_3$ will be interchanged.

So far, we focused on the pre-aggregation stage and the formation of oligomers, since the simulation length is simply not long enough to actually observe fibril formation. Nevertheless, it would be interesting to analyze the stability of $[KIGAKI]_3$ fibrils and their effects on membrane properties. Firstly, because more experimental data for fibrils are available that

allows to validate the simulations. Secondly, it has been reported that fibrils are most likely the toxic species with the desired ability to disrupt bacterial cell-membranes [24]. Since fibril formation cannot be observed on the μs timescale of our simulations, it would be required to start with already formed $[KIGAKI]_3$ fibrils. Since the $[KIGAKI]_3$ fibril structure is not known yet, a fibril model has to be created. These fibrils could be put in different orientations on the bilayer surface in order to investigate, for example, whether the hydrophobic or hydrophilic peptide domain points inside the membrane headgroup region and how deeply they insert. From these simulations it may be possible to conclude how $[KIGAKI]_3$ disrupts negatively charged bilayers. The same can be done for the *D*-labeled peptide, since this shows the lowest hemolytic activity, thus least toxicity for eukaryotic cells, while the antimicrobial activity is similar for the unlabeled and *L*-labeled peptides [24]. Therefore, *D*-labeled $[KIGAKI]_3$ is most suitable for potential drug design.
To our knowledge, there is no precise data available that describes the structure of $[KIGAKI]_3$ fibrils, apart from the 98% β-content derived from CD measurements [27] that indicates an elongated structure. However, in order to build fibril models, it would be beneficial to know specific features of the structure. In particular, if $[KIGAKI]_3$ fibrils consist of elongated peptides and if the β-sheets are parallel or anti-parallel. Therefore, several techniques to obtain these data will be explored. Förster resonance energy transfer (FRET) can be used to measure the distance between a donor and an acceptor, which could be assigned to both termini of the $[KIGAKI]_3$ peptide. A small distance would indicate a β-hairpin structure being involved in fibril formation, a larger distance ($\sim$ 6 nm, corresponding to the N-C termini distance) would point towards an elongated structure. However, some problems arise here: fluorophores that are used as donor or acceptor contain at least one conjugated π-system, which implies a large size of the label compared to the peptide size of 18 aminoacids and therefore is likely to influence its behavior. Furthermore, the peptide sequence is very homogeneous, therefore it might be critical to attach the label to the desired residues.
A more promising option is the H/D exchange combined with nuclear magnetic resonance (NMR) as described in [74, 75]. The buried hydrogen atoms exchange slower with the deuterium atoms in the solvent and therefore the ^{1}H signal of the corresponding residues lasts for a longer time. If an elongated state is present, only the signal for the termini residues would disappear quickly. However, if a β-hairpin structure is the basis of the fibril structure, also residues involved in the turn/bend would exhibit a rapid decreasing signal intensity. Using this method it may be possible to gain important information that are required to construct a fibril model, that could be used in future simulations testing the membrane disruption mechanism of $[KIGAKI]_3$ fibrils.

7 Appendix

7.1 Simulation Setup

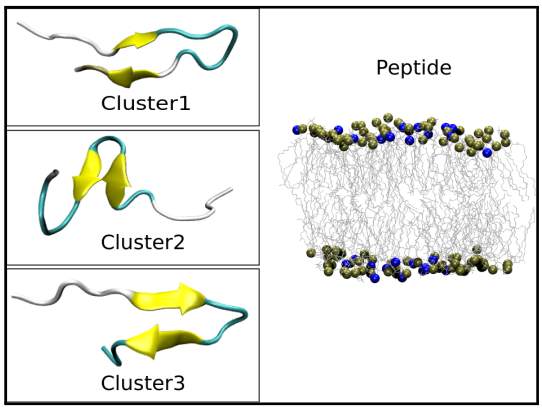

Figure 31: The initial system for the POPC/POPG simulations with the corresponding starting structures is shown here. The peptide is placed around 1.5 nm away from the membrane surface. To illustrate the headgroup region, the phosphorus atoms are shown in VDW representation, here tan spheres correspond to POPC and blue to POPG lipids. The input system for the POPC simulations is the same apart from the absence of the POPG lipids.

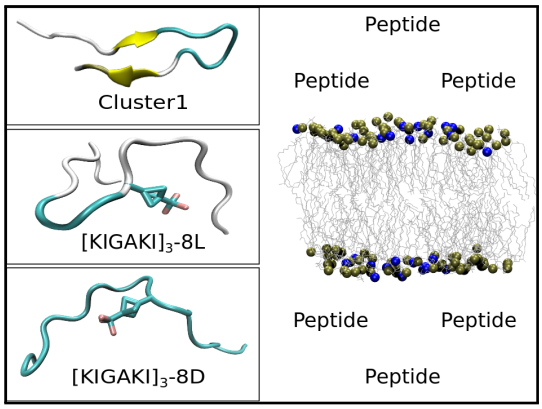

Figure 32: Simulation setup of the simulation with six [KIGAKI]$_3$ peptides on a POPC/POPG bilayer. The peptides are placed with enough space between them and to the bilayer surfaces. The corresponding structures are shown on the left. To illustrate the headgroup region, the phosphorus atoms are shown in VDW representation, here tan spheres correspond to POPC and blue to POPG lipids. The pure POPC system looks similar, again only POPG lipids are substituted by POPC lipids.

7.2 Lipids

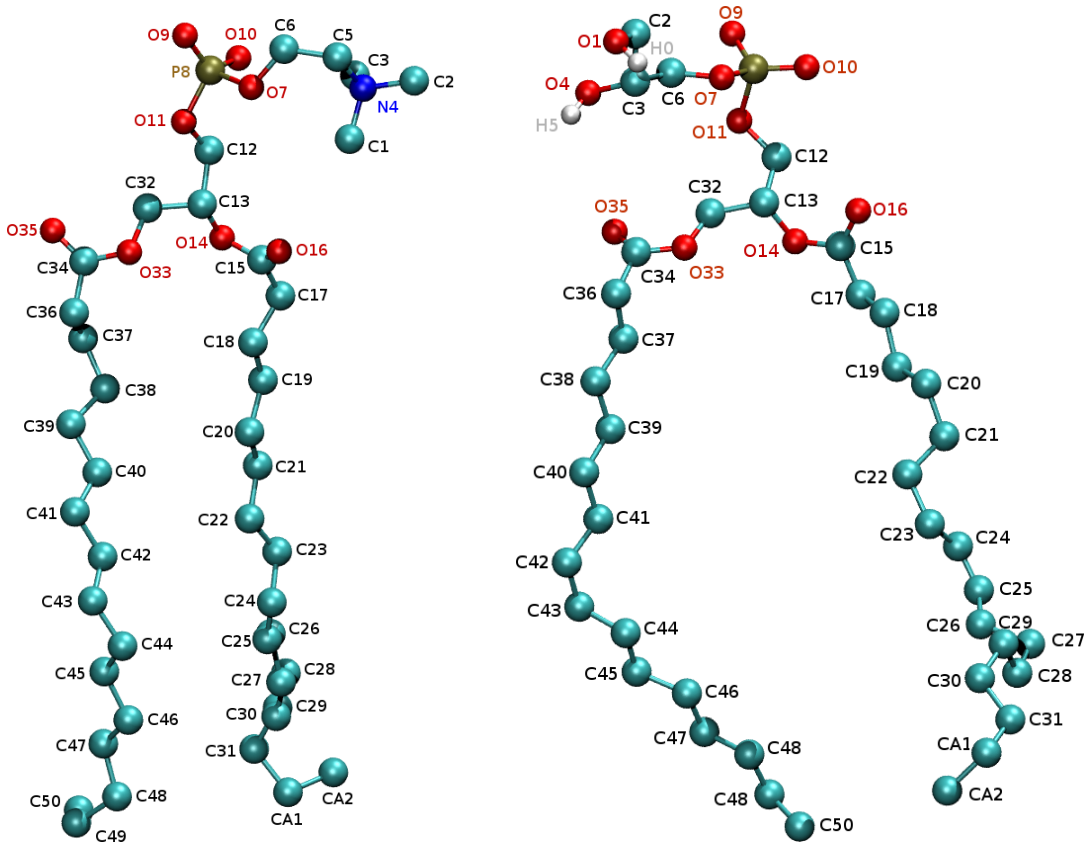

Figure 33: The two lipid types, which are present in the membranes that were in our simulations are presented. (a) illustrates one POPC lipid, (b) shows one POPG lipid.

7.3 Adsorption of six [KIGAKI]$_3$ peptides in the six-peptide simulations

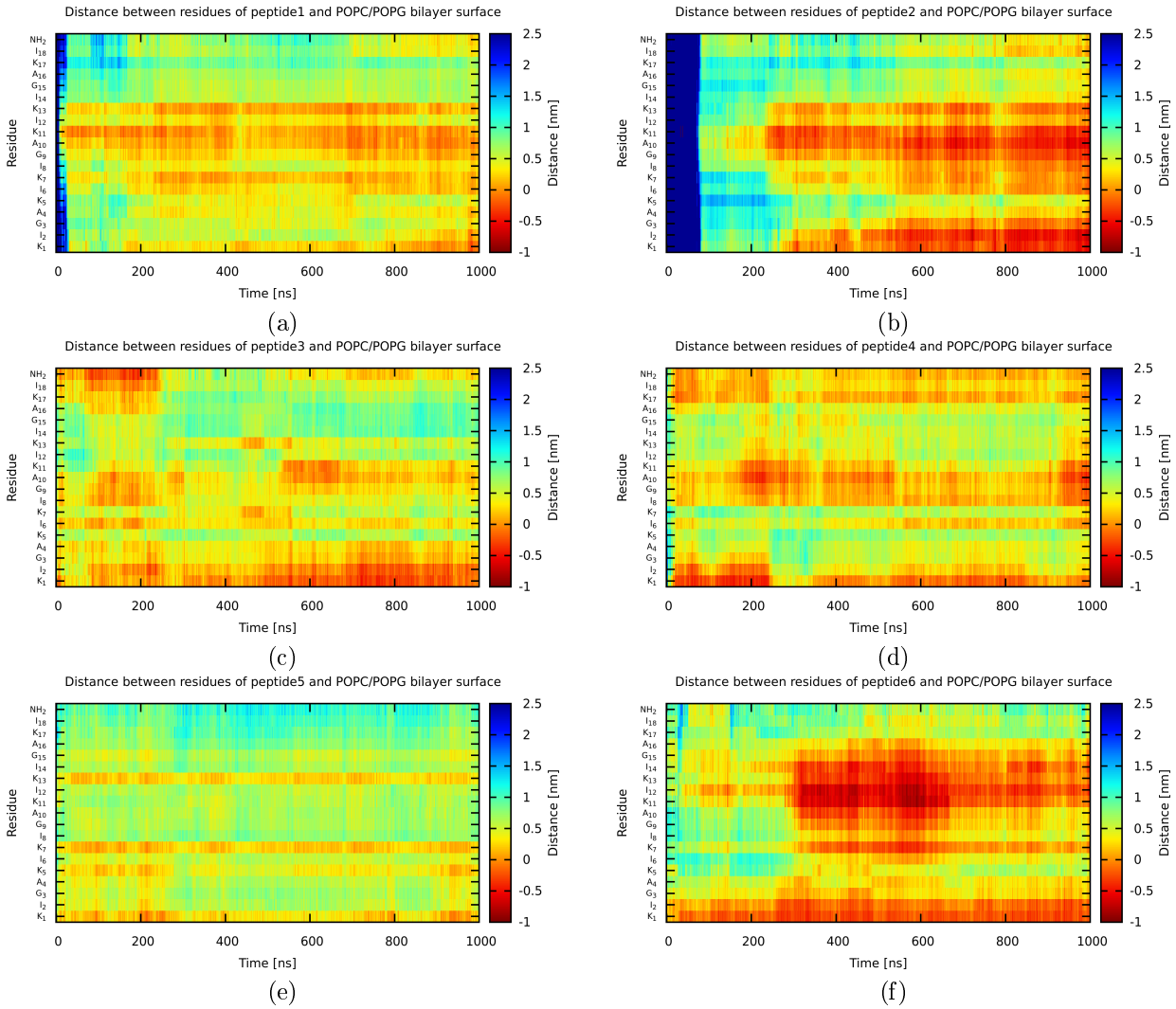

Figure 34: The distance between each residue of the six [KIGAKI]$_3$ peptides and the POPC/POPG membrane surface is shown.

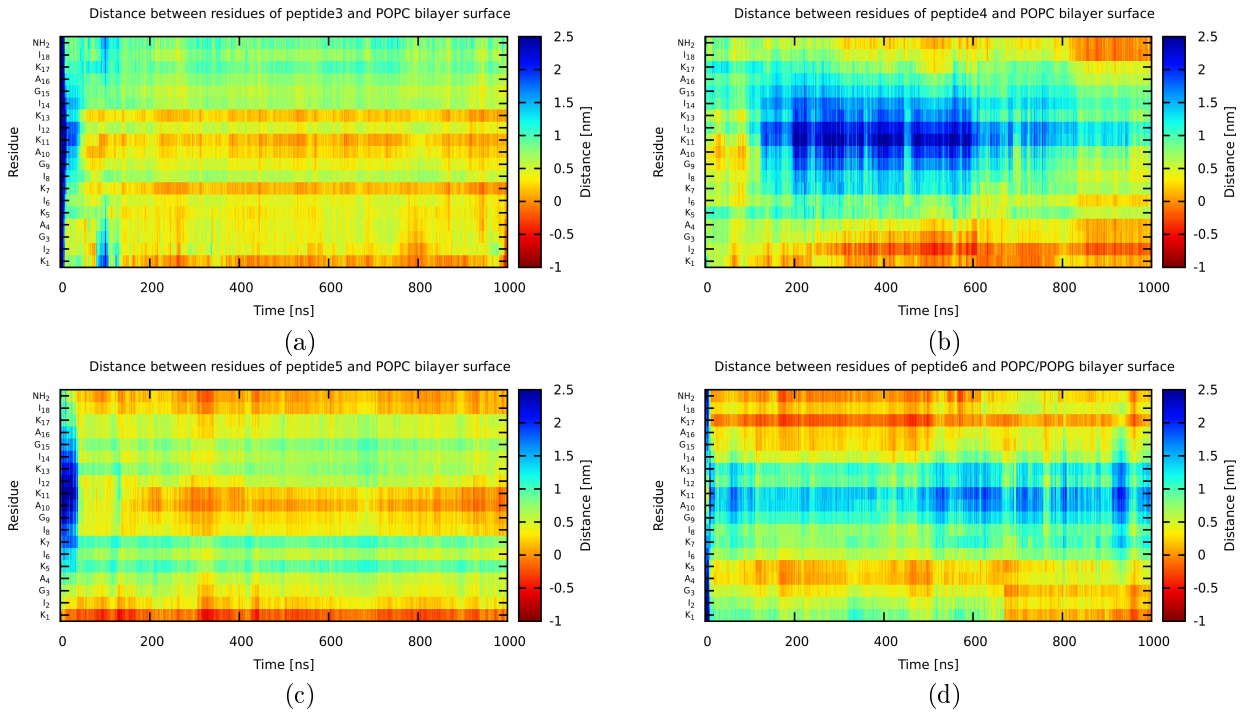

Figure 35: The Distance between each residue of the four adsorbing $[KIGAKI]_3$ peptides and the POPC membrane surface is illustrated here. Peptide1 and peptide2 do not adsorb during the 1 μs simulation, but stay in the water phase.

7.4 Secondary structure of six-peptide simulations

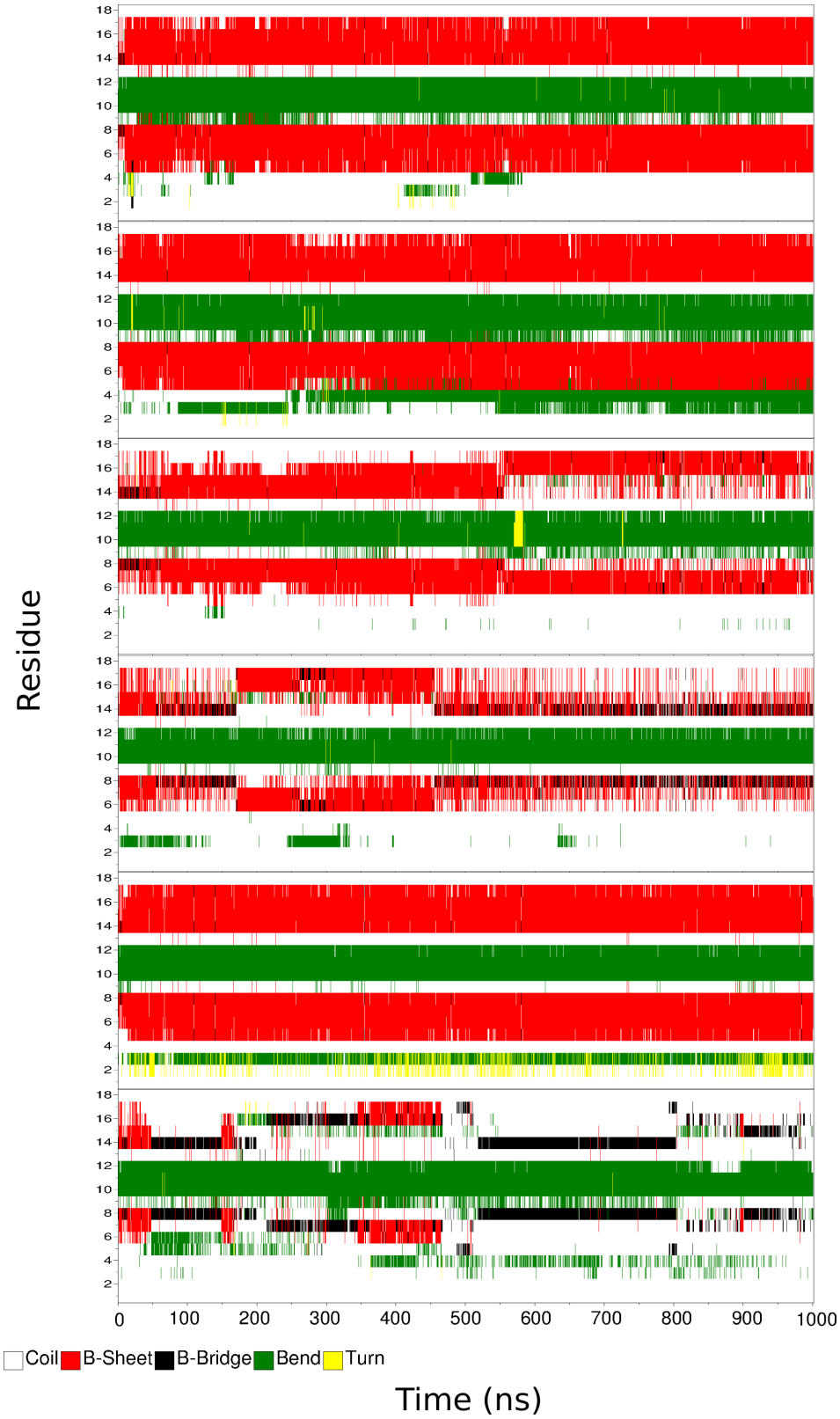

Figure 36: Secondary structure of six $[KIGAKI]_3$ peptides on the POPC/POPG bilayer. Peptide1 to peptide6 are shown from top to bottom.

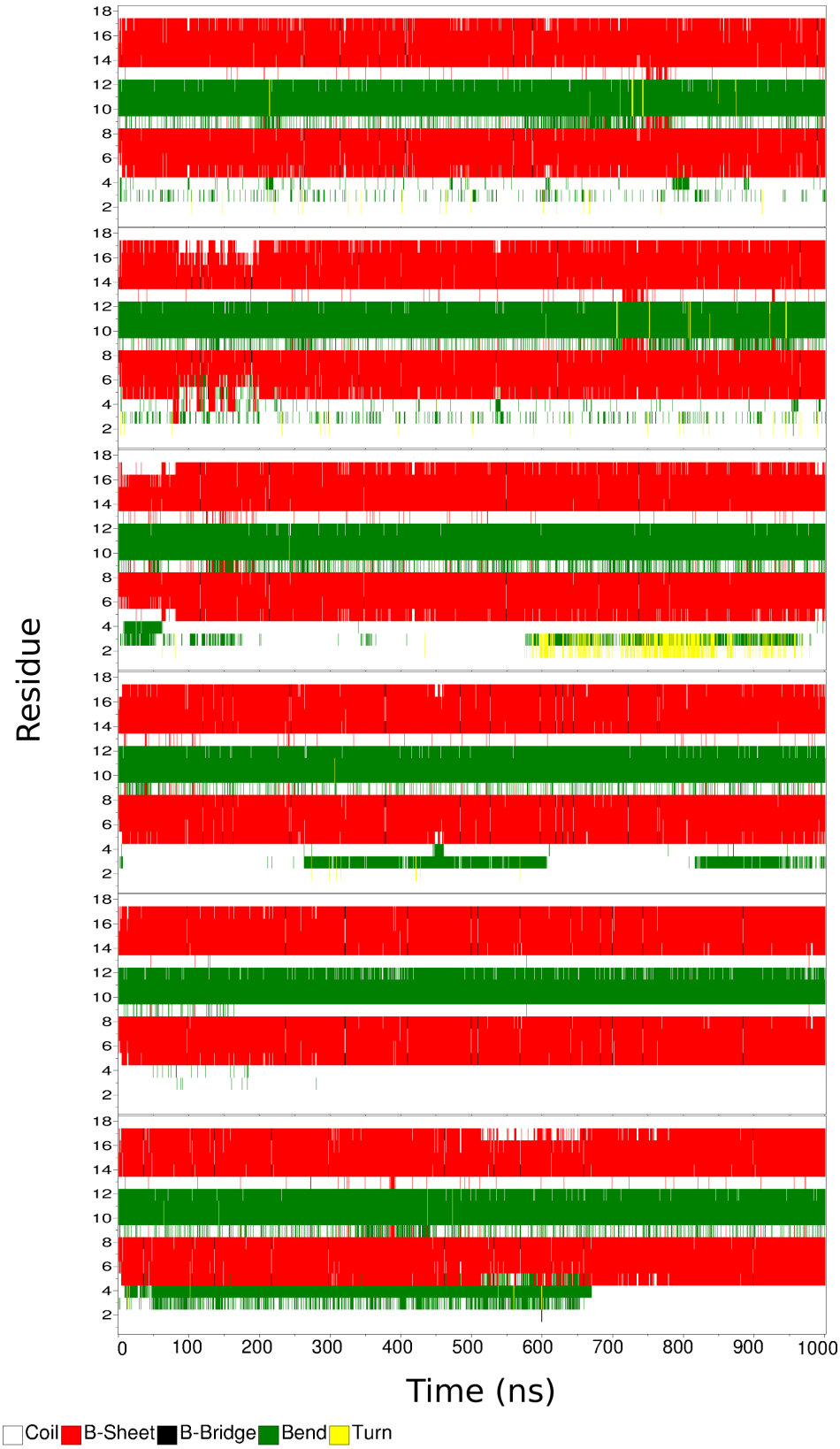

Figure 37: Secondary structure of six $[KIGAKI]_3$ peptides on the POPC bilayer. Peptides1 to peptide6 are shown from top to bottom. Peptides 1 and 2 stay in water during the whole simulation.

7.5 Correlation between secondary structure and insertion depth

Residue	β-Sheet	Bend	Turn	β-Bridge	Coil	insertion Depth [nm]
K_1	0	0	0	0	1	0.08
I_2	0	0	0.05	0	0.95	0.27
G_3	0	0.27	0.05	0	0.68	0.48
A_4	0	0.19	0	0	0.81	0.51
K_5	0.45	0.03	0	0.01	0.51	0.65
I_6	0.72	0.02	0	0.01	0.26	0.43
K_7	0.80	0	0	0.03	0.17	0.37
I_8	0.71	0.01	0	0.13	0.15	0.44
G_9	0.02	0.29	0	0	0.69	0.32
A_{10}	0	0.99	0.01	0	0	0.21
K_{11}	0	0.99	0.01	0	0	0.22
I_{12}	0	0.96	0	0	0.04	0.41
K_{13}	0.02	0	0	0	0.98	0.29
I_{14}	0.68	0	0	0.12	0.20	0.57
G_{15}	0.71	0.04	0	0.015	0.23	0.62
A_{16}	0.72	0.01	0	0.03	0.24	0.66
K_{17}	0.62	0	0	0.01	0.37	0.74
I_{18}	0	0	0	0	1	0.63

Table 7: The average insertion depth of each residue and the corresponding secondary structure element population on the POPC/POPG bilayer is given. The values are averaged over all six peptides after adsorption happened. The insertion depth is calculated by averaging the distance in z-direction between the phosphorous atoms of the lipids and the COM of each residue. The average insertion over all residues is 0.45 nm.

Residue	β-Sheet	Bend	Turn	β-Bridge	Coil	insertion Depth
K_1	0	0	0	0	1	0.17
I_2	0	0	0.03	0	0.97	0.30
G_3	0	0.24	0.03	0	0.73	0.38
A_4	0.01	0.15	0	0	0.84	0.42
K_5	0.91	0.02	0	0	0.70	0.60
I_6	0.98	0	0	0	0.02	0.60
K_7	0.99	0	0	0	0.01	0.75
I_8	0.98	0	0	0.01	0.01	0.71
G_9	0.03	0.24	0	0.01	0.72	0.78
A_{10}	0	1	0	0	0	0.80
K_{11}	0	1	0	0	0	0.91
I_{12}	0	1	0	0	0	0.94
K_{13}	0.03	0	0	0	0.97	0.85
I_{14}	0.98	0	0	0.01	0.01	0.83
G_{15}	0.99	0	0	0	0.01	0.74
A_{16}	0.98	0	0	0	0.02	0.64
K_{17}	0.91	0	0	0	0.9	0.54
I_{18}	0	0	0	0	1	0.44

Table 8: The average insertion depth of each residue and the corresponding secondary structure element population on the POPC bilayer is given. For further details see caption of Table 7. The average insertion over all residues is 0.62 nm, which is 38% higher than for the charged membrane system.

7.6 Na^+ density

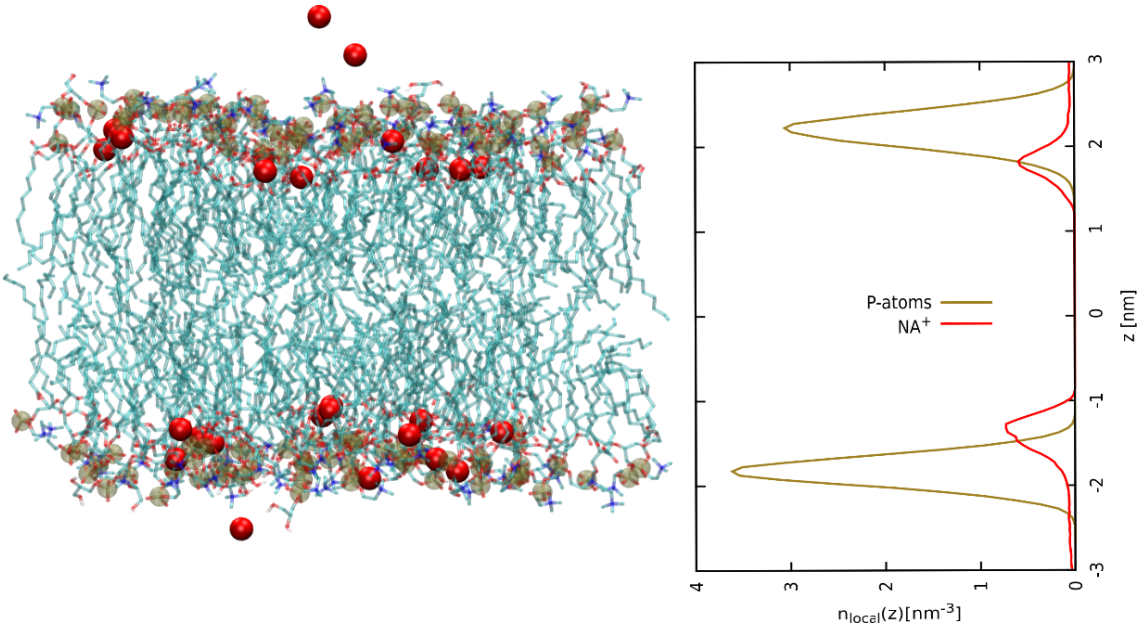

Figure 38: Sodium-ion and phosphorus-atom density in the pure POPC/POPG bilayer simulation. Values are calculated over the last 100 ns of the 200 ns simulation.

7.7 Water density

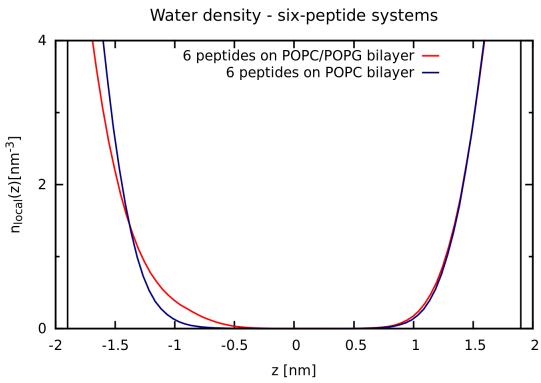

(a)

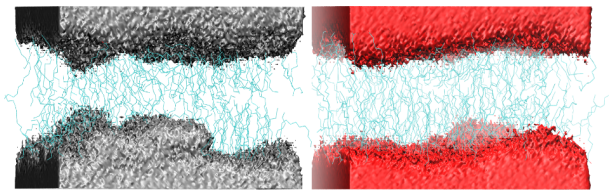

(b)

Figure 39: (a) Water density along the z-axis is presented for the six-peptide simulations. The average position of phosphorus atoms is illustrated with two vertical lines. (b) Illustrates the water density in 3D in (left) POPC/POPG and (right) POPC headgroup region. Over the whole simulation water molecules close to the membrane surface were counted. The positions are presented using the Isosurface representation.

7.8 Adsorption of CF_3-labeled peptides

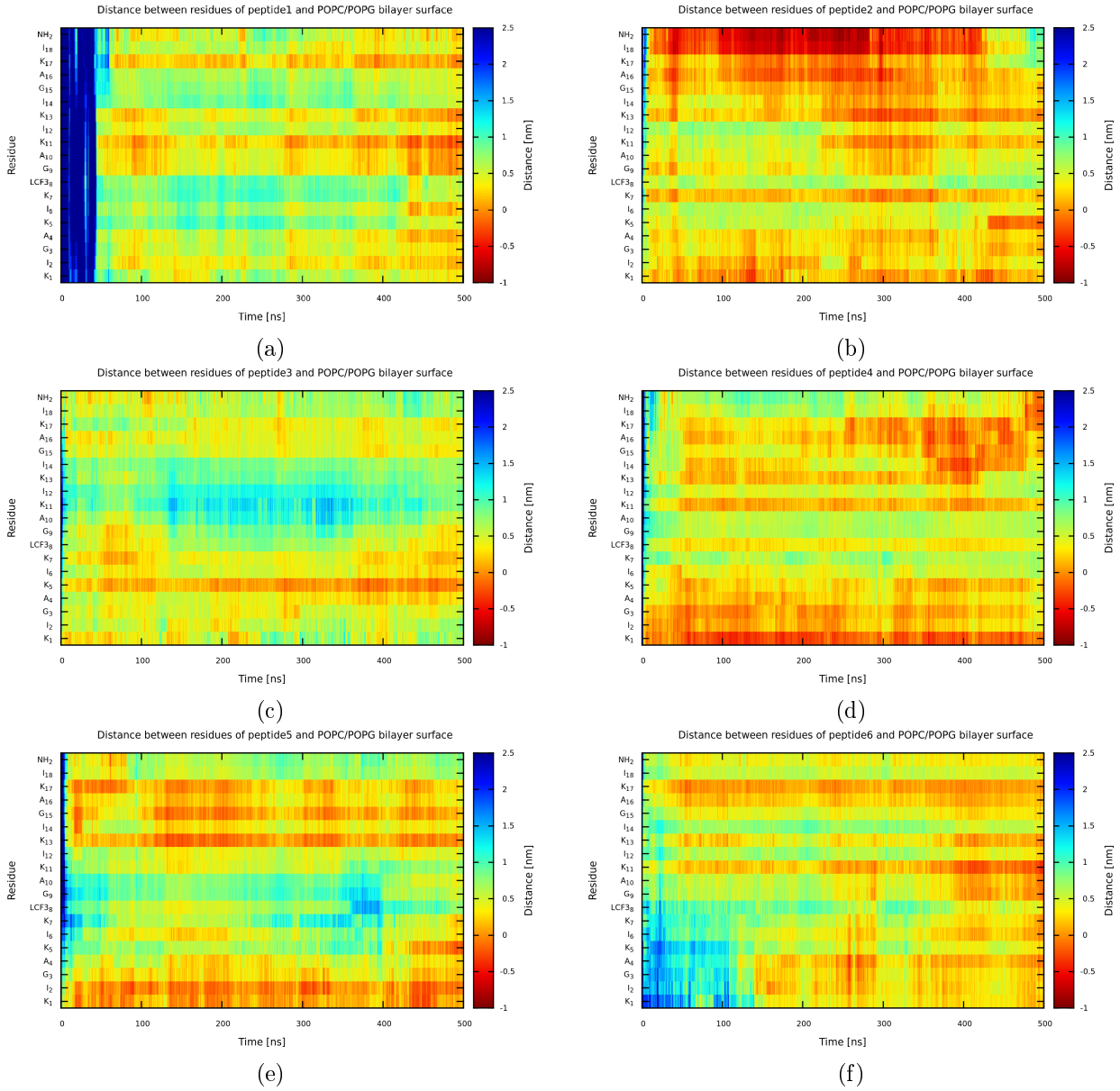

Figure 40: The distance between each residue of the six $[KIGAKI]_3$-8L peptides and the POPC/POPG membrane surface is shown.

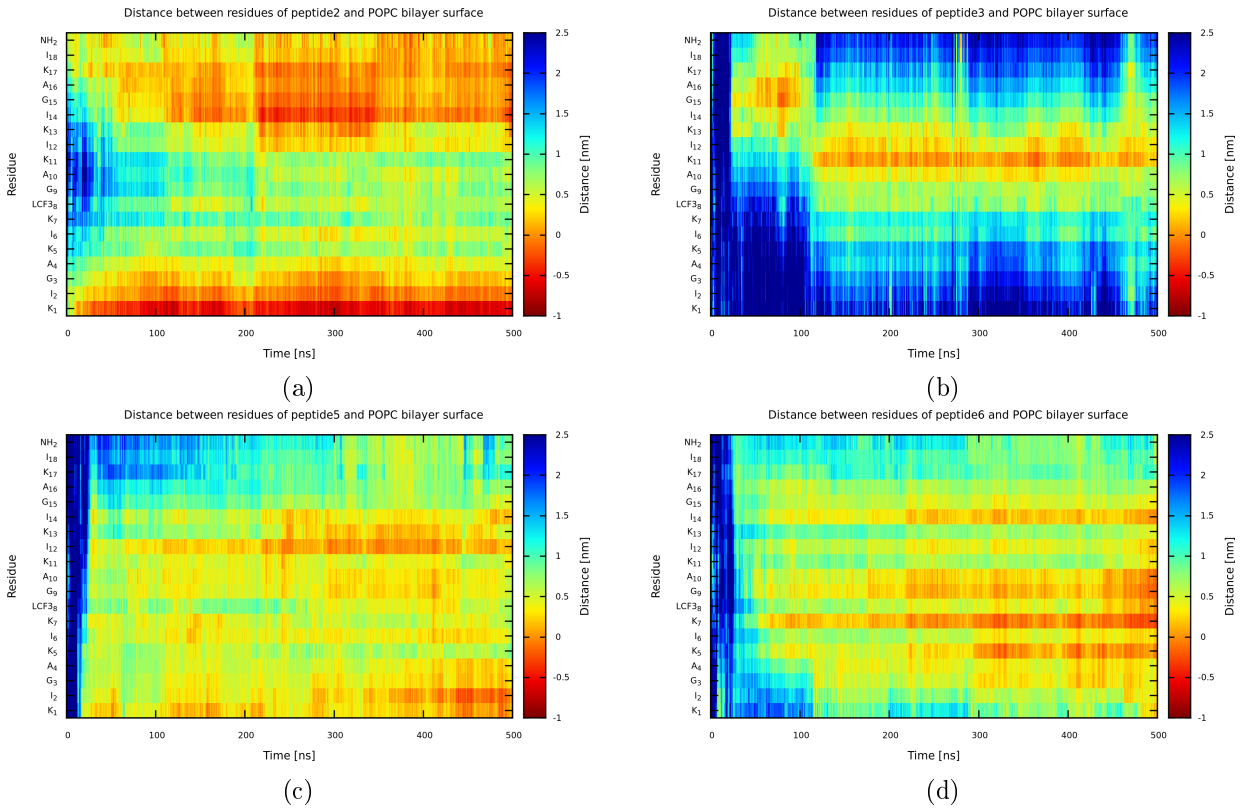

Figure 41: The distance between each residue of the four adsorbing [KIGAKI]$_3$-8L peptides and the POPC membrane surface is illustrated here. Peptide1 and peptide4 do not adsorb during the 500 ns simulation, but stay in the water phase.

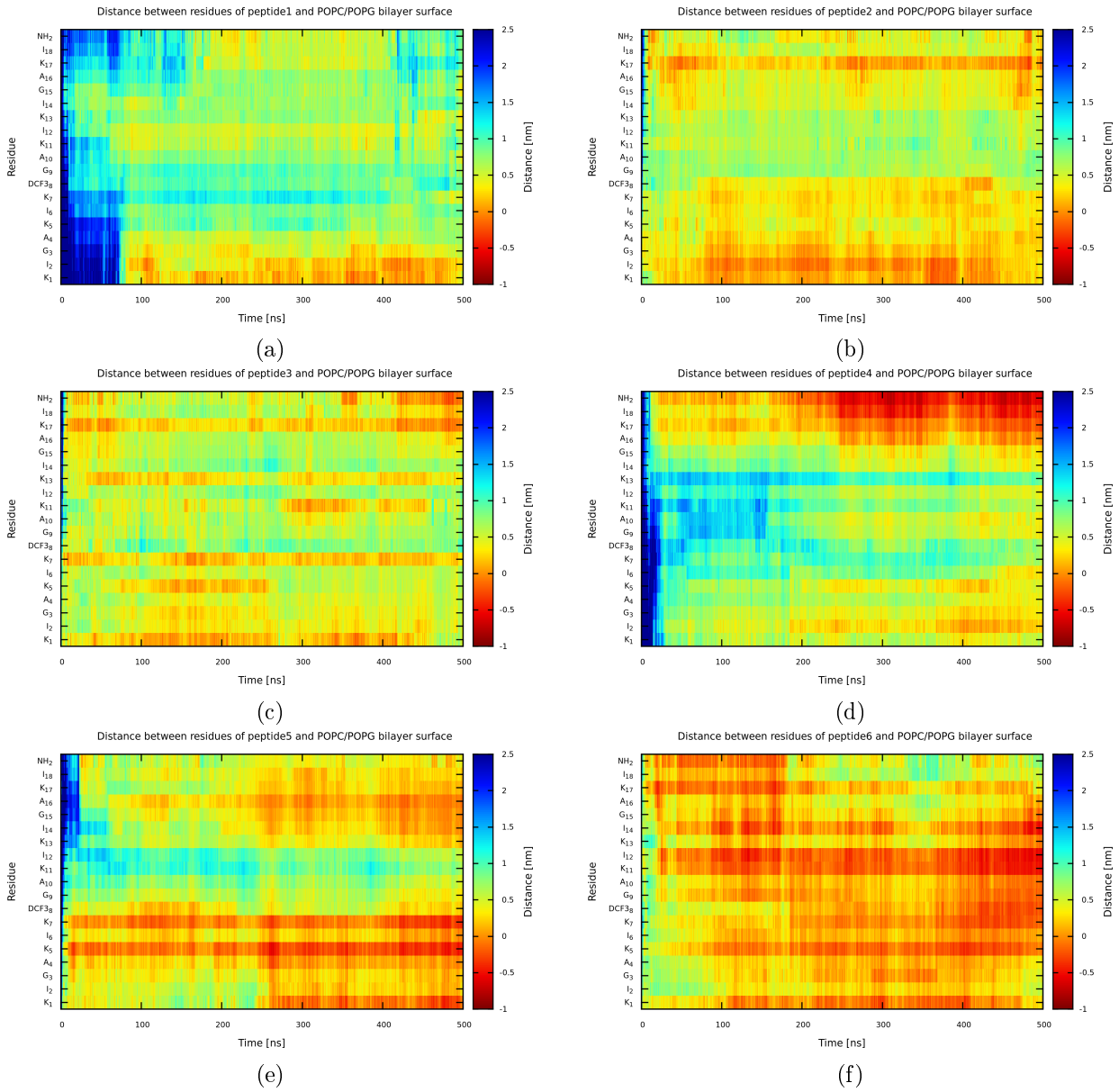

Figure 42: The distance between each residue of the six [KIGAKI]$_3$-8D peptides and the POPC/POPG membrane surface is shown.

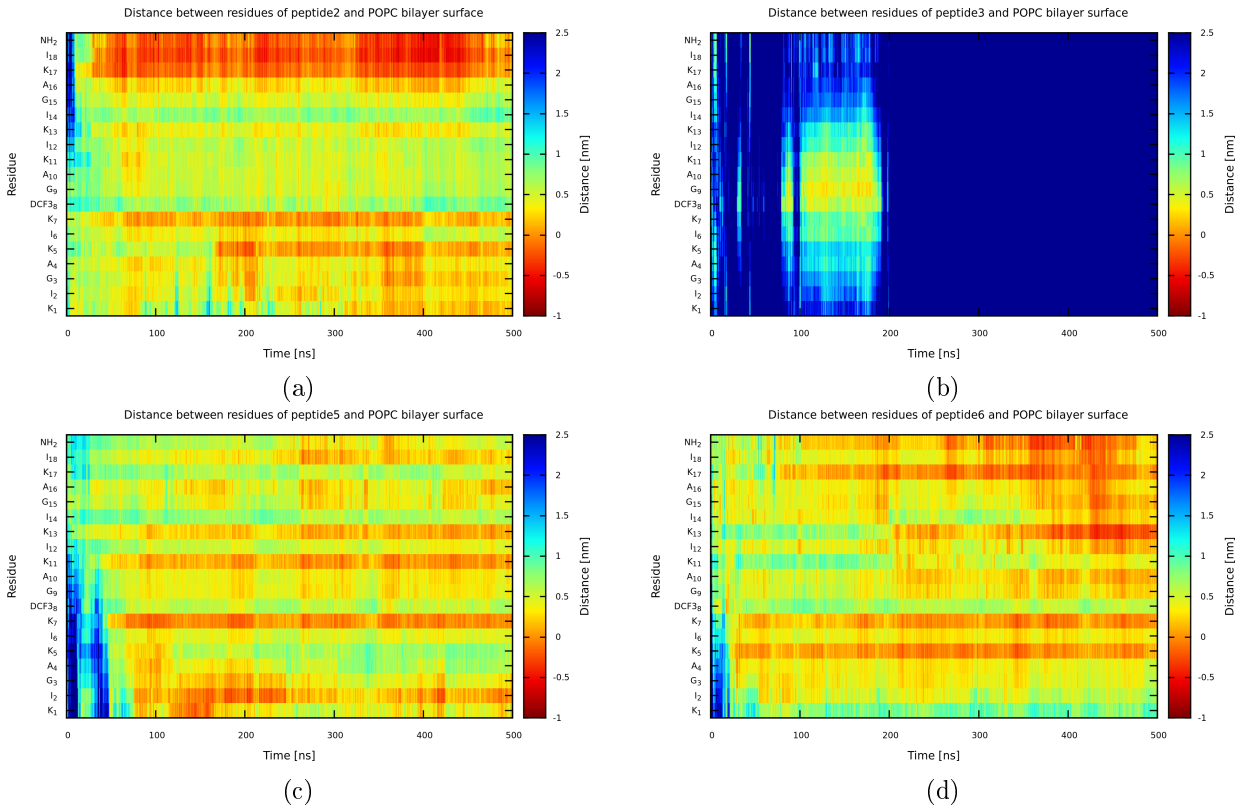

Figure 43: The distance between each residue of the three adsorbing $[KIGAKI]_3$-8D peptides and peptide3, which temporary adsorbs, and the POPC membrane surface is illustrated here. Peptide1 and peptide4 do not adsorb during the 500 ns simulation, but stay in the water phase

7.9 Secondary structure of CF_3 labeled peptides

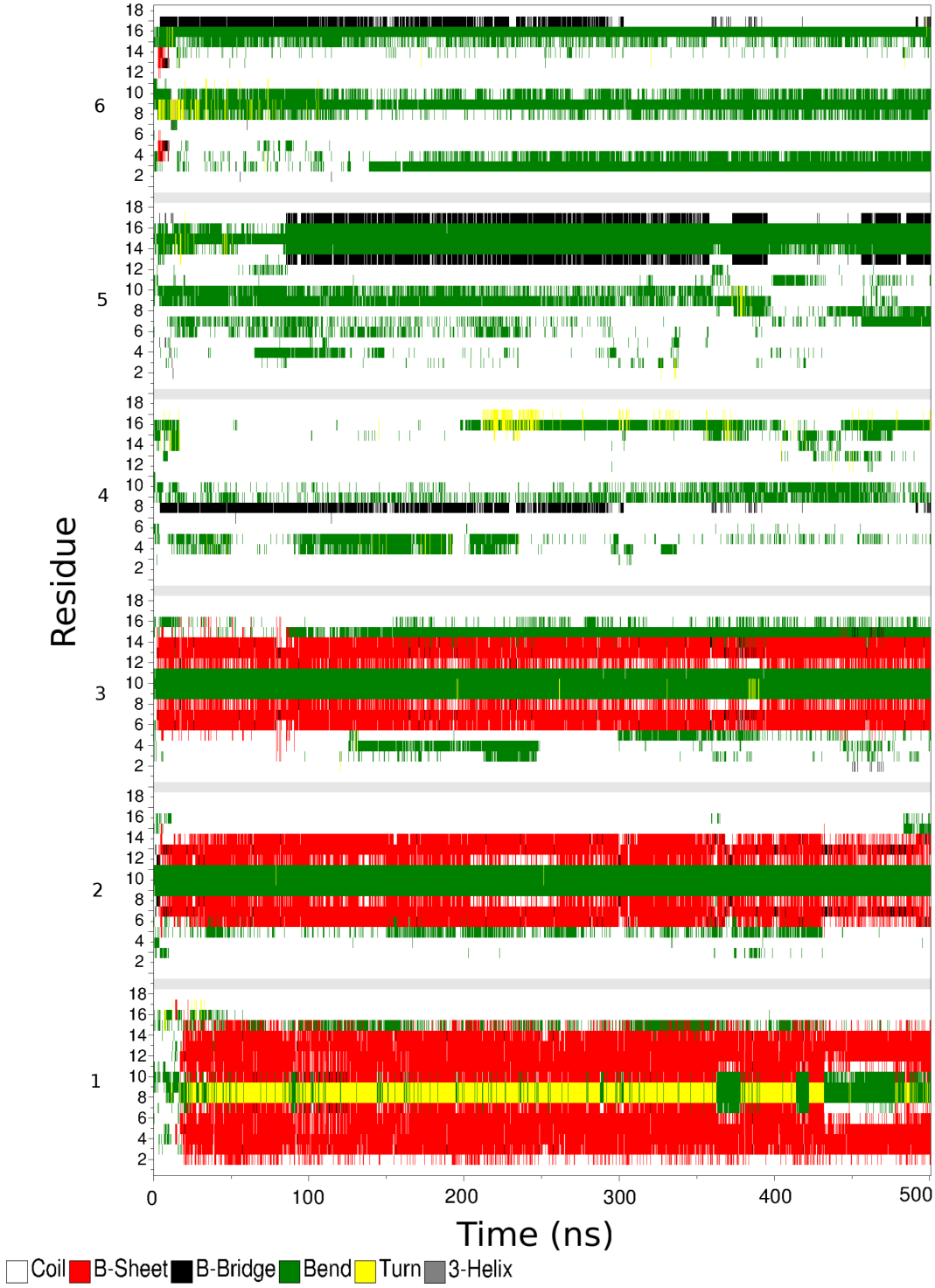

Figure 44: Secondary structure of $[KIGAKI]_3$-8L on the POPC/POPG bilayer. All peptides are adsorbed in the monomeric state on the membrane surface.

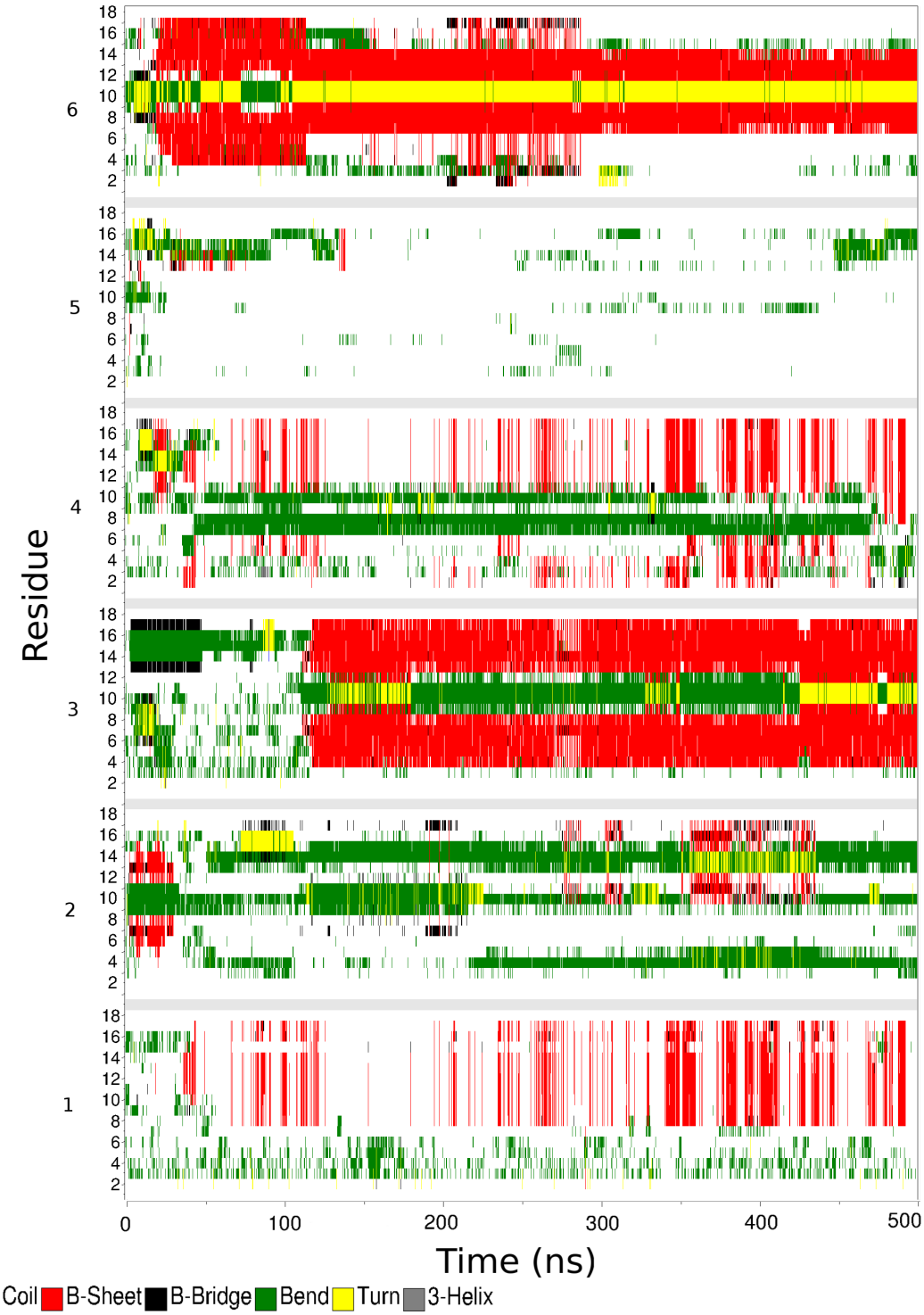

Figure 45: Secondary structure of [KIGAKI]$_3$-8L on the POPC bilayer. Peptides 1 and 4 do not adsorb on the membrane surface, but form a dimer in water.

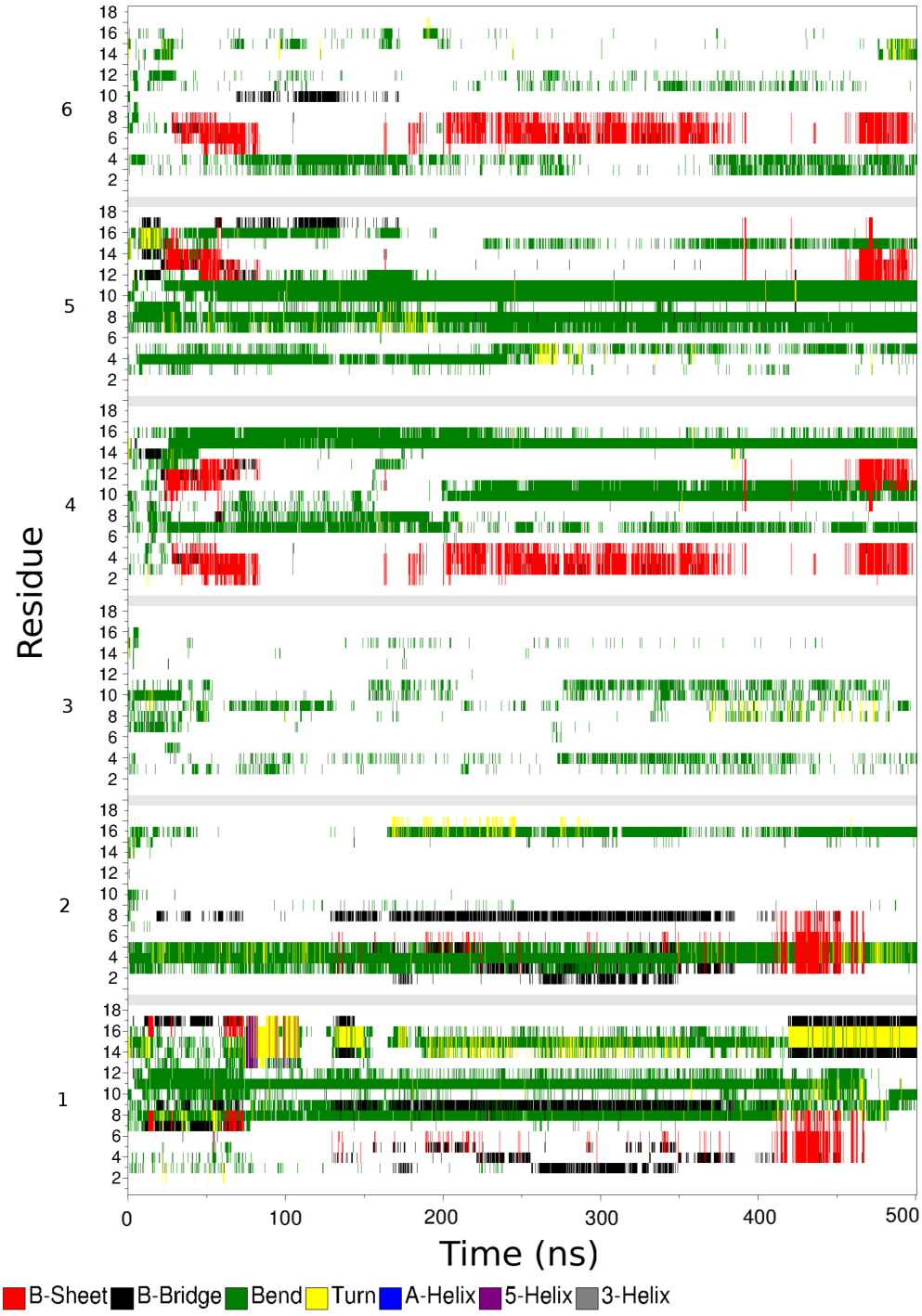

Figure 46: Secondary structure of $[KIGAKI]_3$-8D on the POPC/POPG bilayer. All peptides are adsorbed to the bilayer. Peptide 1 and 2 form a dimer and peptides 4-6 form a trimer on the membrane surface.

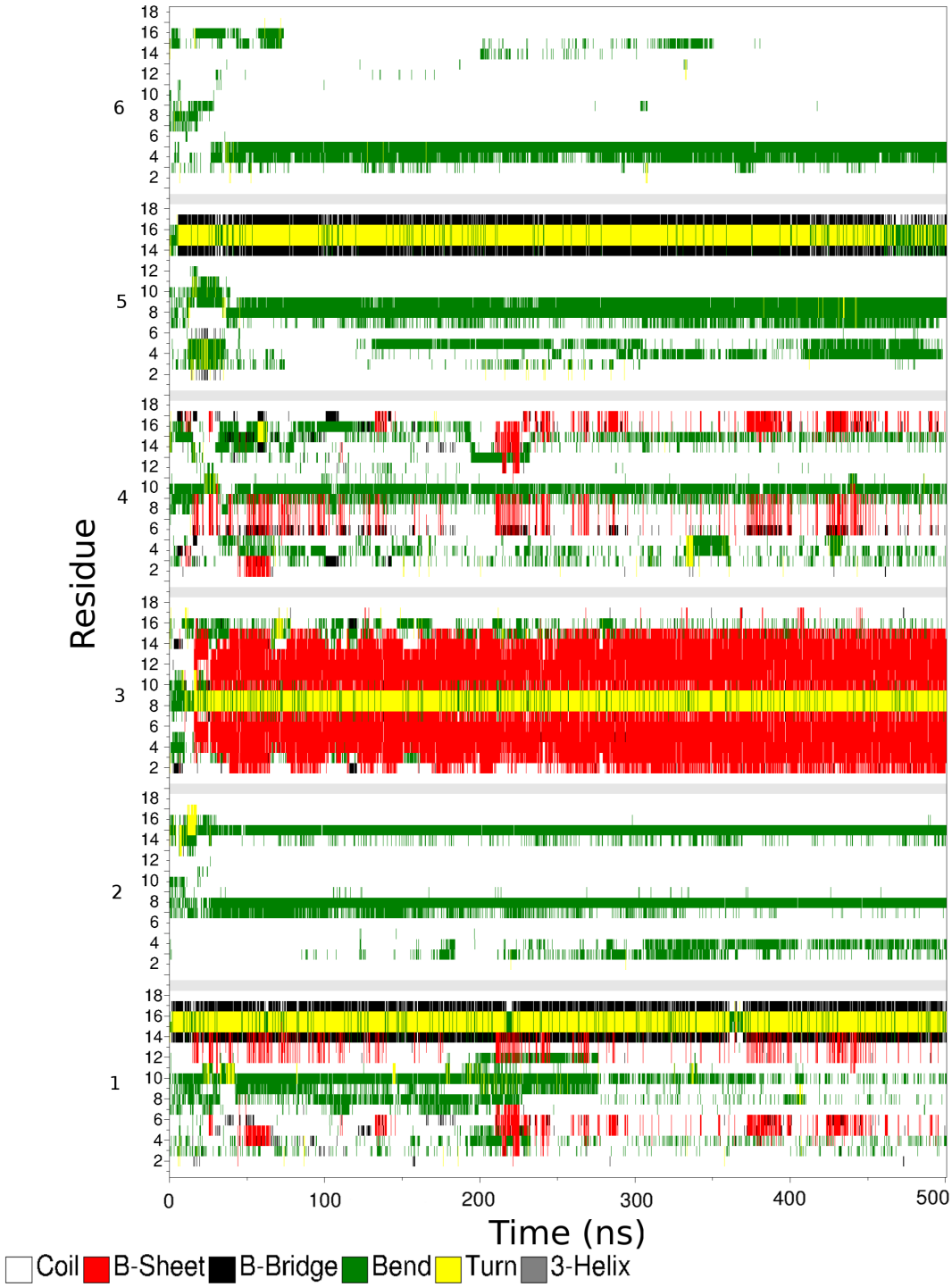

Figure 47: Secondary structure of $[KIGAKI]_3$-8D on the POPC bilayer. Peptides 1 and 4 stay in the water phase during the whole simulation, whereas peptide3 adsorbs from 80 ns to 180 ns. Peptides 1,3 and 4 loosely aggregate to a trimer towards the end of the simulation.

References

[1] Antimicrobial Resistance, Global Report on Surveillance. Technical report, World Health Organization, 2014.

[2] G. L. French. The continuing crisis in antibiotic resistance. *International Journal of Antimicrobial Agents*, 36S3:3 – 7, 2010.

[3] W. Witte. Medical Consequences of Antibiotic Use in Agriculture. *Science*, 279:996 – 997, 1998.

[4] P. S. McManus, V. O. Stockwell, G. W. Sundin, and A. L. Jones. Antibiotic Use In Plant Agriculture. *Annual Review of Phytopathology*, 40:443 – 465, 2002.

[5] R. E. W. Hancock. Peptide antibiotics. *The Lancet*, 349:418 – 422, 1997.

[6] J.-P. S. Powers and R. E. W. Hancock. The relationship between peptide structure and antibacterial activity. *Peptides*, 24:1681 – 1691, 2003.

[7] H. A. Pereira. Novel Therapies Based on Cationic Antimicrobial Peptides. *Current Pharmaceutical Biotechnology*, 7:229 – 234, 2006.

[8] A. Di Giulio and H. Zhao. Antimicrobial Peptides: Basic Mechanisms of Action and Emerging Pharmacological Interest. *Asian Journal of Biochemistry*, 1:28 – 40, 2006.

[9] H. G. Boman. Antibacterial peptides: basic facts and emerging concepts. *Journal of Internal Medicine*, 254:197 – 215, 2003.

[10] S.-J. Kang, D.-H. Kim, T. Mishig-Ochir, and B.-J. Lee. Antimicrobial Peptides: Their Physicochemical Properties and Therapeutic Application. *Archieves of Pharmacal Reserach*, 35:409 – 413, 2012.

[11] Y. J. Gordon and E. G. Romanowski. A Review of Antimicrobial Peptides and Their Therapeutic Potential as Anti-Infective Drugs. *Current Eye Research*, 30:505 – 515, 2005.

[12] M. Zasloff. Antimicrobial peptides of multicellular organisms. *Nature*, 415:389 – 395, 2002.

[13] R. P. Darveau, M. D. Cunningham, C. L. Seachord, L. Cassiano-Clough, W. L. Cosand, J. Blake, and C. S. Watkins. β-Lactam Antibiotics Potentiate Magainin 2 Antimicrobial Activity In Vitro and In Vivo. *Antimicrobial Agents and Chemotherapy*, 35:1153 – 1159, 1991.

[14] G. Roscia, C. Falciani, L. Bracci, and A. Pini. The Development of Antimicrobial Peptides as New Antibacterial Drugs. *Current Protein and Peptide Science*, 14:641 – 649, 2013.

[15] W. van 't Hof, E. C. I. Veerman, E. J. Helmerhorst, and A. V. N. Amerongen. Antimicrobial Peptides: Properties and Applicability. *Journal of Biological Chemistry*, 382:597 – 619, 2001.

[16] C. Friedrich, M. G. Scott, N. Karunaratne, H. Yan, and R. E. W. Hancock. Salt-Resistant Alpha-Helical Cationic Antimicrobial Peptide. *Antimicrobial Agents and Chemotherapy*, 43:1542 – 1548, 1999.

[17] K. Matsuzaki. Why and how are peptide-lipid interactions utilized for self-defense? Magainins and tachyplesins as archetypes. *Biochimica et Biophysica Acta*, 1462:1 – 10, 1999.

[18] L. Yang, T. M. Weiss, R. I. Lehrer, and H. W. Huang. Crystallization of Antimicrobial Pores in Membranes: Magainin and Protegrin. *Biophysical Journal*, 79:2002 – 2009, 2000.

[19] Y. Shai. Mechanism of the binding, insertion and destabilization of phospholipid bilayer membranes by α-helical antimicrobial and cell non-selective membrane-lytic peptides. *Biochimica et Biophysica Acta*, 1462:55 – 70, 1999.

[20] J. P. Bradshaw. Cationic Antimicrobial Peptides. *Biodrugs*, 17:233 – 240, 2003.

[21] J. M. Graham and J. A. Higgins. *Membrane Analysis*. Springer, New York, 1997.

[22] J. Blazyk, R. Wiegand, J. Klein, J. Hammer, R. M. Epand, R. F. Epand, W. L. Maloy, and U. P. Kari. A Novel Linear Amphipathic β-Sheet Cationic Antimicrobial Peptide with Enhanced Selectivity for Bacterial Lipids. *The Journal of Biological Chemistry*, 267:27899 – 27906, 2001.

[23] P. Wadhwani, E. Strandberg, N. Heidenreich, J. Bürck, S. Fanghänel, and A. S. Ulrich. Self-Assembly of Flexible β-Strands into Immobile Amyloid-Like β-Sheets in

Membranes As Revealed by Solid-State ^{19}F NMR. *Journal of the American Chemical Society*, 134:6512 – 6515, 2012.

[24] P. Wadhwani, J. Reichert, E. Strandberg, J. Bürck, J. Misiewicz, S. Afonin, N. Heidenreich, S. Fanghänel, P. K. Mykhailiuk, I. V. Komarov, and A. S. Ulrich. Stereochemical effects on the aggregation and biological properties of the fibril-forming peptide $[KIGAKI]_3$ in membranes. *Physical Chemistry Chemical Physics*, 15:8962 – 8971, 2013.

[25] Y. Jin, J. Hammer, M. Pate, Y. Zhang, F. Zhu, E. Zmuda, and J. Blazyk. Antimicrobial Activities and Structures of Two Linear Cationic Peptide Families with Various Amphipathic β-Sheet and α-Helical Potentials. *Antimicrobial Agents and Chemotherapy*, 49:4957 – 4964, 2005.

[26] J.-X. Lu, J. Blazyk, and G. A. Lorigan. Exploring membrane selectivity of the antimicrobial peptide KIGAKI using solid-state NMR. *Biochimica et Biophysica Acta*, 1758:1303 – 1313, 2006.

[27] M. Meier and J. Seelig. Thermodynamics of the Coil $\leftrightarrow$ β-Sheet Transition in a Membrane Environment. *Journal of Molecular Biology*, 369:277 – 289, 2007.

[28] D. J. Haass, C. Selkoe. Soluble protein oligomers in neurodegeneration: lessons from the Alzheimer's amyloid β-peptide. *Nature Reviews Molecular Cell Biology*, 8:101 – 112, 2007.

[29] K. A. Conway, J. D. Harper, and P. T. Lansbury Jr. Fibrils Formed in Vitro from R-Synuclein and Two Mutant Forms Linked to Parkinson's Disease are Typical Amyloid. *Biochemistry*, 39:2552 – 2563, 2000.

[30] M. Meier. *Thermodynamics and Structure of Peptide-Aggregates at Membrane Surfaces*. PhD thesis, Universität Basel, 2006.

[31] N. B. Hoang. Comparison of force fields to test the membrane adsorption of the amyloid-like $[KIGAKI]_3$ peptide. Master's thesis, German Research School for Simulation Sciences, 2013.

[32] W. Humphrey, A. Dalke, and K. Schulten. VMD – Visual Molecular Dynamics. *Journal of Molecular Graphics*, 14:33 – 38, 1996.

[33] S. A. Adcock and J. A. McCammon. Molecular Dynamics: Survey of Methods for Simulating the Activity of Proteins. *Chemical Reviews*, 106:1589 – 1615, 2006.

[34] L. Verlet. Computer "Experiments" on Classical Fluids. I. Thermodynamical Properties of Lennard-Jones Molecules. *Physical Review*, 159:98 – 103, 1967.

[35] D. v. d. Spoel, E. Lindahl, B. Hess, and the GROMACS development team. *GROMACS User Manual*, 4.6.7. edition, 2014.

[36] W. C. Swope, H. C. Andersen, P. H. Berens, and K. R. Wilson. A computer simulation method for the calculation of equilibrium constants for the formation of physical clusters of molecules: Application to small water clusters. *Journal of Chemical Physics*, 76:637 – 649, 1982.

[37] D. A. McQuarrie. *Statistical Mechanics*. Harper and Row, 1976.

[38] H. J. C. Berendsen, J. P. M. Postma, W. F. v. Gunsteren, A. DiNola, and Haak J. R. Molecular dynamics with coupling to an external bath. *The Journal of Chemical Physics*, 81:3684 – 3690, 1984.

[39] S. Nosé. A molecular dynamics method for simulations in the canonical ensemble. *Molecular Physics*, 52:255 – 268, 1984.

[40] W. G. Hoover. Canonical dynamics: Equilibrium phase-space distributions. *Physical Review A*, 31:1695 – 1697, 1985.

[41] G. Bussi, D. Donadio, and M. Parrinello. Canonical sampling through velocity rescaling. *The Journal of Chemical Physics*, 126:014101–1 – 014101–7, 2007.

[42] M. Parrinello and A. Rahman. Polymorphic transitions in single crystals: A new molecular dynamics method. *Journal of Applied Physics*, 52:7182 – 7190, 1981.

[43] S. Nosé and M. L. Klein. Constant pressure molecular dynamics for molecular systems. *Molecular Physics*, 50:1055 – 1076, 1983.

[44] G. J. Martyna, M. E. Tuckerman, D. J. Tobias, and M. L. Klein. Explicit reversible integrators for extended systems dynamics. *Molecular Physics*, 87:1117 – 1157, 1996.

[45] C. Oostenbrink, A. Villa, A. E. Mark, and W. F. v. Gusteren. A Biomolecular Force Field Based on the Free Enthalpy of Hydration and Solvation: The GROMOS Force-Field Parameter Sets 53A5 and 53A6. *Journal of Computational Chemistry*, 25:1656 – 1676, 2004.

[46] T. J. Piggot, Á. Piñeiro, and S. Khalid. Molecular Dynamics Simulations of Phosphatidylcholine Membranes: A Comparative Force Field Study. *Journal of Chemical Theory and Computation*, 8:4593 – 4609, 2012.

[47] D. Frenkel and B. Smit. *Understanding Molecular Simulation - From Algorithms to Applications*. Academic Press, 2002. ISBN 0-12-267351-4.

[48] T. Darden, D. York, and L. Pedersen. Particle mesh Ewald: An N*log(N) method for Ewald sums in large systems. *Journal of Chemical Physics*, 98:10089 – 10092, 1993.

[49] U. Essmann, L. Perera, and M. L. Berkowitz. A smooth particle mesh Ewald method. *Journal of Chemical Physics*, 103:8577 – 8593, 1995.

[50] V. Gapsys, B. L. de Groot, and R. Briones. Computational analysis of local membrane properties. *Journal of Computer-Aided Molecular Design*, 27:845 – 858, 2013.

[51] W. J. Allen, J. A. Lemkul, and D. R. Bevan. GridMAT-MD:A Grid-based Membrane Analysis Tool for use with Molecular Dynamics. *Journal of Computational Chemistry*, 30:1952 – 1958, 2009.

[52] A. Saupe. Kernresonanzen in kristallinen Flüssigkeiten und in kristallinflüssigen Lösungen. Teil 1. *Zeitschrift Für Naturforschung*, 19a:161 – 171, 1964.

[53] v. d. P. Ploeg and H. J. C. Berendsen. Molecular dynamics simulation of a bilayer membrane. *Journal of Chemical Physics*, 76:3271 – 3276, 1982.

[54] E. Egberts and H. J. C. Berendsen. Molecular dynamics simulation of a smectic liquid crystal with atomic detail. *The Journal of Chemical Physics*, 89:3718 – 3732, 1988.

[55] J.-P. Douliez, A. Ferrarini, and E.-J. Dufourc. On the relationship between C-C and C-D order parameters and its use for studying the conformation of lipid acyl chains in biomembranes. *The Journal of Chemical Physics*, 109:2513 –2518, 1998.

[56] May 2014. `http://bugzilla.gromacs.org/issues/1166`.

[57] May 2014. `http://www.mail-archive.com/gmx-users@gromacs.org/msg41543.html`.

[58] A. K. Malde, L. Zuo, M. Breeze, M. Stoet, D. Poger, P. C. Nair, C. Oostenbring, and A. E. Mark. An Automated Force Field Topology Builder (ATB) and Repository: Version 1.0. *Journal of Chemical Theory and Computation*, 7:4026 – 4037, 2011.

[59] U. C. Singh and A. N. Koller. An Approach to Computing Electrostatic Charges for Molecules. *Journal of Computational Chemistry*, 5:129 – 145, 1984.

[60] S. Pronk, S. Páll, R. Schulz, P. Larsson, P. Bjelkmar, R. Apostolov, M. R. Shirts, J. C. Smith, P. M. Kasson, D. v. d. Spoel, B. Hess, and E. Lindahl. GROMACS 4.5: a high-throughput and highly parallel open source molecular simulation toolkit. *Bioinformatics*, 21:1 –10, 2013.

[61] J. Domański, P. Stansfeld, M. S. P. Sansom, and O. Beckstein. Lipidbook: A Public Repository for Force Field Parameters Used in Membrane Simulations. *Journal of Membrane Biology*, 236:255 – 258, 2010.

[62] L. Martínez, R. Andrade, E. G. Birgin, and J. M. Martínez. Packmol: A Package for Building Initial Configurations for Molecular Dynamics Simulations. *Journal of Computational Chemistry*, 30:2157 – 2164, 2009.

[63] J.-X. Lu, K. Damodaran, J. Blazyk, and G. A. Lorigan. Solid-State Nuclear Magnetic Resonance Relaxation Studies of the Interaction Mechanism of Antimicrobial Peptides with Phospholipid Bilayer Membranes. *Biochemistry*, 44:10208 – 10217, 2005.

[64] J. Lemkul, August 2014. `http://www.bevanlab.biochem.vt.edu/Pages/Personal/justin/Scripts/plot_ss_xpm.txt`.

[65] J. Seelig and N. Waespe-Šarčevič. Molecular order in cis and trans unsaturated phospholipid bilayers. *Biochemistry*, 17:3310 – 3315, 1978.

[66] W. Zhao, R. R. Tomasz, A. A. Gurtovenko, I. Vattulainen, and M. Karttunen. Atomic-scale Structure and Electrostatics of Anionic Palmitoyloleoylphosphatidylglycerol Lipid Bilayers with Na^+ Counterions. *Biophysical Journal*, 2007:1114 – 1124, 2007.

[67] D. E. Elmore. Molecular dynamics simulation of a phosphatidylglycerol membrane. *FEBS Letters*, 580:144 – 148, 2006.

[68] B. Perly, I. C. P. Smith, and H. C. Jarrell. Acyl chain dynamics of phosphatidylethanolamines containing oleic acid and dihydrosterculic acid: deuteron NMR relaxation studies. *Biochemistry*, 24:4659 – 4665, 1985.

[69] N. Kučerka, S. Tristam-Nagle, and J. F. Nagle. Structure of Fully Hydrated Fluid Phase Lipid Bilayers with Monounsaturated Chains. *The Journal of Membrane Biology*, 208:193 – 202, 2005.

[70] J. M. Smaby, M. M. Momsen, H. L. Brockman, and R. E. Brown. Phosphatidylcholine Acyl Unsaturation Modulates the Decrease in Interfacial Elasticity Induced by Cholesterol. *Biophysical Journal*, 73:1492 – 1505, 1997.

[71] N. Kučerka, M.-P. Nieh, and J. Katsaras. Fluid phase lipid areas and bilayer thicknesses of commonly used phosphatidylcholines as a function of temperature. *Biochimica et Biophysica Acta*, 1808:2761 – 2771, 2011.

[72] O. Beckstein and M. S. P. Sansom. Liquid-vapor oscillations of water in hydrophobic nanopores. *Proceedings of the National Academy of Sciences*, 100:7063 – 7068, 2003.

[73] M. R. R. Planque, J. A. W. Kruijtzer, R. M. J. Liskamp, D. Marsh, D. V. Greathouse, R. E. Koeppe II, B. van Kruijff, and J. A. Killian. Different Membrane Anchoring Positions of Tryptophan and Lysine in Synthetic Transmembrane α-Helical Peptides. *The Journal of Biological Chemistry*, 274:20839 – 20846, 1999.

[74] M. Hoshino, H. Katou, Y. Hagihara, K. Hasegawa, H. Naiki, and Y. Goto. Mapping the core of the β_2-microglobulin amyloid fibril by H/D exchange. *Nature structural biology*, 9:332 – 336, 2002.

[75] N. A. Whittemore, R. Mishra, I. Kheterpal, A. D. Williams, R. Wetzel, and E. H. Serpersu. Hydrogen-Deuterium (H/D) Exchange Mapping of Aβ_{1-40} Amyloid Fibril Secondary Structure Using Nuclear Magnetic Resonance Spectroscopy. *Biochemistry*, 44:4434 – 4441, 2005.